

PRODUCTION AND CHARACTERIZATION OF
BORON NITRIDE NANOTUBES

A THESIS SUBMITTED TO
THE GRADUATE SCHOOL OF NATURAL AND APPLIED SCIENCES
OF
MIDDLE EAST TECHNICAL UNIVERSITY

BY

DİDEM ÖZMEN

IN PARTIAL FULFILLMENT OF THE REQUIREMENTS
FOR
THE DEGREE OF MASTER OF SCIENCE
IN
CHEMICAL ENGINEERING

MAY 2008

Approval of the thesis:

**PRODUCTION AND CHARACTERIZATION
OF BORON NITRIDE NANOTUBES**

submitted by **DİDEM ÖZMEN** in partial fulfillment of the requirements for the degree of **Master of Science in Chemical Engineering Department, Middle East Technical University** by,

Prof. Dr. Canan ÖZGEN _____
Dean, Graduate School of **Natural and Applied Sciences**

Prof. Dr. Gürkan KARAKAŞ _____
Head of Department, **Chemical Engineering**

Assoc. Prof. Dr. Naime Aslı SEZGİ _____
Supervisor, **Chemical Engineering Dept., METU**

Prof. Dr. Suna BALCI _____
Co-supervisor, **Chemical Engineering Dept., Gazi University**

Examining Committee Members:

Prof. Dr. Timur DOĞU _____
Chemical Engineering Department, METU

Assoc. Prof. Dr. Naime Aslı SEZGİ _____
Chemical Engineering Department, METU

Prof. Dr. Suna BALCI _____
Chemical Engineering Department, Gazi University

Prof. Dr. Güngör GÜNDÜZ _____
Chemical Engineering Department, METU

Prof. Dr. H. Önder ÖZBELGE _____
Chemical Engineering Department, METU

Date: _____

I hereby declare that all information in this document has been obtained and presented in accordance with academic rules and ethical conduct. I also declare that, as required by these rules and conduct, I have fully cited and referenced all material and results that are not original to this work.

Name, Last name : Didem ÖZMEN

Signature :

ABSTRACT

PRODUCTION AND CHARACTERIZATION OF BORON NITRIDE NANOTUBES

Özmen, Didem

M.S., Department of Chemical Engineering

Supervisor: Assoc. Prof. Dr. Naime Aslı Sezgi

Co-Supervisor: Prof. Dr. Suna Balcı

May, 111 pages

The further developments in nanotechnology in last few years provide usage of nanoscale particles for many applications in various areas such as electronics, pharmaceutical, and biomedical due to their strengthened mechanical, thermal and electrical properties. Boron nitride nanotubes are a good example of nanoparticles. In this study, boron nitride nanotubes were successfully synthesized from the reaction of ammonia gas with mixture of boron and iron oxide. Physical and structural properties of the synthesized materials were determined by X-Ray Diffraction, Energy Dispersive X-Ray Spectroscopy, nitrogen sorption, X-Ray Photoelectron Spectroscopy, Fourier Transform Infrared Spectroscopy, and Scanning Electron Microscopy. Experiments were conducted in a tubular furnace at different temperatures and also at different weight ratios of boron to iron oxide. Qualitative chemical analysis of the reactor effluent stream was carried out using a mass spectrometer.

The mass spectrometer analysis of the reaction products proved formation of nitrogen in addition to hydrogen and water during the reaction of ammonia gas with the mixture of boron and iron oxide.

XRD results showed that hexagonal and rhombohedral boron nitrides and cubic iron were the solid phases formed in the product. FTIR and XPS results also indicated the presence of boron nitride and the atomic ratio of boron to nitrogen was compatible with the chemical stoichiometric relation between boron and nitrogen. It was observed that the crystallinity of the product increased with an increase in temperature.

The diameter of the produced nanotubes varied from 64 nm to 136 nm. The synthesized nanotubes exhibited Type II isotherms. The surface areas of the produced boron nitride nanotubes decreased with a decrease in both temperature and the weight ratio of boron to iron oxide.

The best temperature and weight ratio of boron to iron oxide to produce boron nitride nanotubes were found to be 1300 °C and 20, respectively.

Keywords: Boron Nitride, Nanotubes, Characterization, Synthesis,
Nanotechnology.

ÖZ

BOR NİTRÜR NANOTÜPÜNÜN ÜRETİMİ VE KARAKTERİZASYONU

Özmen, Didem

Yüksek Lisans, Kimya Mühendisliği Bölümü

Tez Yöneticisi: Doç. Dr. Naime Aslı Sezgi

Ortak Tez Yöneticisi: Prof. Dr. Suna Balcı

Mayıs, 111 sayfa

Son yıllarda nanoteknolojideki gelişmeler, nanoboyuttaki partiküllerin güçlü mekanik, ısı ve elektriksel özelliklerinden dolayı elektronik, ilaç sanayi ve biyomedikal gibi çeşitli alanlarda uygulanmasını sağlamaktadır. Bor nitrür nanotüpleri nanopartiküllere iyi birer örnektirler. Bu çalışmada, bor nitrür nanotüpleri, amonyak gazı ile bor ve demir oksit karışımının reaksiyonu sonucunda başarılı bir şekilde sentezlenmiştir. Sentezlenen maddelerin fiziksel ve yapısal özellikleri X-Işını Kırınım Ölçeri (XRD), Enerji Dağılımı X-Işını Spektroskopisi, Azot Sorpsiyon, X-Işını Fotoelektron Spektroskopisi (XPS), Fourier Dönüşüm Kızılötesi Spektroskopisi (FTIR) ve Taramalı Elektron Mikroskobu (SEM) kullanılarak belirlenmiştir. Deneyler tüp fırında farklı sıcaklıklarda ve farklı bor/demir oksit kütle oranlarında gerçekleştirilmiştir. Reaktörden çıkan maddelerin nitel kimyasal analizleri kütle spektrometresi kullanılarak yapılmıştır.

Reaksiyon ürünlerinin kütle spektrometre analizi, hidrojen ve suya ek olarak azotun da oluştuğunu kanıtlamıştır.

XRD sonuçları, hekzagonal ve rombohedral bor nitrür ile kübik demirin üründe oluşan katı fazlar olduğunu göstermiştir. FTIR ve XPS sonuçları da bor nitrürün ortamda varlığını işaret etmiştir ve borun azota olan atomik oranı borla azot arasındaki kimyasal stokiometrik ilişkiyle uyumludur. Sıcaklıktaki artışla birlikte üründeki kristallığın de arttığı gözlenmiştir.

Üretilen nanotüplerin çapları 64 nm ile 136 nm arasında değişmektedir. Sentezlenen nanotüpler Tip II izotermelerini göstermişlerdir. Sıcaklıktaki ve bor/demir oksit kütle oranındaki azalmayla birlikte üretilen bor nitrür nanotüplerinin yüzey alanları azalmıştır.

Bor nitrür nanotüplerini üretmek için en iyi sıcaklık ve bor/demir oksit kütle oranı 1300 °C ve 20 olarak bulunmuştur.

Anahtar Sözcükler: Bor Nitrür, Nanotüpler, Karakterizasyon, Sentez, Nanoteknoloji.

To My Family

ACKNOWLEDGEMENTS

First of all, I would like to express my deepest appreciation to my supervisor Assoc. Prof. Dr. Naime Aslı Sezgi for her invaluable guidance, her humanity, her kindly attitude toward me, and help throughout this study. I would also like to thank my co-supervisor Prof. Dr. Suna Balcı for her suggestions, her kindly attitude toward me and help.

I would like to thank Canan Gücüyener, Belma Soydaş, Özge Aktaş, and Funda Başoğlu for their help in characterization experiments.

I would also like to thank to Zeynep Obalı, Ahmet Göktaş, Nihan Karakoç, Erkan Biber, Canan Şener Martı, Derya Silibolatlaz for their help, friendship and motivation during the hard course of this study. Thanks to all technicians and machine shop workers of the Department of Chemical Engineering who helped me in this study.

Thanks to Scientific and Technological Research Council of Turkey (TÜBİTAK) (Project No:106M379) for financial support, METU Central Laboratory for EDX, XPS and SEM analysis, Department of Metallurgical and Materials Engineering for XRD analysis, Department of Chemical Engineering of Gazi University for FTIR, single point surface area and nitrogen sorption analysis.

Finally, I would like to present my greatest thanks to my family for their continuous support, love, patience for me that made the accomplishment of this work.

TABLE OF CONTENTS

ABSTRACT.....	iv
ÖZ.....	vi
ACKNOWLEDGMENTS.....	ix
TABLE OF CONTENTS.....	x
LIST OF TABLES.....	xiii
LIST OF FIGURES.....	xvi
NOMENCLATURE.....	xxi
CHAPTER	
1. INTRODUCTION.....	1
1.1 Nanotubes.....	1
1.2 Types of Nanotubes.....	2
1.3 Carbon Nanotubes (CNTs).....	4
1.3.1 Properties of Carbon Nanotubes.....	4
1.3.2 Applications of Carbon Nanotubes.....	5
1.4 Boron Nitride and Similarities between Hexagonal Boron Nitride and Graphite.....	6
1.5 Boron Nitride Nanotubes (BNNTs).....	8
1.5.1 Properties of Boron Nitride Nanotubes.....	8
1.5.2 Applications of Boron Nitride Nanotubes.....	9
1.5.3 Production Methods for Boron Nitride Nanotubes.....	10
1.5.3.1 Arc-Discharge and Arc-Melting Methods....	10
1.5.3.2 Laser Ablation Method.....	11
1.5.3.3 Ball Milling + Annealing Method.....	12

1.5.3.4	Chemical Vapor Deposition (CVD)	
	Method.....	13
1.6	Literature Survey.....	14
1.7	Objective of the Study.....	20
2.	EXPERIMENTAL.....	22
2.1	Experimental Set-up.....	22
2.2	Experimental Procedure.....	24
2.3	Hiden HPR20 Gas Analysis System.....	25
2.3.1	Working Principles of Mass Spectrometer.....	28
2.4	Characterization Techniques.....	29
2.4.1	X-ray Diffraction (XRD) Technique.....	30
2.4.2	X-ray Photoelectron Spectroscopy (XPS).....	31
2.4.3	Scanning Electron Microscopy (SEM).....	31
2.4.4	Energy Dispersive X-ray Spectroscopy (EDX).....	32
2.4.5	Fourier Transform Infrared Spectroscopy (FTIR).....	32
2.4.6	Single Point Surface Area Measurement.....	33
2.4.7	Nitrogen Adsorption/Desorption Isotherms.....	34
3.	RESULTS AND DISCUSSION.....	35
3.1	Qualitative Chemical Analysis of Reactor Effluent Stream.....	35
3.2	Characterization of Synthesized Boron Nitride Nanotubes.....	37
3.2.1	X-ray Diffraction Results.....	37
3.2.2	Fourier Transform Infrared Spectroscopy (FTIR).....	43
3.2.3	X-ray Photoelectron Spectroscopy (XPS).....	48
3.2.4	Energy Dispersive X-ray Spectroscopy (EDX).....	51
3.2.5	Scanning Electron Microscopy (SEM).....	54

3.2.6 Single Point Surface Area Measurement.....	58
3.2.7 Nitrogen Adsorption/Desorption Isotherms.....	58
3.3 Reproducibility of the Experimental Data.....	65
4. CONCLUSIONS.....	68
5. RECOMMENDATIONS.....	70
REFERENCES.....	71
APPENDICES	
A. VOLUMETRIC FLOW RATE CALIBRATION CURVES FOR ARGON AND AMMONIA ROTAMETERS.....	77
A.1 Calibration Curve for Argon Rotameter.....	77
A.2 Calibration Curve for Ammonia Rotameter.....	78
B. THE MASS SPECTROMETER CRACKING PATTERN DATA FOR THE SYSTEM GASES.....	79
C. X-RAY DIFFRACTION DATA.....	81
C.1 X-ray Diffraction Data of Reference Compounds.....	81
C.2 XRD Data of Synthesized Materials.....	86
D. FTIR SPECTRA OF BORON AND IRON OXIDE.....	92
E. XPS SPECTRA OF SYNTHESIZED MATERIALS.....	94
F. EDX SPECTRA OF PRODUCTS.....	105
G. NITROGEN ADSORPTION/DESORPTION ISOTHERMS.....	109
G.1 BET Method.....	109
G.2 Single Point BET Method.....	110

LIST OF TABLES

TABLES

Table 1.1 Properties of CNTs and BNNTs.....	8
Table 2.1 Experimental conditions for synthesis of BNNTs	25
Table 3.1 B to N atomic ratios of the products synthesized with different B:Fe ₂ O ₃ weight ratios and boron sources at different temperatures.....	51
Table 3.2 Atomic ratios of boron to nitrogen for the materials synthesized with B to Fe ₂ O ₃ weight ratio of 15 and boron purchased from Merck at different temperatures.....	52
Table 3.3 Boron to nitrogen atomic ratios of BNNTs synthesized at 1300°C at different B to Fe ₂ O ₃ weight ratios and boron purchased from Merck.....	53
Table 3.4 Single point surface areas of products synthesized at different temperatures with B to Fe ₂ O ₃ weight ratio of 15.....	58
Table 3.5 Physical properties of the synthesized materials.....	62
Table B.1 Mass spectrometer cracking pattern data for NH ₃	79
Table B.2 Mass spectrometer cracking pattern data for Ar.....	79
Table B.3 Mass spectrometer cracking pattern data for H ₂	80
Table B.4 Mass spectrometer cracking pattern data for H ₂ O.....	80
Table B.5 Mass spectrometer cracking pattern data for N ₂	80

Table C.1.1 XRD data for hexagonal BN.....	81
Table C.1.2 XRD data for hexagonal BN.....	82
Table C.1.3 XRD data for hexagonal BN.....	82
Table C.1.4 XRD data for hexagonal BN.....	82
Table C.1.5 XRD data for cubic Fe.....	83
Table C.1.6 XRD data for cubic Fe.....	83
Table C.1.7 XRD data for rhombohedral boron nitride.....	83
Table C.1.8 XRD data for cubic Fe.....	84
Table C.1.9 XRD data for cubic Fe.	84
Table C.1.10 XRD data for Fe ₂ O ₃	85
Table C.2.1 XRD data for BNNTs produced at 1400°C with a B to Fe ₂ O ₃ weight ratio of 15.....	86
Table C.2.2 XRD data for BNNTs produced at 1300°C with a B to Fe ₂ O ₃ ratio of 15.....	86
Table C.2.3 XRD data for BNNTs produced at 1200°C with a B to Fe ₂ O ₃ ratio of 15.....	87
Table C.2.4 XRD data for BNNTs produced at 1100°C with a B to Fe ₂ O ₃ ratio of 15.....	87
Table C.2.5 XRD data for BNNTs produced at 1000°C with a B to Fe ₂ O ₃ ratio of 15.....	87
Table C.2.6 XRD data for BNNTs produced at 900°C with a B to Fe ₂ O ₃ ratio of 15.....	88

Table C.2.7 XRD data for BNNTs produced at 1300°C with a B to Fe ₂ O ₃ ratio of 5.....	88
Table C.2.8 XRD data for BNNTs produced at 1300°C with a B to Fe ₂ O ₃ ratio of 20.....	89
Table C.2.9 XRD data for BNNTs produced at 1300°C with a B to Fe ₂ O ₃ ratio of 1.....	89
Table C.2.10 XRD data for BNNTs produced at 1300°C with a B to Fe ₂ O ₃ ratio of 0.5.....	90
Table C.2.11 XRD data for BNNTs produced at 1300°C with a B to Fe ₂ O ₃ ratio of 20 with boron source of Sigma-Aldrich.....	90
Table C.2.12 XRD data for BNNTs produced at 1200°C with a B to Fe ₂ O ₃ ratio of 20 with boron source of Sigma-Aldrich.....	90
Table C.2.13 XRD data for BNNTs produced at 1100°C with a B to Fe ₂ O ₃ ratio of 20 with boron source of Sigma-Aldrich.....	91
Table C.2.14 XRD data for BNNTs produced at 900°C with a B to Fe ₂ O ₃ ratio of 20 with boron source of Sigma-Aldrich.....	91

LIST OF FIGURES

FIGURES

Figure 1.1 An example of a nanotube.....	2
Figure 1.2 (a) Multi-wall nanotube (MWNNT), (b) Single-wall nanotube (SWNT).....	2
Figure 1.3 Structural types of nanotubes.....	3
Figure 1.4 Boron nitride crystal structures: (a) hexagonal, (b) rhombohedral (c) cubic.....	6
Figure 1.5 Hexagonal structures of graphite and BN.....	7
Figure 1.6 Experimental apparatus for (a) arc-discharging, and (b) arc-melting methods.....	11
Figure 1.7 Experimental set-up for laser ablation method.....	12
Figure 1.8 Experimental set-up for ball milling+annealing method.....	13
Figure 1.9 Experimental set-up for CVD method.....	13
Figure 2.1 Schematic drawing of experimental system.....	23
Figure 2.2 HPR 20 Gas analysis system.....	26
Figure 2.3 Schematic representation of a quadrupole mass analyzer.....	28

Figure 2.4 Components of a mass spectrometer.....	29
Figure 2.5 Reflection of X-rays from two planes of atoms in a solid.....	30
Figure 3.1 Typical mass spectrum of the reactor effluent at 1400°C with B to Fe ₂ O ₃ weight ratio of 15.....	36
Figure 3.2 XRD patterns of products synthesized with B to Fe ₂ O ₃ weight ratio of 15 and Merck boron source at different reaction temperatures: (a)1400°C, (b)1300°C, (c)1200°C, (d)1100°C, (e)1000°C, and (f)900°C....	38
Figure 3.3 XRD patterns of products synthesized at 1300°C, with Merck boron source and B to Fe ₂ O ₃ weight ratios of a) 20, (b) 15, and (c) 5.....	39
Figure 3.4 XRD pattern of product synthesized at 1300°C, with Merck boron source and B to Fe ₂ O ₃ weight ratio of 1.....	40
Figure 3.5 XRD pattern of product synthesized at 1300°C, with Merck boron source and B to Fe ₂ O ₃ weight ratio of 0.5.....	41
Figure 3.6 XRD pattern of product synthesized at 1300°C, with Sigma-Aldrich boron source and B to Fe ₂ O ₃ weight ratio of 20.....	42
Figure 3.7 FTIR spectra of BNNTs synthesized with B to Fe ₂ O ₃ weight ratio of 15 and boron purchased from Merck at different reaction temperatures: (a) 1300°C, (b) 1200°C, (c) 1100°C, (d) 1000°C, and (e) 900°C.....	44
Figure 3.8 FTIR spectra of BNNTs synthesized at 1300°C with Merck boron source and different B to Fe ₂ O ₃ weight ratios: (a) 20, (b) 15, (c) 5, (d) 1, and (e) 0.5.....	46
Figure 3.9 FTIR spectrum of BNNTs synthesized at a temperature of 1300°C with B to Fe ₂ O ₃ weight ratio of 20 and Sigma-Aldrich boron source.....	47
Figure 3.10 XPS spectrum of the product synthesized with a B: Fe ₂ O ₃ weight ratio of 15 at 1300°C.....	48

Figure 3.11 XPS spectrum of the product synthesized with a B:Fe ₂ O ₃ weight ratio of 15 at 1300°C after bombarding with Ar ⁺ ions.....	49
Figure 3.12 EDX spectrum of BNNTs produced at 1300°C with B to Fe ₂ O ₃ weight ratio of 20.....	52
Figure 3.13 SEM images of BNNTs synthesized at B to Fe ₂ O ₃ weight ratios of 15 with boron purchased from Merck at different reaction temperatures: (a) 1300°C, (b) 1300°C, (c) 1200°C, (d) 1100°C, (e) 1000°C, and (f) 900°C.....	55
Figure 3.14 SEM images of BNNTs synthesized at 1300°C with boron purchased from Merck and B to Fe ₂ O ₃ weight ratios of (a) 20 (b)15, (c) 5, (d) 1, and (e) 0.5.....	56
Figure 3.15 SEM images of BNNTs synthesized at 1200°C with boron purchased from Sigma-Aldrich and B to Fe ₂ O ₃ weight ratio of 20.....	57
Figure 3.16 Adsorption/desorption isotherms of the BNNTs synthesized with B to Fe ₂ O ₃ weight ratio of 15 at: (a) 1300°C and (b) 1200°C.....	59
Figure 3.17 Adsorption/desorption isotherm of the BNNTs synthesized with B to Fe ₂ O ₃ weight ratio of 5 at 1300 °C.....	60
Figure 3.18 Pore size distributions for products produced at: (a) 1300°C and (b) 1200°C.....	64
Figure 3.19 Pore size distribution for BNNTs produced at 1300°C with B to Fe ₂ O ₃ weight ratio of 5.....	65
Figure 3.20 XRD patterns of BNNTs produced at 1300°C at B to Fe ₂ O ₃ weight ratio of 15.....	66
Figure 3.21 FTIR spectra of BNNTs produced at 1300°C at B to Fe ₂ O ₃ weight ratio of 15.....	67
Figure A.1 Volumetric flow rate calibration curve for argon rotameter.....	77

Figure A.2 Volumetric flow rate calibration curve for ammonia rotameter.....	78
Figure D.1 FTIR spectrum of boron.....	92
Figure D.2 FTIR spectrum of iron oxide.....	93
Figure E.1 XPS spectrum of BNNTs produced at 1400°C with B to Fe ₂ O ₃ ratio of 15.....	94
Figure E.2 XPS spectrum of BNNTs produced at 1100°C with B to Fe ₂ O ₃ ratio of 15.....	95
Figure E.3 XPS spectrum of BNNTs produced at 1200°C with B to Fe ₂ O ₃ ratio of 15.....	96
Figure E.4 XPS spectrum of BNNTs produced at 1000°C with B to Fe ₂ O ₃ ratio of 15.....	97
Figure E.5 XPS spectrum of BNNTs produced at 900°C with B to Fe ₂ O ₃ ratio of 15.....	98
Figure E.6 XPS spectrum of BNNTs produced at 1300°C with B to Fe ₂ O ₃ ratio of 20 with boron source of Sigma-Aldrich.....	99
Figure E.7 XPS spectrum of BNNTs produced at 1300°C with B to Fe ₂ O ₃ ratio of 20 with boron source of Merck.....	100
Figure E.8 XPS spectrum of BNNTs produced at 1300°C with B to Fe ₂ O ₃ ratio of 5 with boron source of Merck.....	101
Figure E.9 XPS spectrum of BNNTs produced at 1300°C with B to Fe ₂ O ₃ ratio of 1 with boron source of Merck.....	102
Figure E.10 XPS spectrum of BNNTs produced at 1300°C with B to Fe ₂ O ₃ ratio of 0.5 with boron source of Merck.....	103
Figure E.11 XPS spectrum of BNNTs produced at 1300°C with B to Fe ₂ O ₃ ratio of 20 with boron source of Sigma-Aldrich.....	104

Figure F.1 EDX spectrum of BNNTs produced at 1300°C with B to Fe ₂ O ₃ weight ratio of 15.....	105
Figure F.2 EDX spectrum of BNNTs produced at 1200°C with B to Fe ₂ O ₃ weight ratio of 15.....	105
Figure F.3 EDX spectrum of BNNTs produced at 1200°C with B to Fe ₂ O ₃ weight ratio of 20 with boron source from Sigma-Aldrich.....	106
Figure F.4 EDX spectrum of BNNTs produced at 900°C with B to Fe ₂ O ₃ weight ratio of 15	106
Figure F.5 EDX spectrum of BNNTs produced at 1300°C with B to Fe ₂ O ₃ weight ratio of 5.....	107
Figure F.6 EDX spectrum of BNNTs produced at 1300°C with B to Fe ₂ O ₃ weight ratio of 20.....	107
Figure F.7 EDX spectrum of BNNTs produced at 1300°C with B to Fe ₂ O ₃ weight ratio of 1.....	108
Figure F.8 EDX spectrum of BNNTs produced at 1300°C with B to Fe ₂ O ₃ weight ratio of 0.5.....	108

NOMENCLATURE

A_{cs}	Crosssectional adsorbate area, m^2
BNNT	Boron Nitride Nanotube
C	Isotherm constant depending on the pore structure of the adsorbate
CNT	Carbon Nanotube
CVD	Chemical Vapor Deposition
EDX	Energy Dispersive X-Ray Spectroscopy
FTIR	Fourier Transform Infrared Spectroscopy
GPa	Giga Pascal
h-BN	Hexagonal Boron Nitride
MWBNNT	Multi-wall Boron Nitride Nanotube
MWCNT	Multi-wall Carbon Nanotube
P	Equilibrium pressure
P_o	Saturation vapor pressure of the adsorbate
r-BN	Rhombohedral Boron Nitride
R	Gas constant, $atm.cm^3.mol^{-1}.K^{-1}$
SEM	Scanning Electron Microscopy
S_t	Total surface area
SWBNNT	Single-wall Boron Nitride Nanotube
SWCNT	Single-wall Carbon Nanotube
T	Temperature, K
TPa	Tera Pascal
V	Volume adsorbed
V_m	Volume adsorbed for monolayer coverage
XPS	X-ray Photoelectron Spectroscopy
XRD	X-ray Diffractometer
2θ	Bragg angle, degree

CHAPTER 1

INTRODUCTION

Nanotechnology is the creation of small materials by manipulating single atoms at the scale of molecules up to nanometers and use in structures, devices, and systems. Nanotechnology term was introduced by Eric Drexler in mid 1980s [1].

Nanoparticles have high thermal, electrical and mechanical properties and these properties cause nanoparticles to be used for different applications in electronics, pharmaceuticals, medicine etc. So, nanotechnology is one of the fastest growing areas in materials and engineering science and biotechnology.

Nanotubes are one of the important types of nanoparticles and nanotechnology.

1.1 Nanotubes

Nanotubes are produced by rolling and folding into cylindrical forms of sheets of specific atoms. The length of the nanotubes varies from a few nanometers to 100 micrometers. They can be made from a variety of materials and they can be organic or inorganic depending on the particles used in nanotube construction. An example of a nanotube is shown in Figure 1.1

Nanotubes are the strongest materials known to humankind. They have an extremely broad range of electronic, thermal and structural properties that vary depending on the type of nanotube. Nanotubes are made of various atoms like carbon or boron nitride.

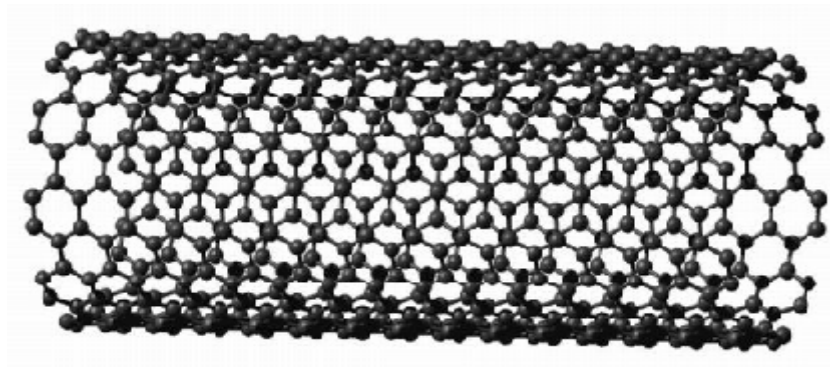


Figure 1.1 An example of a nanotube [2].

1.2 Types of Nanotubes

A nanotube may consist of one tube or a number of concentric tubes. Single layer of atoms forms *single-wall nanotubes (SWNTs)* and *multi-wall nanotubes (MWNTs)* consist of many concentric tubes wrapped one inside another. Examples of single and multi-wall nanotubes can be seen in Figure 1.2.

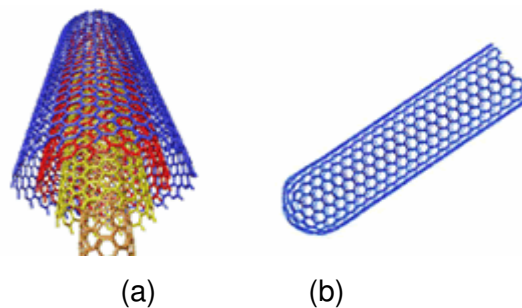


Figure 1.2 (a) Multi-wall nanotube (MWNT), (b) Single-wall nanotube (SWNT) [3].

Nanotubes are classified as armchair, chiral and zigzag nanotubes according to the rolling direction of sheets of atoms. Zig-zag or armchair nanotubes are formed by rolling up the sheets of atoms along the one of the symmetry axis. If equivalent atoms of each unit cell are aligned on a spiral, chiral nanotubes are formed (Figure 1.3).

These structural differences affect the properties of nanotubes such as; mechanical strength, thermal conductivity, density and electrical conductance. According to their structural types, some of the nanotubes are conductor because they are metallic and some are semi-conductor. Furthermore, nanotubes can be open or closed ended depending on their material composition and growth mechanism [4].

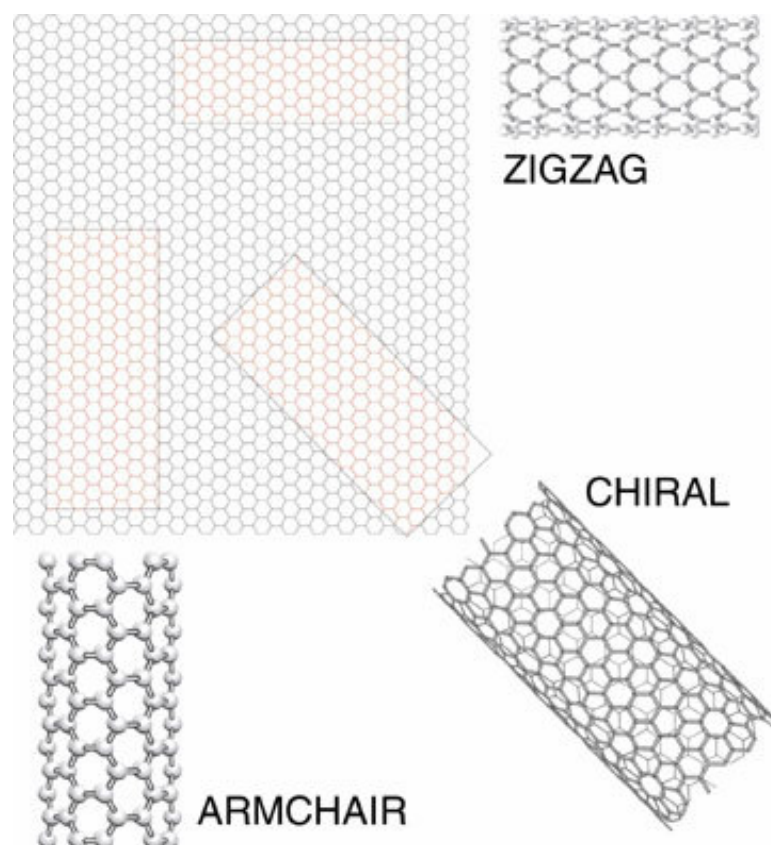


Figure 1.3 Structural types of nanotubes [5].

1.3 Carbon Nanotubes (CNTs)

A carbon nanotube, the most popular type of nanotube, is a cylinder which has single wall or multiwall of graphite atoms. They are about 1-3 nanometers in diameter and hundreds to thousands of nanometers long.

CNTs were first produced and characterized by Iijima in 1991 by arc discharge method. In this method, two graphite rods were used as electrodes and electrical sparks passing between these electrodes vaporized them and allowed to condense carbon to form the product. Although it was expected to produce C_{60} in the product, tiny tubes of carbon with many layers called multi-wall carbon nanotubes were formed [6]. Two years later, single-wall nanotubes were produced using transition metals as the catalyst by arc-discharge method [7, 8].

Beside arc-discharge method, carbon nanotubes are mainly produced by laser ablation and chemical vapor deposition (CVD) methods. Laser ablation apparatus consists of target material, furnace, laser apparatus and water cooled collector. In this method, graphite target is vaporized by using a laser beam under an inert gas atmosphere and the vaporized product is carried by a carrier gas and condenses on the water cooled collector. In CVD method, the catalyst is heated under a hydrocarbon gas atmosphere in a high temperature furnace and the products grow over the catalyst [9].

1.3.1 Properties of Carbon Nanotubes

The electrical properties of the CNTs depend on how the graphene sheet coiled up to form a nanotube. Armchair-type CNTs are metallic. On the other hand, zigzag-type CNTs are semiconductive or metallic. The electrical properties of MWCNTs are quite similar to the SWCNTs [1].

Although CNTs are strong, durable and flexible, they tend to undergo buckling when put under compressive, torsional or bending stress due to their hollow structure. Their tensile strength and Young's Modulus values vary from 10 to 150GPa and from 0.27 to 4.15TPa, respectively. Their average Young's Modulus value is around 1.8TPa. A single perfect nanotube has a tensile strength of nearly 60GPa. On the other hand, MWCNTs have tensile strength of 150GPa. Although the weight of CNTs is one sixth of the weight of steel, CNTs are 100 times stronger than steel [1].

The maximum thermal conductivity of the CNTs is 6000 W/(m·K) at room temperature and this high thermal conductivity makes CNTs as a good thermal conductor. The temperature stability of CNNTs is 2800°C in vacuum and about 750°C in air [10].

1.3.2 Applications of Carbon Nanotubes

Due to their excellent thermal conductivity, high tensile strength, high Young's modulus and electrical properties, carbon nanotubes have many application areas in materials and engineering science, biotechnology, electronics, pharmaceuticals, medicine, and so on.

Having the high length to diameter ratio and strength makes SWCNTs ideal probes for atomic force microscopy.

Due to their electronic properties, CNTs are used in many application areas. The semi conducting properties of CNTs are better than that of silicon. Thus, semi-conductive carbon nanotubes are used to produce field effect transistors instead of the silicon based transistors. Conductive carbon nanotubes are used to produce the tips of scanning tunneling microscopes (STM) and electric force microscopy (EFM) [1].

Carbon nanotubes are also used as electrodes in batteries and as electrode catalyst supports in fuel cell because of their high surface area and thermal conductivity. They play a role in hydrogen storing in fuel cells [10].

The other applications of carbon nanotubes are; artificial muscles, solar cells, filters, clothes, computers, displays and sports equipment like tennis rackets, golf balls etc [11].

1.4 Boron Nitride and Similarities between Hexagonal Boron Nitride and Graphite

After the discovery of carbon nanotubes, the researchers started to work on the other possible nanotubes. Boron nitride is one of them.

Boron nitride (BN) is a molecule that is the combination of boron (B) and nitrogen (N) atoms. Hexagonal, cubic and rhombohedral are the crystal structures of the BN caused by the arrangements of nitrogen and boron atoms (Figure 1.4).

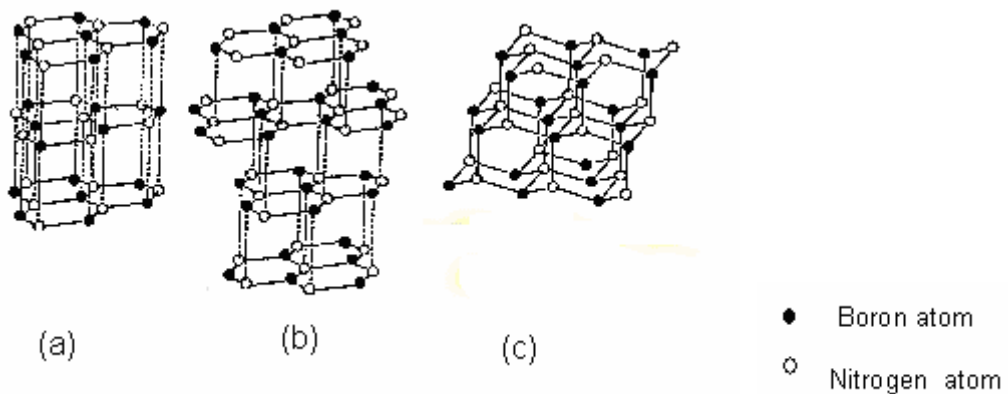


Figure 1.4 Boron nitride crystal structures: (a) hexagonal, (b) rhombohedral (c) cubic [12].

Cubic BN is produced by treating hexagonal BN at high temperature and pressure. It is a very hard material and used in the cutting tools. It is a good conductor of heat and used as an electrical insulator. It has good thermal conductivity. The cubic phase of boron nitride is similar to diamond and the second hardest material after diamond. Rhombohedral BN is similar to hexagonal BN. Hexagonal BN is a graphite-like material and called as white graphite. It is stable up to temperatures of 1000°C under air, up to temperatures of 1400°C under vacuum, and up to temperatures of 2800°C under inert atmosphere. The hexagonal structures of BN and graphite are given in Figure 1.5. Their crystallographic parameters are almost equal. The nearest neighboring distances for graphite and hexagonal BN are 0.142nm and 0.144nm, respectively and inter-layers spacing for graphite and hexagonal BN are 0.33nm and 0.35nm, respectively. They are almost identical. At high temperature and pressure, both graphite and boron nitride are in liquid phase. At high pressure, they are ultra hard materials [14].

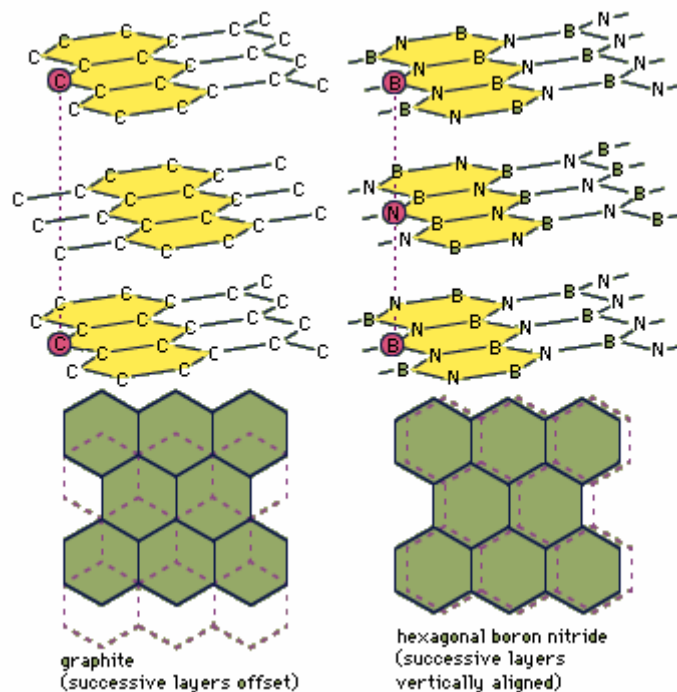


Figure 1.5 Hexagonal structures of graphite and BN [13].

1.5 Boron Nitride Nanotubes (BNNTs)

As it is mentioned in the previous section, nanotubes have outstanding properties and they can be made of various materials. Boron nitride nanotubes are one of them.

BNNTs are formed by folding and rolling the boron nitride sheet into cylindrical forms having zigzag, armchair and chiral structures.

1.5.1 Properties of Boron Nitride Nanotubes

The electronic properties of BNNTs are different than that of CNTs. Carbon nanotubes are either metallic or semi-conductive. However all boron nitride nanotubes are semi-conductive. BNNTs have uniform electronic band gap of 5.5 eV that is independent of the diameter and chirality of the tube [15].

Properties of nanotubes are given in Table 1.1. It is observed that mechanical properties of BNNTs are better than that of CNTs. The elastic modulus of BNNTs is approximately 6 times that of CNTs. Chemical properties of BNNTs is also better than that of CNTs. However, thermal conductivity of BNNTs is not higher than that of CNTs.

Table 1.1 Properties of CNTs and BNNTs.

	BNNTs	CNTs
Elastic Modulus (GPa)^[16]	~ 850	150
Young's Modulus (TPa)^[17]	1.22 ± 0.24	1.8
Oxidation Temperature (°C)^[18]	800	400
Thermal conductivity (W/mK)^[19]	600	3000

1.5.2 Applications of Boron Nitride Nanotubes

Having these outstanding properties makes BNNTs suitable for many applications in which CNNTs are used and researchers are working on to find new application areas for BNNTs.

As it is mentioned, BNNTs are more resistant to oxidation than CNNTs. So, they are used for high temperature applications in which CNNTs would burn.

BNNT is a good candidate for producing composite materials due to its high mechanical, electrical and chemical properties.

They are used for hydrogen storage. Comparing the BNNTs and CNTs with same diameter, boron and nitrogen atoms attract the hydrogen molecule better than carbon. So, BNNTs are preferable to CNTs. Also by increasing the diameter of nanotubes, more hydrogen is stored [20].

In atomic force microscopy (AFM), BNNTs are used as a nano-tip to improve the resolution of the image [21].

BNNTs are being investigated for a wide array of potential applications, such as high-temperature transistors, high-temperature lubricants, photoluminescent devices, reinforcements for weaker materials, and flat-panel displays.

1.5.3 Production Methods for Boron Nitride Nanotubes

Several BNNTs synthesis methods for this outstanding nano material have been investigated in the literature. These methods are summarized in the following sections.

1.5.3.1 Arc-Discharge and Arc-Melting Methods

It is the first technique for the production of both carbon and boron nitride nanotubes. In this method, the reactants are used as electrodes and an arc-discharge is applied between these electrodes. Schematic drawing of experimental apparatus is given in Figure 1.6(a). During the production of nanotubes, the pressure inside the chamber is a few hundred torr. Discharge is typically carried out at a voltage of 20 to 40 V and at a current up to 150 A. The gap between these electrodes is adjusted approximately 1mm or less. Discharging operation takes several minutes and during this operation, the temperature reaches ~4000K. The anode is the consumed electrode because large quantity of electrons from the arc-discharge is accelerated toward the anode and collides with the anode. Nanotubes and other nanoscale structures deposit on the cathode and the inner wall of the chamber.

Arc-melting method is similar to the arc-discharge method. In this method, the reactants are put on the anode which is a Cu mold and cathode is made of tungsten. When voltage and current are applied between the electrodes, arc is generated, the reactant powders are melt on the anode. The experimental set-up for the arc melting method is given in Figure 1.6(b).

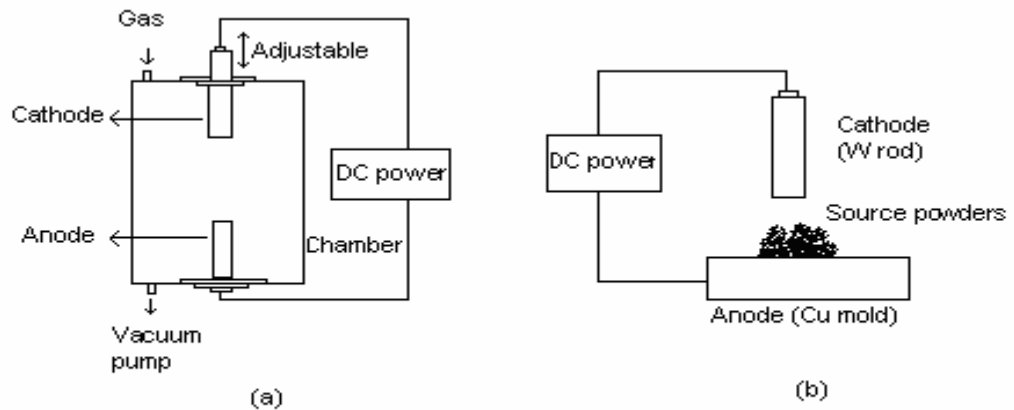


Figure 1.6 Experimental apparatus for (a) arc-discharging, and (b) arc-melting methods [22].

1.5.3.2 Laser Ablation Method

The target material which is a source of boron is placed inside a furnace and a continuous beam of laser or discrete pulses are sent to the target and reacts with nitrogen source gas. The energy caused by the light coming from laser increases the temperature of the irradiated zone to the several hundred Kelvin in a very short time. During laser ablation, carrier gas is passed through the furnace. The produced nanotubes are carried by this carrier gas and collect on the cold metal trap. The experimental set-up for the laser ablation method is given in Figure 1.7. The laser ablation method involves significant amount of energy and high temperature and produces BNNTs with small size range [22].

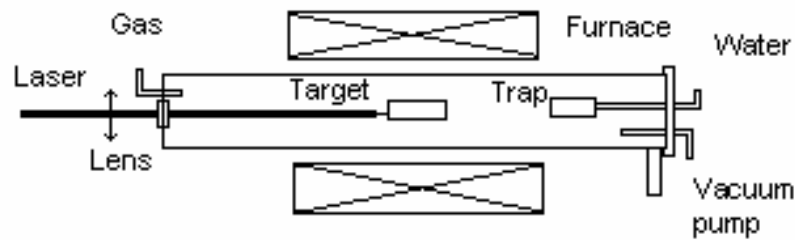


Figure 1.7 Experimental set-up for laser ablation method [22].

1.5.3.3 Ball Milling + Annealing Method

This is a two step method. First, ball milling is carried out at room temperature and then annealing is performed. Boron source powders are loaded into a cell which is made of stainless steel. Inside this cell, there are several steel balls. The milling chamber is filled with nitrogen source gas like N_2 or NH_3 at a pressure of 300 kPa (Figure 1.8). Then, the milling chamber starts to rotate and balls start to collide with the boron source powders for 100 h. By the help of the magnet, milling energy increases. After ball milling process, boron powders are put into a furnace and anneal with nitrogen source gas up to $1000^\circ C$. By this method, large quantities of BNNTs are produced. This method is a practical production with low cost.

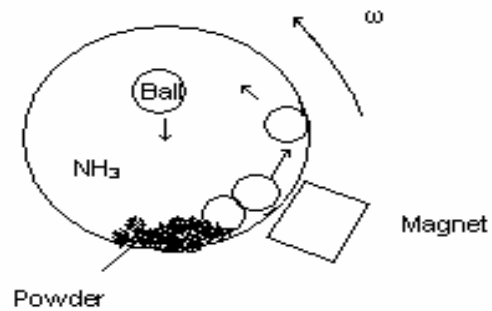


Figure 1.8 Experimental set-up for ball milling+annealing method [22].

1.5.3.4 Chemical Vapor Deposition (CVD) Method

A volatile boron source compound reacts with nitrogen source gas and produces nonvolatile solid product and this product deposits on the substrate (Figure 1.9). CVD method has a low cost and produces pure and long nanotubes.

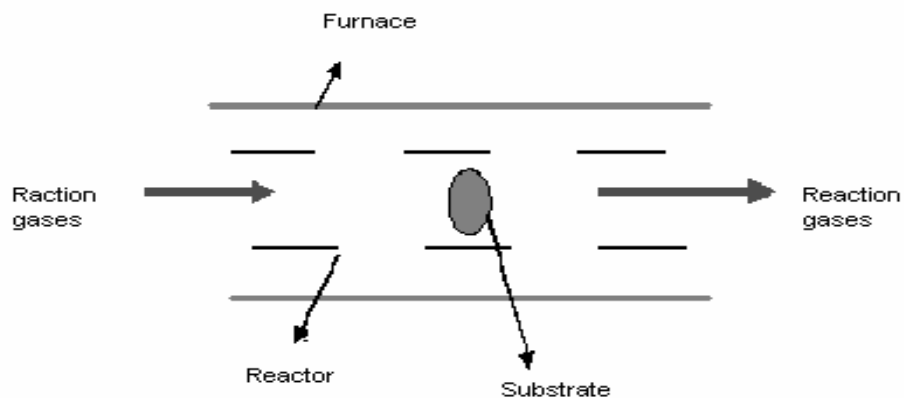


Figure 1.9 Experimental set-up for CVD method.

Researchers have been working on to find new synthesis methods to obtain highest purity, highest yield and new properties of BNNTs for finding new application areas and using them for commercial purposes.

1.6 Literature Survey

Due to outstanding properties of BNNTs, researchers have been working on the production of BNNTs. First studies in production of BNNTs have begun in 1990's and many studies have been doing since 1990's.

BNNTs were first produced by Chopra et al. in 1995 by using arc-discharge method. In this study, while pure hexagonal BN packed tungsten rode was used as anode, pure copper electrode was used as cathode. The inner diameters of produced nanotubes were 1 to 3nm; their outer diameter was 6 to 8 nm and their length was over 200 nm [23].

In 1998, Loiseau et al. synthesized pure BNNTs by applying arc between electrodes made of HfB_2 under nitrogen atmosphere. As a result, high crystalline, open and closed ended BNNTs with one or two layers were produced [24].

In 2003, Narita et al. used arc-melting method to produce BNNTs from boride based powders such as NbB_2 , YB_6 , and YB_6/Ni , under nitrogen and argon atmosphere. Y and Y/Ni metals were chosen because of showing good catalytic properties for the production of carbon nanotubes. Boride based powders were set on a copper mold in an electric-arc furnace at a pressure of 1×10^{-6} Pa. Bundled MWBNNTs containing YB_2 particles having a length of 4-6 μm and a width of 4-10 nm were produced with the help of YB_6 powder. Length and width of MWBNNTs produced from NbB_2 powder were in the range of 80-120 and 12-15 nm, respectively. It was observed

that Nb_2 , YB_6 and YB_6/Ni powders acted as a catalytic material to produce BN nanotubes [25].

Laser ablation is another method that researchers are working on. In 1998, Yu et al. produced BNNTs using this method. They tried to observe the effect of different carrier gases on the production of BNNTs. As a target material hot pressed mixture of BN and nanosized Ni and Co powders was used for the laser ablation at 1200°C using argon, nitrogen and helium as the carrier gas. The ablated materials which were light gray powders were collected on the water cooled copper collector. It was observed that when helium and argon were used as the carrier gas, one layered BNNTs were formed. On the other hand, two layered BNNTs were obtained when nitrogen gas was used. Diameters of the nanotubes were in the range of 1.5 to 8 nm [26].

Zhou et al. also worked on laser ablation process and investigated the effect of catalysts on the growth of BNNTs. Ni and Co powder catalysts were used with pure BN powder and Ar gas was the carrier gas. The ablation process took place at 1200°C and water cooled collector was used to collect the product. SWBNNTs were produced at a diameter range of 1.5 to 4.5 nm with these catalysts. The length of the nanotubes is longer than the one produced without catalyst. No metal particles were observed inside the nanotubes [27].

In 2000, long ropes of BNNTs were produced by a continuous laser heating by Laude et al. Firstly, the reaction chamber was evacuated and then, it was filled by nitrogen gas and CO_2 laser beam was focused on a surface of hexagonal boron nitride. Production of well crystalline BNNTs with three or four layers was observed [28].

Lee et al. synthesized SWBNNTs using laser ablation method. CO₂ laser beam was sent to a rotating BN target under a flow of nitrogen atmosphere. The produced SWBNNTs were long and well crystallized bundles made of about ten tubes and they have zigzag configuration [29].

High energy ball milling method was first developed by Chen et al. in 1999 for the production of BNNTs. Elemental boron powder was the boron source and ammonia was used as the reacting gas. Ball milling process took 150 h and the initial pressure was 300kPa. After ball milling process, annealing was performed. During the first 36h of ball milling process, pressure decreased to 190kPa and then increased to a stable value of 315kPa. The pressure reduction was due to the absorption of ammonia onto the boron particle surfaces created by ball impacts. On the other hand, dissociation of ammonia and formation of BN caused an increase in the pressure. It was also observed that annealing time affected the size of the BNNTs. In other words, an increase in the annealing time caused an increase in the diameter of the produced nanotubes [30].

Chen et al. produced BNNTs using the hexagonal BN powder in ball milling process in an ammonia atmosphere and then annealing was done in nitrogen atmosphere up to 1400°C. The effect of annealing temperature on the production of BNNTs was investigated. BNNTs had an outer diameter and inner diameter of 11 nm and 3 nm were produced at 1200°C, respectively. Above 1200°C, disordered BN nanostructures were obtained such as bamboo like tubes having a diameter range of 120 nm to 280 nm were produced. As a result, both cylindrical and bamboo-like BNNTs with diameters from 20 to 150 nm were produced [31].

Bae et al. worked on ball milling method. Boron nitride nanotubes were synthesized on the alumina substrate deposited with iron through a reaction of the ball-milled boron and hexagonal BN powder mixture with ammonia.

They investigated the effect of reaction temperature on the MWBNNTs in the range of 1000-1200°C. Diameters of the synthesized nanotubes varied from 40nm to 100nm and their lengths varied from 10 μm to 20 μm. At the temperatures less than 1100°C, bamboo- like nanotubes were produced. However, at a temperature higher than 1100°C, cylindrical BNNTs were produced. The crystallinity of the products also increased with an increase in temperature [32].

In 2006, Fengqiu et al. used the ball milled boron powders to produce BNNTs with pure hexagonal BN phase under an ammonia flow at a temperature of 1200°C. The produced BNNTs had closed tips. The diameters of nanotubes changed from 40 nm to 120 nm and the lengths of the nanotubes were higher than 10 μm [33].

CVD method is another method for the production of BNNTs. The first group that worked on the CVD method was Lourie et al. in 2000. The volatile compound was chosen as borazine ($B_3N_3H_6$). Si covered Co, Ni, NiB_2 and NiB catalysts were used to produce BNNTs. It was observed that among the catalysts, nickel boride catalysts were the best catalyst. BNNTs having bulbous tips with length of ~5 μm were produced [34].

Ma et al. produced BNNTs without metal catalyst by CVD method. Melamine diborate ($C_3N_6H_6 \cdot 2H_3BO_3$) was annealed under N_2 atmosphere. As a result, B-N-O powder precursor having a formula of $B_4N_3O_2H$ was produced. The produced BNNTs had 12 concentric layers with inner and outer diameters of 5.2 nm and 13.1 nm, respectively and the nanotubes had bulbous tips [35].

In 1991, Tang et al. produced BNNTs by heating boron and iron oxide powder mixture in flowing ammonia gas. It was observed that reaction temperature and weight ratio of B/Fe_2O_3 powder mixture played an

important role in structure of the BNNTs. The increase in the temperature and Fe_2O_3 concentration caused an increase in the bamboo like BNNTs [36].

Tang et al. synthesized nanotubes by heating a mixture of boron and alumina supported nickel boride catalyst under nitrogen or ammonia atmosphere at the temperature range of 1100°C - 1300°C . As a result, BNNTs having 5-30 nm diameters and several micrometers length were produced. Tang et al. also tried to synthesize BNNTs at temperature higher than 1300°C and it was observed that BNNTs with structural defects were produced and when the temperature was higher than 1500°C , no BNNTs formation was observed [37].

Tang et al. also produced BNNTs with a large diameter distribution from several nm to 70 nm in an ammonia flow with a mixture of boron and magnesium oxide with a molar ratio of 1:1. Mg was evaporated from the final product, so pure BNNTs were produced [38].

Cai et al. (2005) synthesized BNNTs by the reaction of boron powder, iron oxide and ammonium chloride. As a result of the reaction of B with Fe_2O_3 , B_2O_2 was formed. At the same time, NH_4Cl decomposed and formed NH_3 which was nitrogen source for the formation of BNNTs. Thus, the productions of BNNTs were obtained from the reaction of B_2O_2 with NH_3 [39].

In 2007, Yu et al. worked on the ball milling and annealing process to find out the influence of nitriding gases on the growth of BNNTs. Annealing was performed under different gases. Amorphous boron powder was used as a boron source. MWBNNTs with diameters less than 10 nm were produced as a result of annealing in NH_3 without using metal catalyst. Annealing under N_2 or $\text{N}_2\text{-H}_2$ mixture gases, thin cylindrical tubes and thick bamboo

nanotubes with diameter up to 120 nm were produced. As a result, they observed that use of different annealing gases changed the diameter and the appearance of the products [40].

In 2002, Tang et al. produced multi-walled and highly crystalline BNNTs that have diameter of about 10-30 nm. Boron, silica and iron oxide were supported on alumina and then reacted with ammonia gas. Due to the reaction between boron and oxides (SiO_2 and Fe_2O_3), boron oxide gases (B_2O_2 or B_2O_3) were produced. Then, BN formed with the reaction of these oxide gases with ammonia. Beside BNNTs, Si nanowires were also observed due to the Si content in reactants. No BNNTs formation was observed with low amount of catalyst. When excess amount of catalyst was used, BNNTs were obtained at higher temperature. It was concluded that oxide atmosphere (SiO_2 and Fe_2O_3) plays an important role in the production of BNNTs [41].

Fu et al. synthesized BNNTs from the reaction of nitrogen with ammonia gas over nanoscale Fe-B particles at 1100°C . In this method the product was deposited on the liquid catalyst droplet. It was observed that the boron concentration in the Fe-B mixture affected the morphology of the products. Low boron concentration in the Fe-B mixture brought about the formation of BNNTs. On the other hand, high boron concentration in the Fe-B mixture brought about the formation of BN nanowires. The produced bamboos like BNNTs had diameter of 20nm and lengths up to microns and contained some iron particles [42].

In 2005, Rosas et al. tried to synthesize BNNTs based on mechanical alloying technique. The main advantage of this mechanical alloying is no annealing required to produce nanotubes. Boron powder and nitrogen gas were mixed in mechanical alloying device using steel balls at room temperature. As a result, multiwalled BNNTs were produced [43].

1.7 Objective of the Study

BNNTs were produced using different synthesis methods. In most of the literature studied, effect of synthesis methods on the structure of BNNTs has been investigated. Also, there is no study which was based on the chemical analysis of the gaseous products and reactants. Only boron nitride nanotube formation reaction was suggested [37]. But there is no experimental evidence of formation of gaseous products. In other words, in none of the published studies, qualitative or quantitative chemical analysis of the reactor effluent was reported.

As described in the literature survey section, the influence of the reaction temperature and boron to iron oxide weight ratio and characterization of the product were not studied in details. There is not any published information in the literature related to boron nitride nanotubes' surface area, pore size distribution, and pore type. Basing on these factors, the objectives of this study were determined as follows:

- To set up experimental system for synthesis of BNNTs,
- To synthesize BNNTs by the reaction of ammonia gas with the powder mixture of boron and iron oxide,
- To determine gaseous products qualitatively,
- To investigate the influence of reaction temperature and boron to iron oxide weight ratio on the structure of BNNTs,
- To characterize the products using XRD, FTIR, XPS, EDX and SEM,

- To get information about surface area, pore size distribution, average pore size, and pore volume of synthesized boron nitride nanotubes.

CHAPTER 2

EXPERIMENTAL

In this study, it was aimed to synthesize boron nitride nanotubes from the reaction of ammonia gas with the mixture of boron and iron oxide. Experimental studies conducted in this work can be summarized in two groups. The first group is synthesis of boron nitride nanotubes (BNNTs). BNNTs were synthesized at different boron to iron oxide weight ratios within the temperature range of 900°C to 1400°C. The total number of experiments performed in the synthesis of BNNTs is 14. The second group of experiments is related to the characterization studies of BNNTs. Physical and structural properties of the synthesized materials were determined by X-ray diffraction (XRD), Energy Dispersive X-ray Spectroscopy (EDX), nitrogen sorption, X-ray Photoelectron Spectroscopy (XPS), Fourier Transform Infrared Spectroscopy (FTIR), and Scanning Electron Microscopy (SEM).

2.1 Experimental Set-up

Boron nitride nanotubes were synthesized from the reaction of ammonia gas with a powder mixture composed of boron and iron oxide. Ammonia gas and the powder mixture were nitrogen and boron sources, respectively. Two different boron compounds (B) and iron oxide (Fe_2O_3) with a purity of 99% were purchased from Merck-Sigma-Aldrich and Sigma-Aldrich, respectively. Figure 2.1 shows a sketch of the experimental set-up for synthesis of BNNTs. Anhydrous ammonia gas with high purity (Oksan) was the reactant gas. In addition to this gas, argon gas with high purity (Oksan)

was used for purging the system before and after each run. Regulators' pressures for argon and ammonia gases were set at 2 bars. The flow rates of gases were adjusted using rotameters (Cole-Parmer). They were calibrated for these gases. The calibration curves are given in Appendix A. A three way valve was located after the ammonia rotameter. By the help of this valve, the volumetric flow rate of ammonia gas was adjusted before entering the furnace. The gases flowed through ¼ in stainless steel tubing. They were mixed and then entered a horizontal tubular furnace (Protherm PTF 16/50/450) having an inner diameter of 50 mm and a length of 1 m. The temperature of the furnace was measured with a Type B thermocouple, which was placed at the center of the furnace and connected to a temperature controller. Alumina boat in which boron nitride nanotube formation reaction takes place was placed at the middle of the alumina tube. Alumina probe having an outer diameter of 2.5 mm was put inside of the alumina tube. This alumina tube was connected to a mass spectrometer (Hiden HPR20) for on-line qualitative chemical analysis of the effluent stream. Two soap bubble meters were used to measure total inlet and outlet volumetric flow rates of gases.

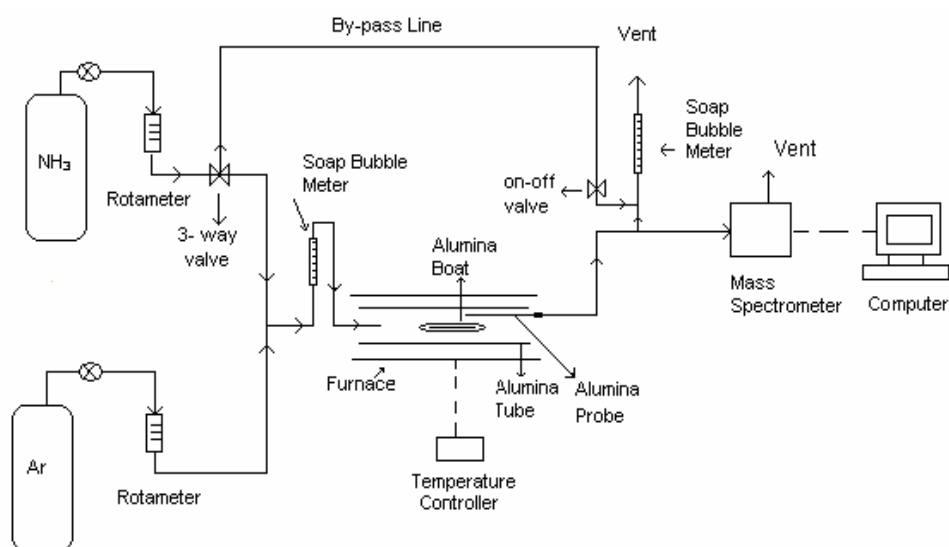


Figure 2.1 Schematic drawing of experimental system.

2.2 Experimental Procedure

The experiments were carried out at an atmospheric pressure of 1 atm, and at different reaction temperatures (900 °C-1400 °C), with a constant inlet gas temperature of 25 °C and a constant total volumetric flow rate of 50 cm³/min.

Desired amounts of boron and iron oxide were mixed and homogenized in an agate pestle. This mixture was placed in an alumina boat and this boat was put into the center of the tubular furnace. While the furnace was heated to the desired temperature with a heating rate of 8 °C/min, the argon gas was passed through the alumina tube of furnace to remove oxygen from the system with a flow rate of 50 cm³/min. When the furnace temperature approached to the reaction temperature, by the help of the three way valve, the ammonia gas passed through the bypass line to adjust the volumetric flow rate of the reactant gas to the desired value. After the temperature of the furnace had reached to the desired temperature, the argon gas was shut off and the ammonia gas was fed into the system with a volumetric flow rate of 50 cm³/min. The qualitative chemical analysis of the reactor effluent stream was carried out using the mass spectrometer. MASsoft program was used for the data analysis. After 135 minutes, the ammonia gas was shut off and the argon gas was fed to the system with a volumetric flow rate of 50 cm³/min. The furnace cooled down to the room temperature with a cooling rate of 5 °C/min. Afterwards, the alumina boat was taken from the furnace and the material was taken into the sample folder.

The operating conditions of experiments conducted in this work are tabulated in Table 2.1.

Table 2.1 Experimental conditions for synthesis of BNNTs.

Reaction Temperature (°C)	B to Fe₂O₃ Weight Ratio	Boron Source
1400	15	Merck
1300	15	Merck
1200	15	Merck
1100	15	Merck
1000	15	Merck
900	15	Merck
1300	20	Merck
1300	5	Merck
1300	1	Merck
1300	0.5	Merck
1300	20	Sigma-Aldrich
1200	20	Sigma-Aldrich
1100	20	Sigma-Aldrich

2.3 Hiden HPR20 Gas Analysis System

Hiden HPR20 Gas Analysis System (Figure 2.2) was used in this study to perform qualitative chemical analysis of the reactor effluent stream.

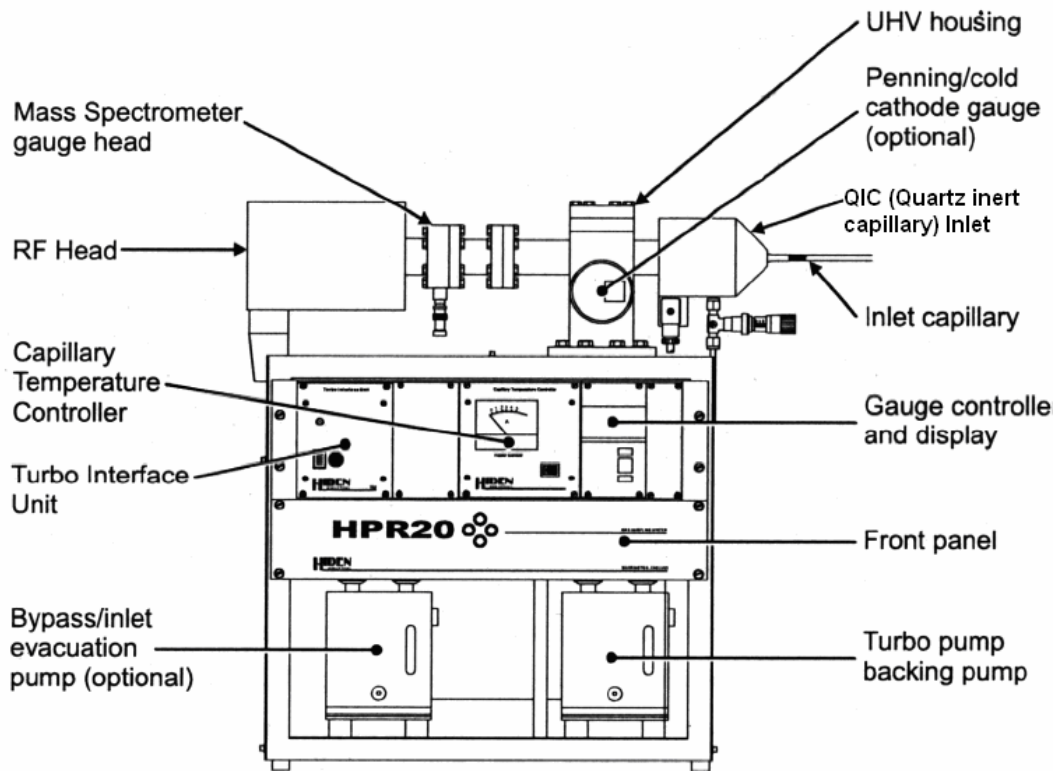


Figure 2.2 HPR 20 Gas analysis system [45].

The HPR20 Gas Analysis System consists of ultra high vacuum (UHV) housing, vacuum pumping system, QIC (Quartz Inert Capillary) capillary inlet; quadruple mass spectrometer, computer and MASsoft PC software.

Ultra high vacuum pumping system contains; turbo pump, turbo pump backing pump, turbo controller interface unit and the venting device. High vacuum system provides the molecules entering the ion source be in gas phase and prevents the gases not to condense on the surfaces of the spectrometer. Besides preventing the condensation, high vacuum system protects the metal surfaces of the ion source, mass analyzer and the detector from the corrosion caused from the sample gases.

QIC fast sampling capillary inlet provides a method of sampling reactive or condensable gases. As it was mentioned above, high vacuum is needed and for this purpose, the QIC inlet employs two pressure reduction stages to reduce sample pressure to a proper low level for operation of the mass spectrometer. In the first stage, bypass pumping line helps the sample gas to be drawn down the silica capillary to provide the sample gas exits the capillary at low pressure and high velocity. In the second stage, the sample gas which has high velocity and at low pressure impinges on a platinum orifice and this provides the pressure reduction directly into the mass spectrometer ion source [45].

In HPR20 Gas analysis system, quadrupole mass filter was used as a mass analyzer. The schematic representation of a quadrupole mass analyzer is shown in Figure 2.3. It consists of four cylindrical stainless steel rods having 15 cm length and 6 mm diameter. These rods are the electrodes of the filter. Opposite rods are connected electrically. One pair is attached to the positive side and the other pair to the negative terminal. Radio frequency is applied to the rods and rods are connected to the direct current generators. With the right DC voltage and radio frequency, ions travel along the each rod. Detector converts the beam of ions into an electric signal that can be processed, and stored in a computer and displayed [46]. For the detection of the ions which pass through the quadrupole analyzer, “Faraday Cup” and “Secondary Electron Multiplier (SEM)” detectors are used in HPR20 Gas Analysis System. Faraday cup is an ion collector that is connected after the ion analyzer. It is ideal for the ion partial pressures between 10^{-10} - 10^{-4} torr and SEM is used where the ion partial pressures between 10^{-13} - 10^{-6} torr. SEM gives high sensitivity with low background noise.

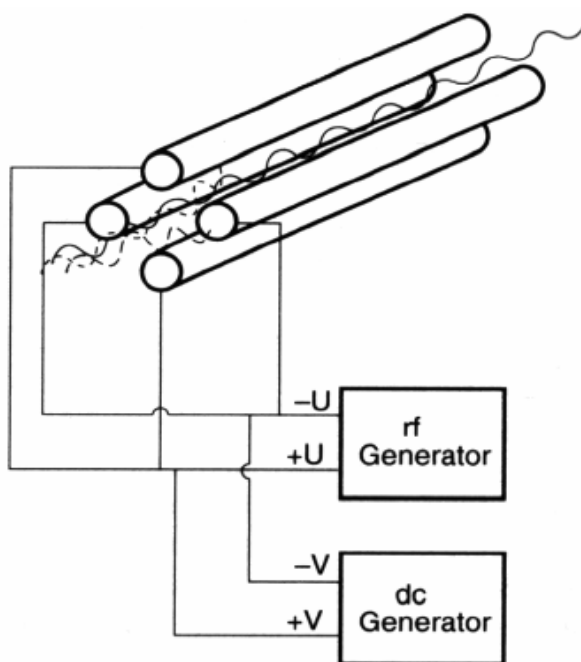


Figure 2.3 Schematic representation of a quadrupole mass analyzer [47].

2.3.1 Working Principles of Mass Spectrometer

Mass spectrometry is widely used for providing information about the qualitative and quantitative composition of both organic and inorganic compounds. The components of a mass spectrometer are given in Figure 2.4. The inlet system introduces small amount of sample into the mass spectrometer. The ion source converts sample into ions by bombardment with highly energetic electrons. Generally, the inlet system and ion source are a single component. If not, the output stream of commonly positive ions is accelerated into the mass analyzer. In mass analyzer, dispersion is based upon the mass to charge ratios of the ions.

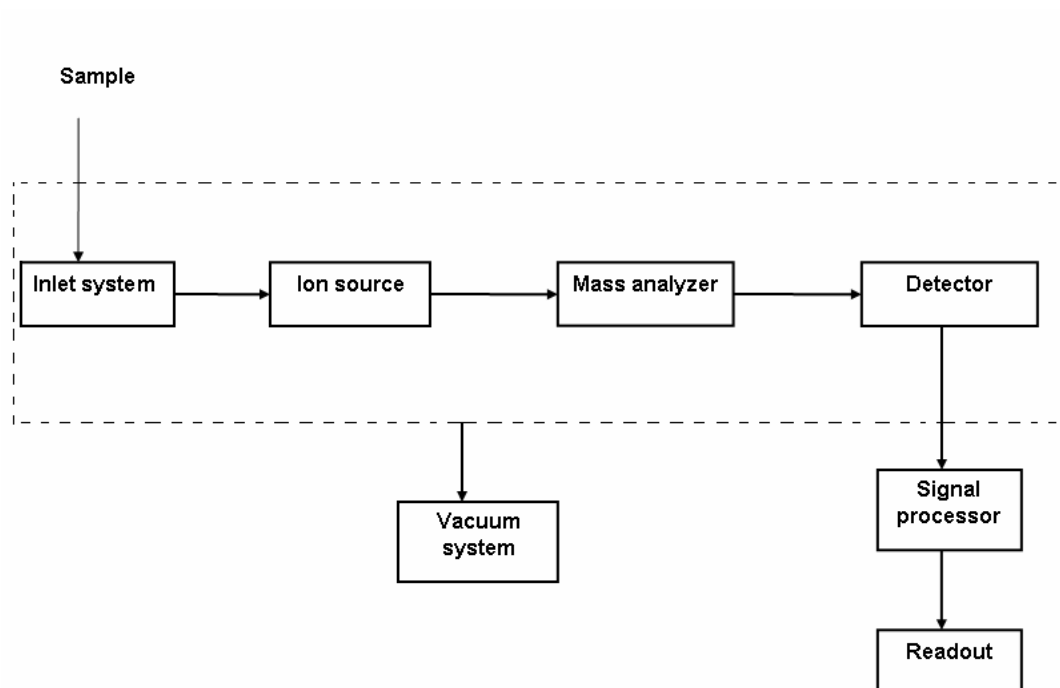


Figure 2.4 Components of a mass spectrometer [46].

2.4 Characterization Techniques

Product characterization is an important part of this study. It helps to find out the crystallography, structure and surface area of the synthesized material.

The synthesized boron nitride nanotubes were characterized by X-ray Diffraction (XRD), X-ray Photoelectron Spectroscopy (XPS), Energy Dispersive X-ray Spectroscopy (EDX), Scanning Electron Microscopy (SEM), Fourier Transform Infrared Spectroscopy (FTIR), and nitrogen physisorption in order to determine the crystalline structures, B/N atomic ratios in the surface and in the bulk, chemical compositions, the shapes and dimensions of nanotubes, surface areas, pore size distributions and nitrogen adsorption/desorption isotherms of the synthesized material.

2.4.1 X-ray Diffraction (XRD) Technique

X-ray Diffraction is a technique which is used for characterization and understanding the morphology of the crystalline material.

Bragg equation (Eq. 2.1) was developed by Sir W. H. Bragg and Sir W. L. Bragg to explain the reflection of X-rays from a crystal (Figure 2.5) According to Bragg equation, X-rays reflect from a crystal if the angle of incidence satisfies the Bragg equation. In Bragg equation, d represents the interplanar distance of the crystal, λ is the wavelength of the incident X-ray beam, θ is the diffraction angle and n is the integer.

$$n\lambda = 2d \sin \theta \quad (2.1)$$

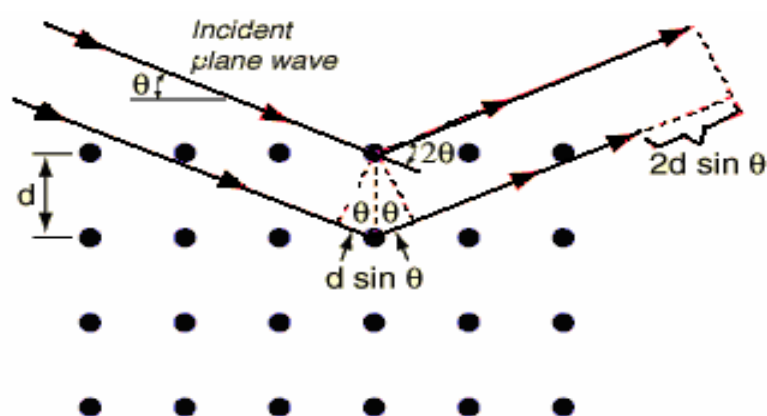


Figure 2.5 Reflection of X-rays from two planes of atoms in a solid [48].

In this work, X-ray diffraction for the identification of the crystallography of the products was performed by 'Philips PW 1729 X-ray Diffractometer' with nickel filtered $\text{CuK}\alpha$ radiation having a characteristic wavelength of 1.5406 \AA . During the operation, the voltage and current were 30 kV and 24 mA ,

respectively. The diffraction patterns were taken in the Bragg angle range of 20° - 80° with a goniometric velocity of 0.01° . Beside this instrument, 100 kV Philips twin tube X-ray Diffractometer (PW/1050) was also used. During the operation, the voltage and current were 30 kV and 40 mA, respectively. The diffraction patterns were taken in the Bragg angle range of 20° - 90° with a goniometric velocity of 0.02° . Philips PW 1729 and PW 1050 X-ray Diffractometers were used for the products synthesized at different temperatures with boron purchased from Merck and the products synthesized with different B to Fe_2O_3 weight ratios and boron purchased from Merck and Sigma-Aldrich Philips, respectively.

2.4.2 X-ray Photoelectron Spectroscopy (XPS)

XPS is a surface characterization technique which gives information about elements that exist in the material and elemental compositions of the species. For every element, there is a characteristic binding energy associated with each core atomic orbital and each element give rise to a characteristic set of peaks in the XPS spectrum at kinetic energies determined by the photon energy and the respective binding energies.

In this study, XPS measurements were performed with the SPECS instrument. The Mg K_{α} radiation was employed as an X-ray source.

2.4.3 Scanning Electron Microscopy (SEM)

The SEM was used to understand the morphology of the products. In SEM, electrons are used to produce images.

Gold, gold/palladium alloy, platinum, tungsten or graphite is used as an ultra thin coating of electrically-conducting material to prevent the accumulation of static electric charge on the specimen during electron

irradiation. Another reason for coating is to improve contrast and resolution of the SEM images [49, 50].

In this study, 'FEI Quata 400F Scanning Electron Microscopy' was used. Au-Pd alloy coating was performed for the preparation of the samples.

2.4.4 Energy Dispersive X-ray Spectroscopy (EDX)

Energy dispersive X-ray Spectroscopy (EDX or EDS) identifies elemental compositions of materials imaged in a Scanning Electron Microscope. EDX analysis system works as an integrated part of a SEM and not operates without it. By the help of the EDX spectrum, quantitative and qualitative analyses of the elements present in the sample are performed [51, 52].

In this study, EDX spectrometer that is connected to the 'FEI Quata 400F Scanning Electron Microscopy' was used for the chemical characterization of the synthesized material.

2.4.5 Fourier Transform Infrared Spectroscopy (FTIR)

Fourier Transform Infrared Spectroscopy is used to identify the chemical bonds or functional groups in the synthesized material.

The infrared spectrum is divided into three regions: the far infrared (400 cm^{-1} - 0 cm^{-1}), the mid infrared (4000 cm^{-1} - 400 cm^{-1}) and the near infrared (14285 cm^{-1} - 4000 cm^{-1}). Mid infrared is generally used for the characterization of the samples. Infrared spectrum represents the molecular absorption and transmission. Two different molecular structures do not produce the same infrared spectrum. So it is like a fingerprint of the sample to provide the identification of the unknown material [53].

In this study, Bruker Vertex 70 instrument was used to identify the chemicals in the synthesized material. The sample was prepared by the synthesized material to KBr approximate weight ratio of 1/100.

2.4.6 Single Point Surface Area Measurement

Single point surface area measurements were performed using Quantachrome Monosorb Direct Surface Analyzer. This instrument gives rapid and accurate single point B.E.T (Brunauer-Emmett-Teller) surface area measurement under the flow of N₂-He gas mixture at the specified relative pressure of 0.30.

Before surface area measurement, the synthesized material was dried in an oven at a temperature of 140°C overnight and degassing was additionally performed at 140°C for 30 minutes to remove the moisture from the material under the flow of N₂-He gas mixture. Measurements were carried out at liquid nitrogen temperature of 77 K under the flow of gas mixture composed of 30% nitrogen and 70% helium. Before starting the measurements, the calibration of the analyzer was performed with 1 cm³ of air at atmospheric pressure. The surface area value corresponding to nitrogen content of 1 cm³ of air is 2.84 m². After degassing process had been completed, the sample was taken from the degassing unit and transferred to the analysis station for the measurement. To remove air entering to the system while placing the sample to the analysis station, the indicator of the analyzer was set to zero. The liquid nitrogen tank rose, and the sample cell was introduced to the liquid nitrogen and then adsorption of the nitrogen to the sample began. After adsorption was completed, the liquid nitrogen tank lowered down and the desorption of nitrogen from the sample started at equilibrium pressure/saturation vapor pressure of the nitrogen (P/P₀) ratio of 0.30. The surface area value was read from the instrument panel and then this value was divided by the weight of the

sample (approximately 0.02 grams) to obtain the surface area of the material per gram.

2.4.7 Nitrogen Adsorption/Desorption Isotherms

Nitrogen adsorption and desorption isotherms are used to get information about the surface area, pore size distribution, average pore size and pore volume of the synthesized material. For this purpose, Quantachrome Autosorb 1C Physical Adsorption instrument was used. The instrument consists of two parts; degassing unit and sample analyzing unit. Degassing unit is used to get rid of the moisture from the samples' pores. Before surface area measurement, the synthesized materials were dried in an oven at a temperature of 110°C overnight and degassing was additionally performed at 300°C for 4 hours. Approximately a sample weight of 0.03 grams was used for all analyses. The analysis was carried out at a relative pressure range of 5×10^{-2} to 0.99 at liquid nitrogen temperature.

CHAPTER 3

RESULTS AND DISCUSSION

Boron nitride nanotubes were synthesized from the reaction of ammonia gas with boron and iron oxide powder mixture at different temperatures and boron to iron oxide weight ratios. Physical, chemical and structural properties of synthesized materials were determined by using XRD, XPS, FTIR, SEM, EDX, nitrogen adsorption/desorption experiments. In the following subheadings, qualitative chemical analysis and characterization results are given and discussed.

3.1 Qualitative Chemical Analysis of Reactor Effluent Stream

On-line qualitative chemical analysis of the reactor outlet stream was performed by using a mass spectrometer. The spectrum of the reactor effluent was continuously taken. From the analysis of the spectrum, the chemical composition of the outlet stream was evaluated. A typical mass spectrum of the reactor effluent stream taken during the experiment is given in Figure 3.1. From the mass spectrum analysis result, in addition to the ammonia gas, the formation of hydrogen, water and nitrogen was detected in the effluent of the reactor. As shown in Figure 3.1, typical peaks of hydrogen were observed at masses 1 and 2. Peaks at masses 2, 17, 18, and 20 belong to water. On the other hand, peaks at masses 14, 17, and 18 correspond to the reactant gas, which is ammonia. In addition to the peaks corresponding to hydrogen, water and ammonia, some peaks were also observed at masses 14, 28, and 29. These peaks show the presence of

nitrogen in the reactor effluent stream. The cracking patterns of the species are consistent with the standard cracking patterns given in the literature. The reference cracking pattern data obtained from the database of Hiden analytical HPR20 Mass Spectrometer's software 'MASsoft' is presented in Appendix B.

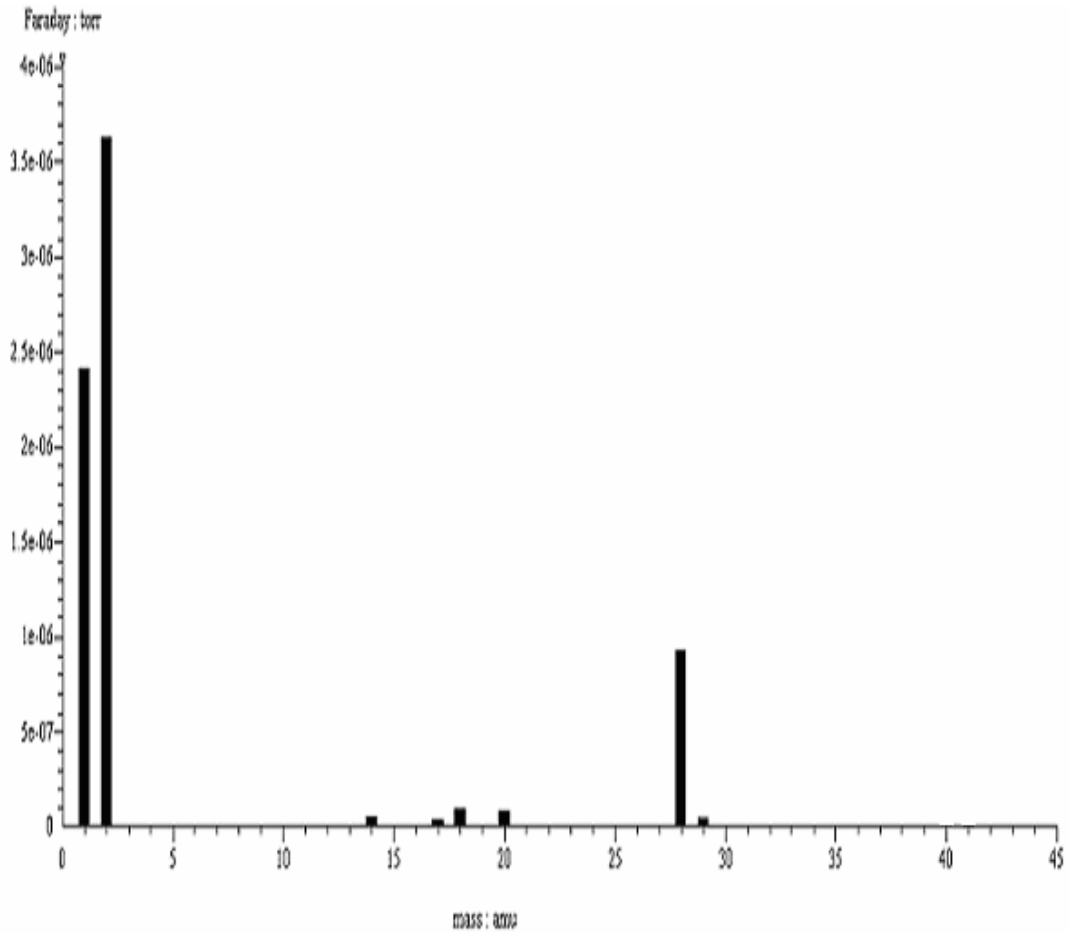
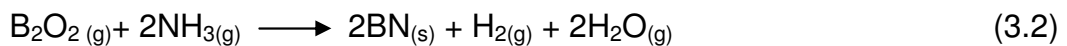


Figure 3.1 Typical mass spectrum of the reactor effluent at 1400°C with B to Fe₂O₃ weight ratio of 15.

In the work of Tang et al. (2001), for the formation of boron nitride the following probable reactions were proposed:



According to the above reactions, diboron dioxide (B_2O_2), hydrogen and water must be in the reactor effluent stream. In this work, formation of hydrogen and water was detected. However B_2O_2 formation was not observed in the reactor effluent stream. This may be due to consumption of B_2O_2 in the reaction in a very short time. In other words, B_2O_2 reacts with ammonia as soon as it forms. In this study, in addition to hydrogen and water gases, formation of nitrogen was also observed. With the analysis of mass spectrum obtained in this work, evidence of formation of nitrogen was revealed for the first time and formation of water and hydrogen was experimentally justified.

3.2 Characterization of Synthesized Boron Nitride Nanotubes

3.2.1 X-ray Diffraction Results

X-ray diffraction patterns of boron nitride deposits produced at different temperatures and at different B to Fe_2O_3 ratios were taken in order to obtain information about the crystal structure. XRD patterns of the materials synthesized with boron to iron oxide weight ratio of 15 at a temperature range of $900^\circ C$ to $1300^\circ C$ are shown in Figure 3.2. In Figure 3.2.b, peaks observed at Bragg angle values of 25.9° , 41.9° , 43.7° , 50.0° , 55.1° , 76.2° correspond to hexagonal boron nitride and the peaks at Bragg angle values of 25.9° , 42.5° , 45.8° , 55.36° , 75.74° belong to rhombohedral boron nitride. In addition to hexagonal and rhombohedral boron nitride phases, cubic iron was observed at Bragg angle values of around 44.65° and 65.2° . d spacing values of cubic iron, hexagonal and rhombohedral boron nitrides, and synthesized materials are listed in Appendix C. Another XRD pattern of the material synthesized at $1200^\circ C$ is shown in Figure 3.2.c. Again this X-ray diffraction pattern showed the presence of cubic iron, hexagonal and

rhombohedral boron nitrides. However, additional unassigned peak at Bragg angle value of 28.03 was observed.

These results showed that hexagonal and rhombohedral boron nitrides and cubic iron were the phases formed in the temperature range of 900°C to 1300°C.

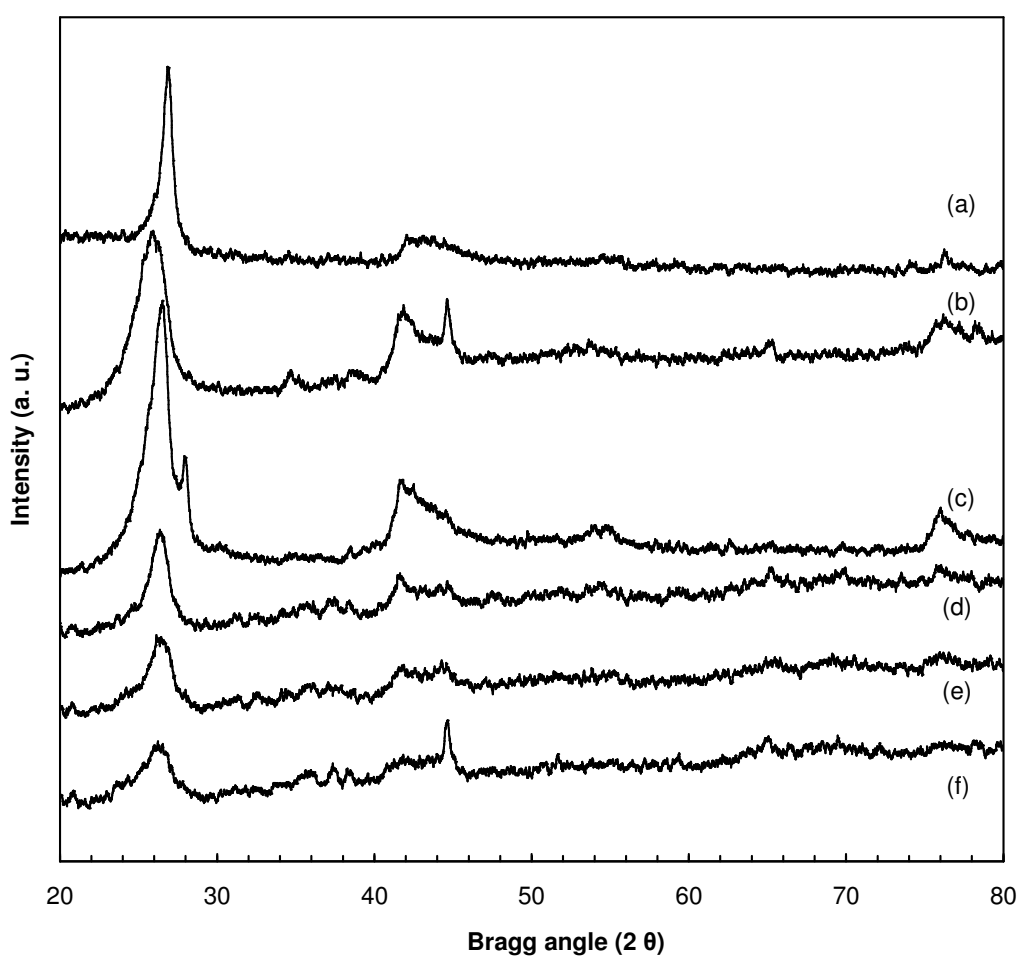


Figure 3.2 XRD patterns of products synthesized with B to Fe₂O₃ weight ratio of 15 and Merck boron source at different reaction temperatures: (a) 1400°C, (b) 1300°C, (c) 1200°C, (d) 1100°C, (e) 1000°C, and (f) 900°C.

Figure 3.3 shows XRD patterns of the material synthesized at 1300°C with boron to iron oxide weight ratio range of 5 to 20. These XRD patterns are similar to XRD patterns shown in Figure 3.2. Again these XRD patterns

revealed the presence of hexagonal and rhombohedral boron nitrides and cubic iron.

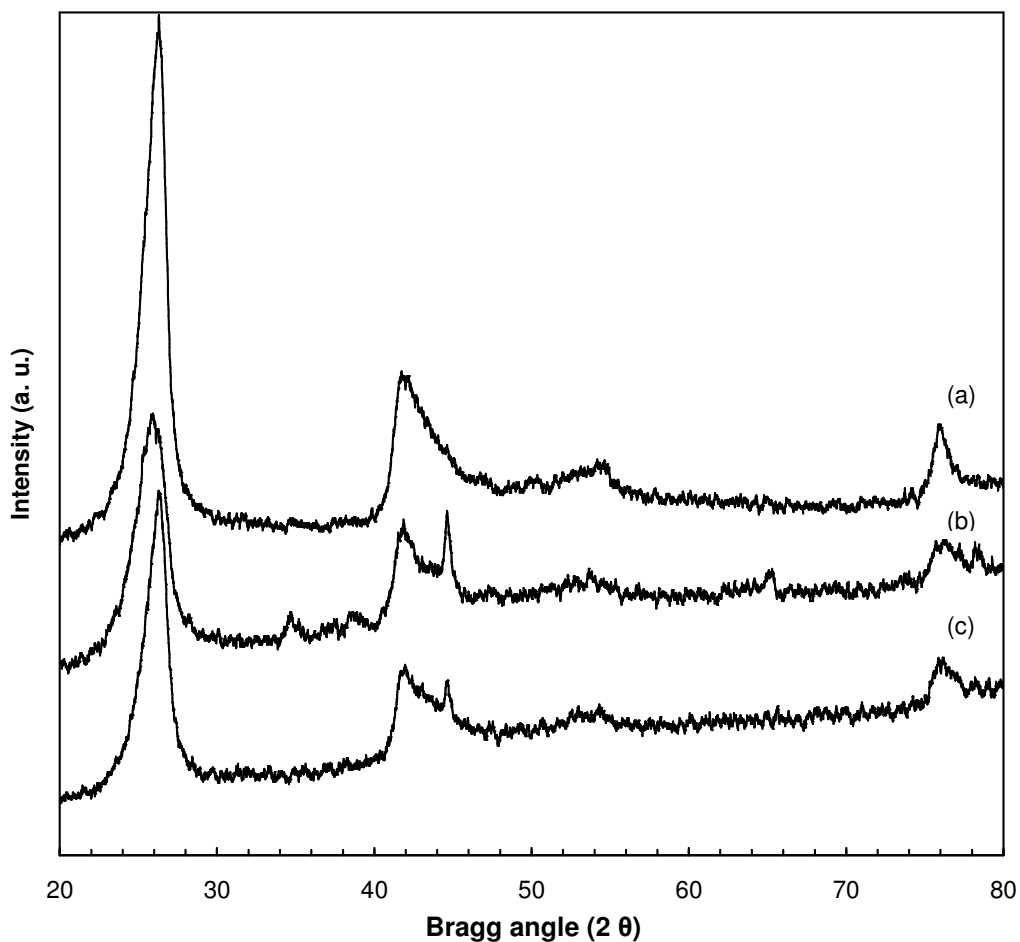


Figure 3.3 XRD patterns of products synthesized at 1300°C, with Merck boron source and B to Fe₂O₃ weight ratios of (a) 20, (b) 15, and (c) 5.

Figure 3.4 shows XRD pattern of the material synthesized at 1300°C with boron to iron oxide weight ratio of 1. In addition to the peaks of cubic iron, hexagonal and rhombohedral boron nitrides, additional peaks at Bragg angle values of 33.3°, 35.66°, 40.83°, 49.38°, 54.36° were observed. These peaks belong to iron oxide. Another XRD pattern of the material synthesized with boron to iron oxide weight ratio of 0.5 at 1300°C is shown

in Figure 3.5. In this figure, peaks observed at Bragg angle values of 23.78°, 33.42°, 35.88°, 39.92°, 49.46°, 54.44°, and 64.3° correspond to iron oxide and the peaks at Bragg angle values of 26.5°, 41.42°, 50.1° belong to hexagonal boron nitride. In addition to hexagonal boron nitride and iron oxide, cubic iron was observed at Bragg angle values of 44.72°, 65.94°, and 82.32°.

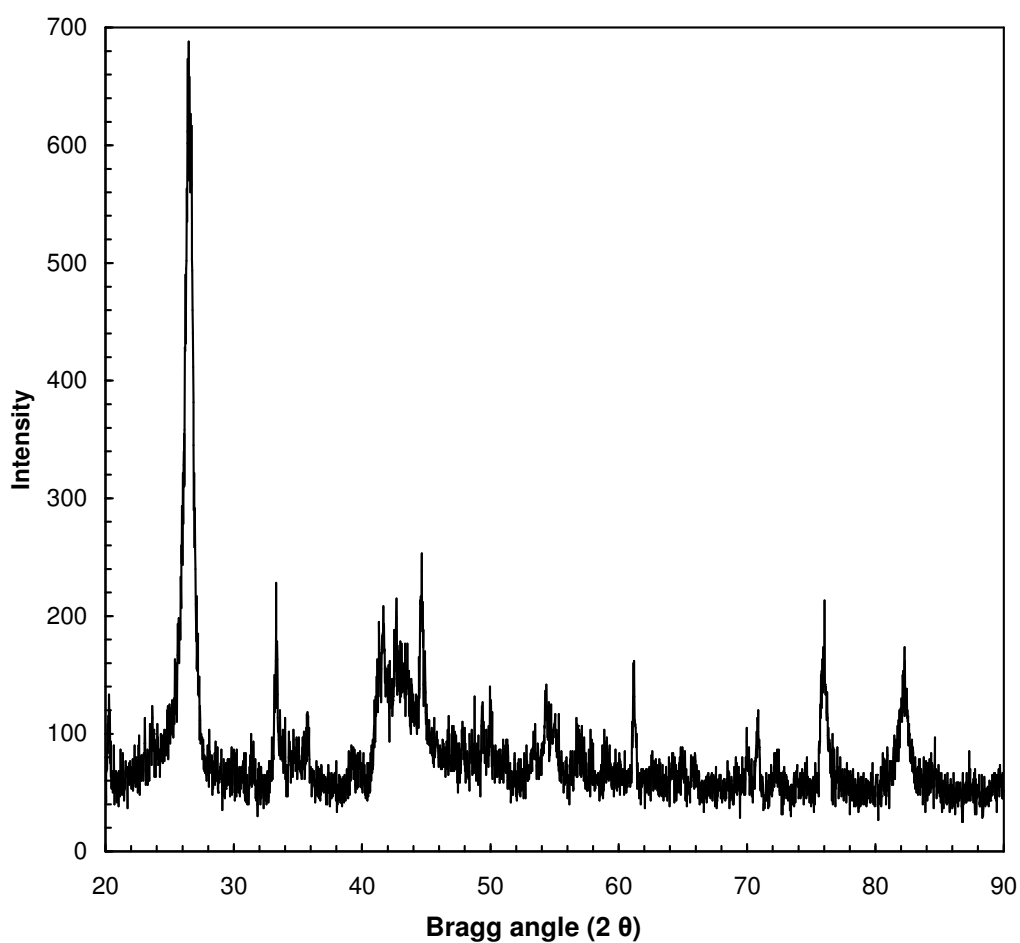


Figure 3.4 XRD pattern of product synthesized at 1300 °C, with Merck boron source and B to Fe₂O₃ weight ratio of 1.

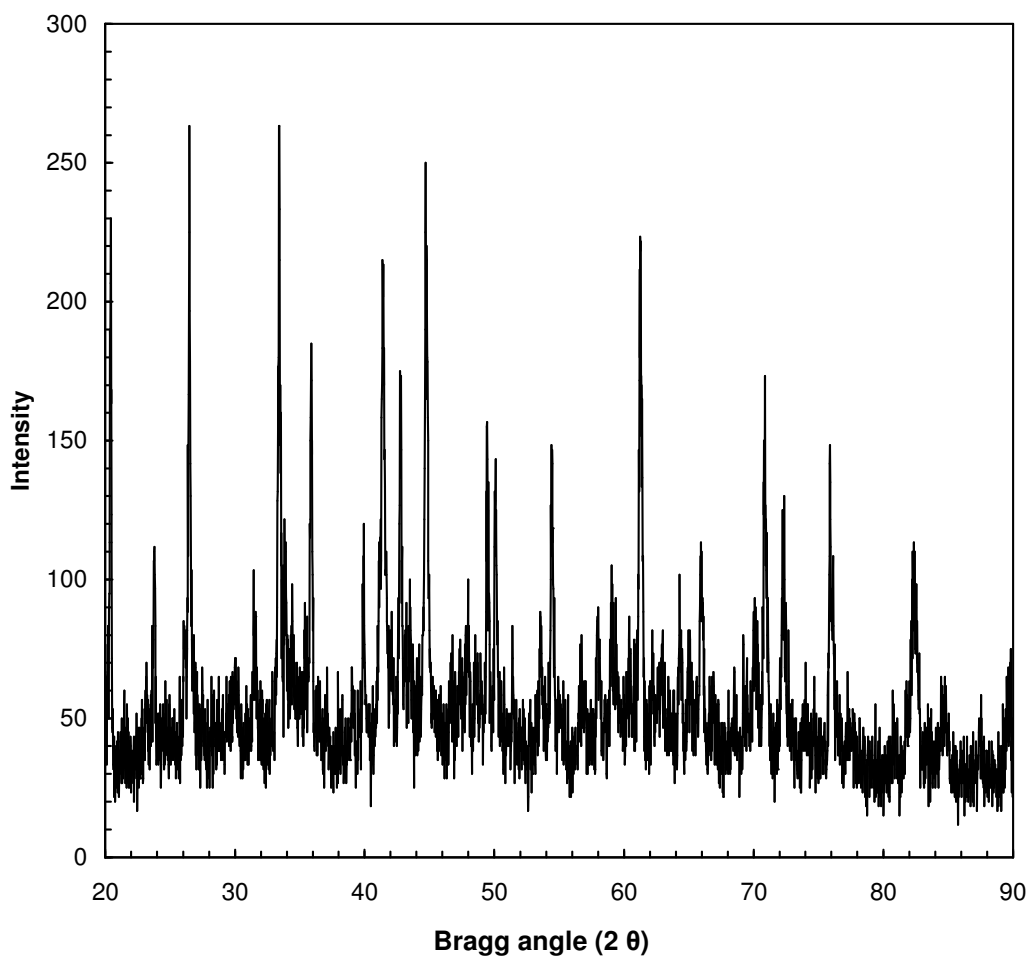


Figure 3.5 XRD pattern of product synthesized at 1300 °C, with Merck boron source and B to Fe₂O₃ weight ratio of 0.5.

Figure 3.6 shows XRD pattern of the material synthesized with boron to iron oxide ratio of 20 and Sigma-Aldrich boron source. Again this XRD pattern showed the presence of hexagonal and rhombohedral boron nitrides, cubic iron. Similar XRD patterns for the materials synthesized with Sigma-Aldrich and Merck boron sources were observed (Figures 3.3.a and 3.6). Both XRD patterns revealed the presence of hexagonal and rhombohedral boron nitride and cubic iron. Using different boron sources did not change the structure of the synthesized material.

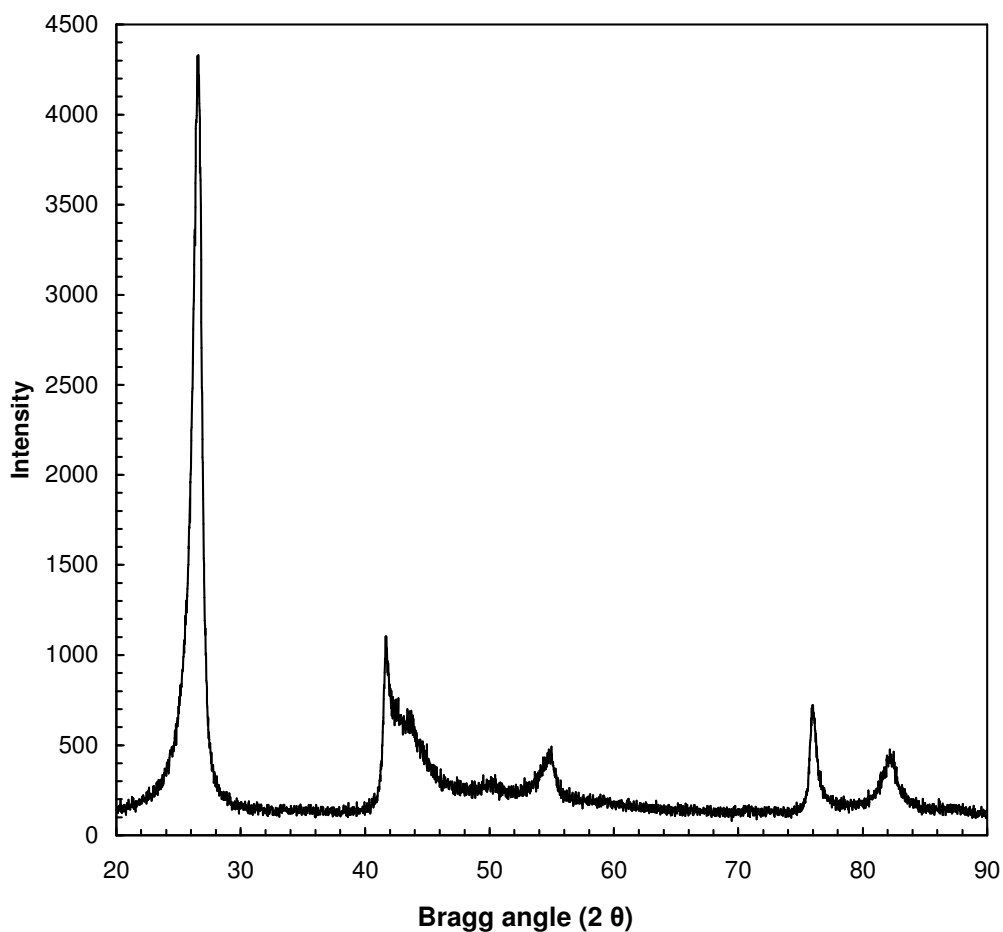


Figure 3.6 XRD pattern of product synthesized at 1300°C, with Sigma-Aldrich boron source and B to Fe₂O₃ weight ratio of 20.

BNNT production was first observed at 900°C and the crystallinity of the product increased with an increase in temperature (Figure 3.2). The color and appearance of the product also changed with temperature. The product was light brown and in particular structure at 900°C and 1000°C. However, at 1100°C, it was brown and in powder form. At 1200°C, it was grey and in particular form, at 1300°C, it was a mixture of grey and white particles and at 1400°C, it was white and in particular form.

BNNT production was observed at all weight ratios. The crystallinity of the product decreased with an increase in the iron oxide amount

(Figures 3.3-3.5). The best crystallinity of the product was obtained with B to Fe_2O_3 weight ratio of 20 and its color was light grey in a particular form. As in temperature case, the color of the product was also affected with boron to iron oxide weight ratio. All products were in particular form. The color of the product became darker with a decrease in boron to iron oxide weight ratio.

Although similar XRD patterns were observed for the synthesized materials with different boron sources, their color and appearance were not the same. The material synthesized with Sigma-Aldrich boron source was in sponge like form and its color was between white and grey.

3.2.2 Fourier Transform Infrared Spectroscopy (FTIR)

The FTIR spectra of the synthesized materials were taken to reveal the information about the chemicals present in the synthesized material.

Figure 3.7 represents FTIR spectra of the material synthesized at different temperatures with boron to iron oxide weight ratio of 15. As shown in this figure, typical infrared peaks of boron nitride were observed at around 1370 cm^{-1} and 810 cm^{-1} . This spectrum is consistent with the standard boron nitride spectrum given in the literature [54]. The peaks at 1370 cm^{-1} and 810 cm^{-1} are assigned to the B-N stretching vibrations and B-N-B bending vibrations, respectively. The broad peak at wavenumbers between 2200 cm^{-1} and 2300 cm^{-1} belongs to boron. FTIR spectrum of boron used in this study is given in Appendix D. In addition to the peaks corresponding to boron nitride and boron, characteristic peak was also observed at 3210 cm^{-1} . The presence of this peak is due to the water absorbed on the sample. There are other peaks at wavenumbers 547 cm^{-1} and 482 cm^{-1} . They are characteristic peaks of iron oxide. Iron oxide's spectrum is given in Appendix D.

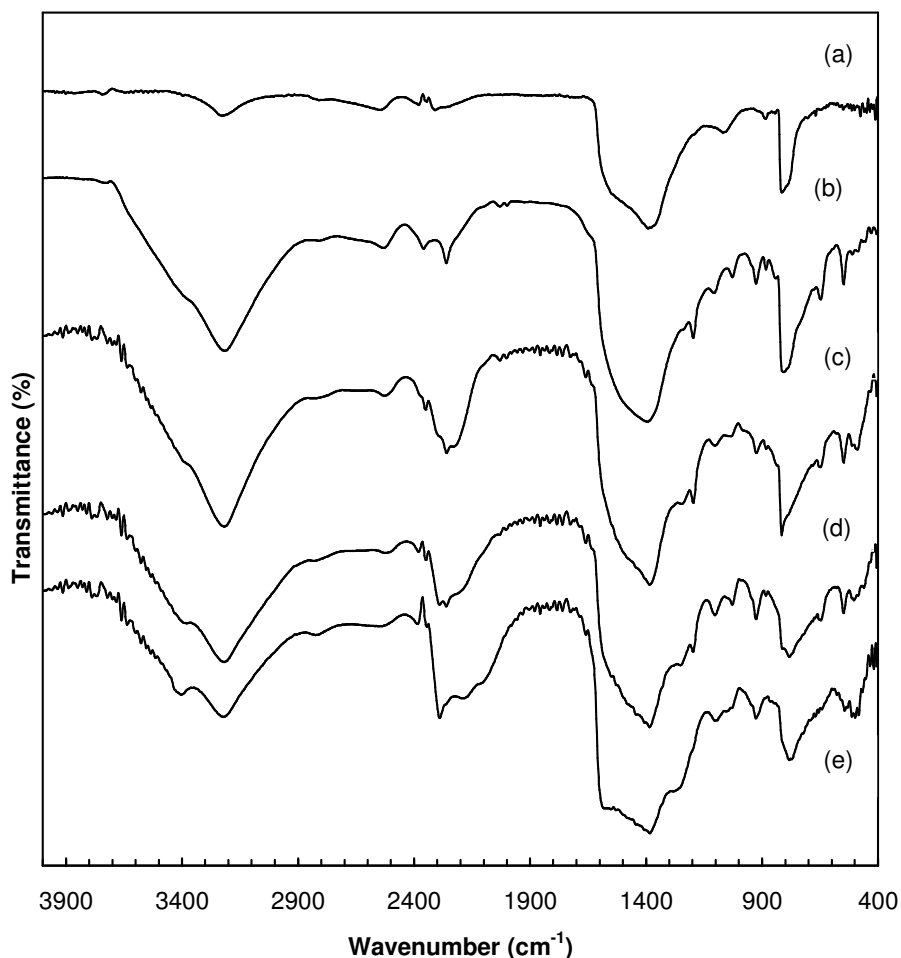


Figure 3.7 FTIR spectra of BNNTs synthesized with B to Fe_2O_3 weight ratio of 15 and boron purchased from Merck at different reaction temperatures: (a) 1300°C, (b) 1200°C, (c) 1100°C, (d) 1000°C, and (e) 900°C.

These results showed that boron nitride was formed at the temperature range of 900°C to 1300°C and in this temperature range, unreacted boron and iron oxide were also observed except at the temperature of 1300°C. The FTIR results are not consistent with the XRD results. Characteristic peaks of boron were not observed in the XRD pattern, because boron source used in the synthesis of BNNT was amorphous. Absence of iron

oxide peaks in the XRD patterns may be due to analyzing different part of the same sample.

Figure 3.8 represents the FTIR spectra of BNNTs synthesized at the temperature of 1300 °C, with Merck boron source and different B to Fe₂O₃ weight ratios. The spectra are similar to the one shown in Figure 3.7. For B to Fe₂O₃ weight ratios except 0.5, the characteristic peaks of B-N stretching vibrations and B-N-B bending vibrations at 1370 cm⁻¹ and 810 cm⁻¹ were observed. The absorbed water peak at 3210 cm⁻¹ was also detected. From Figure 3.8.e, it was observed that boron nitride was not formed at B to Fe₂O₃ weight ratio of 0.5. This result is not consistent with XRD result. This may be due to analyzing different part of the same sample. Amount of boron nitride in the material increased with an increase in boron to iron oxide weight ratio, except B to Fe₂O₃ weight ratio of 5.

FTIR spectrum of the material synthesized at a temperature of 1300°C with B to Fe₂O₃ weight ratio of 20 and Sigma-Aldrich boron source is shown in Figure 3.9. This FTIR spectrum is similar to FTIR spectrum shown in Figure 3.8 (a). This spectrum revealed the presence of boron nitride in the synthesized material.

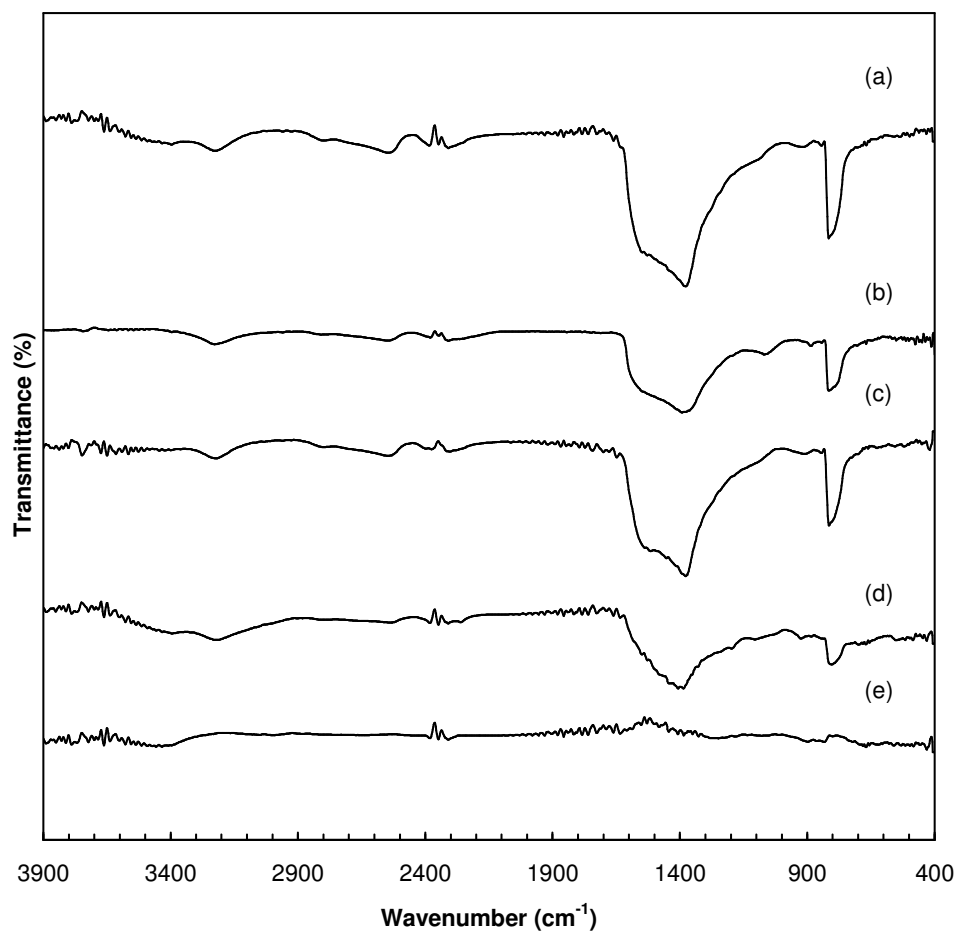


Figure 3.8 FTIR spectra of BNNTs synthesized at 1300°C with Merck boron source and different B to Fe₂O₃ weight ratios: (a) 20, (b) 15, (c) 5, (d) 1, and (e) 0.5.

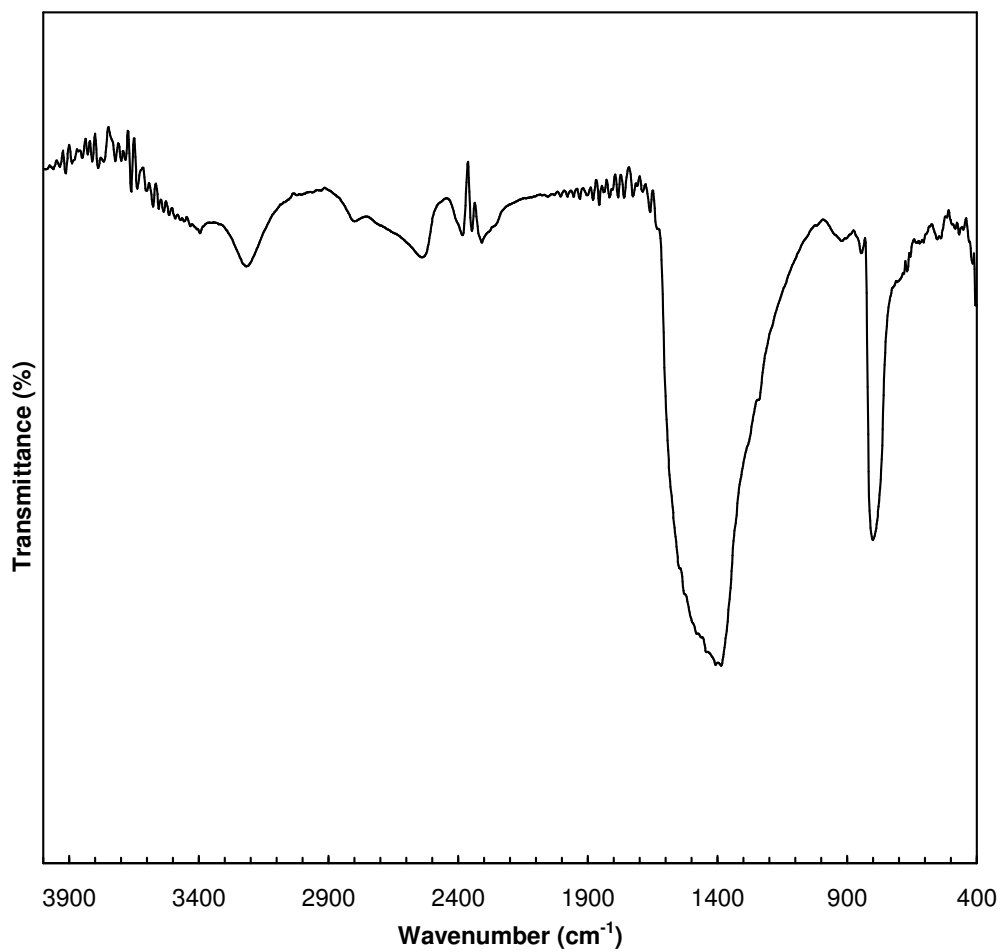


Figure 3.9 FTIR spectrum of BNNTs synthesized at a temperature of 1300 °C with B to Fe_2O_3 weight ratio of 20 and Sigma-Aldrich boron source.

3.2.3 X-ray Photoelectron Spectroscopy (XPS)

A typical XPS spectrum of the product synthesized at 1300°C with a B to Fe₂O₃ weight ratio of 15 is given in Figure 3.10.

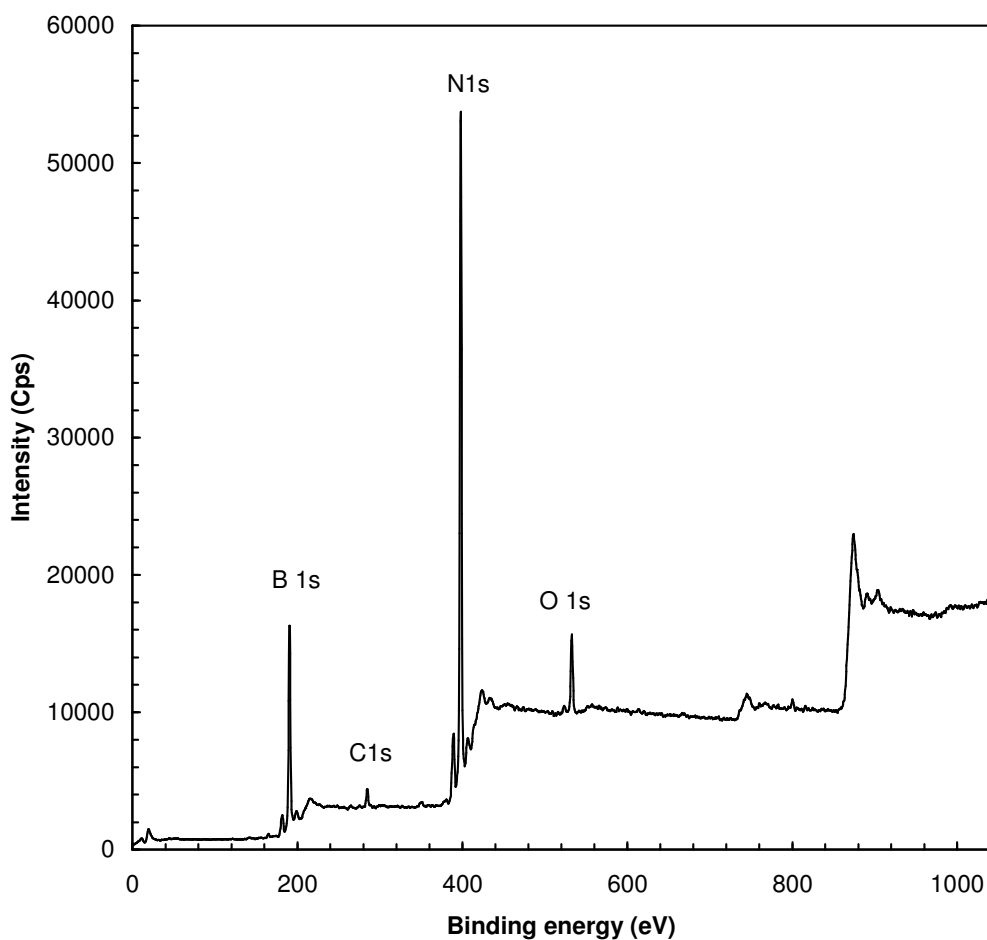


Figure 3.10 XPS spectrum of the product synthesized with a B: Fe₂O₃ weight ratio of 15 at 1300°C.

XPS spectrum showed the existence of B and N elements. Beside B and N elements, oxygen and carbon elements were also present in the spectrum. This is may be due to adsorption of impurities such as oxygen and carbon dioxide on the surface of the sample. Iron element was not observed at surface of the material. The B 1s peak at 190.2 eV and N 1s peak at

398.2 eV represent boron nitride [55]. The peaks observed at 741.4 eV and 873.8 eV correspond to the Auger peaks of oxygen and nitrogen, respectively. The atomic ratio of boron to nitrogen was found to be 0.87 from the peak intensities. This result is close to the chemical stoichiometric relation between boron and nitrogen, which is one. After taking this spectrum, the same sample was bombarded with 4000eV Ar^+ ions for 5 minutes. Similar XPS spectrum was obtained and the atomic ratio of boron to nitrogen remained approximately the same after etching (Figure 3.11). It was observed that the intensities of adsorbed oxygen and carbon increased. This increase was due to the spectrometer used for XPS measurements.

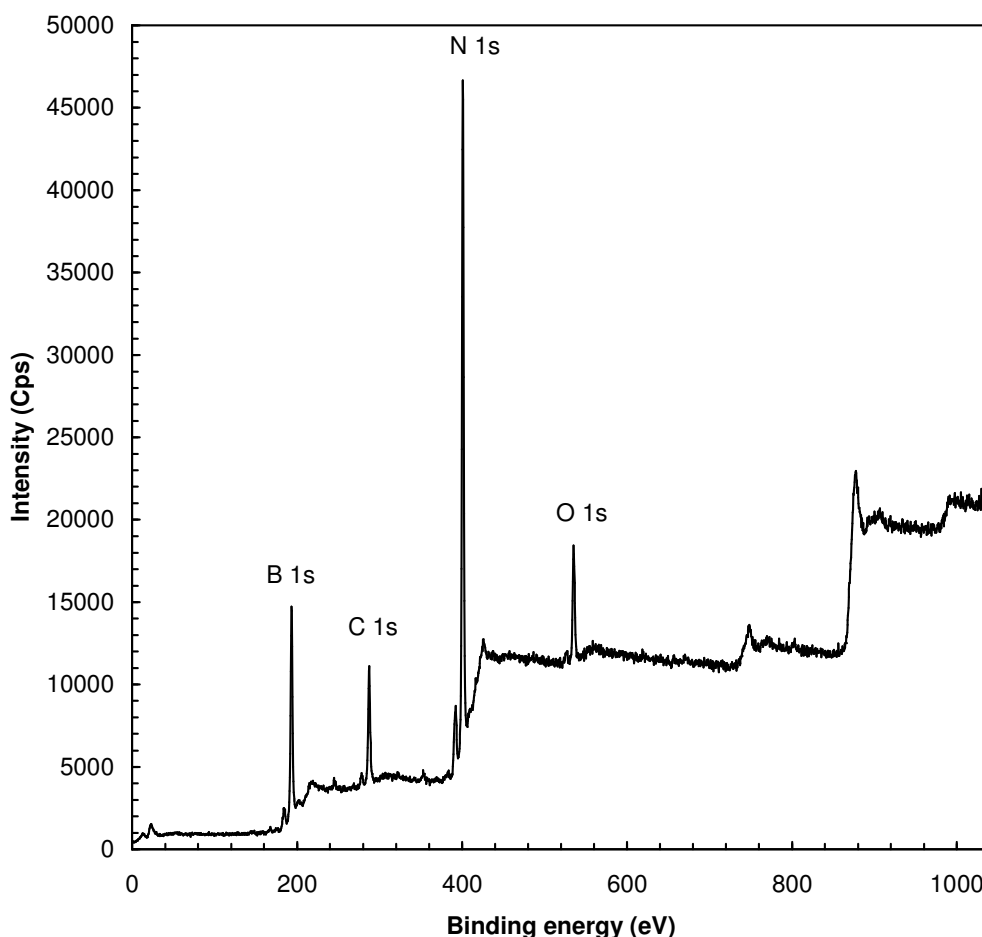


Figure 3.11 XPS spectrum of the product synthesized with a B: Fe_2O_3 weight ratio of 15 at 1300°C after bombarding with Ar^+ ions.

XPS spectra of the materials produced at different temperatures, different B to Fe_2O_3 weight ratios and boron sources are given in Appendix E. B 1s peak with the binding energies from 190.2 eV to 191.4 eV, N 1s peak with the binding energies from 398.2 eV to 399 eV, and O 1s peak with binding energies from 532.6 eV to 533.8 eV were observed. Presence of these peaks in all spectra showed that surfaces of the materials were made of boron, nitrogen and oxygen. This result verified the existence of boron nitride. In addition to these peaks, C 1s peak with the binding energy 285 eV was observed due to the adsorption of CO_2 on the surface of the sample. Iron element was not observed at the surface of the prepared material.

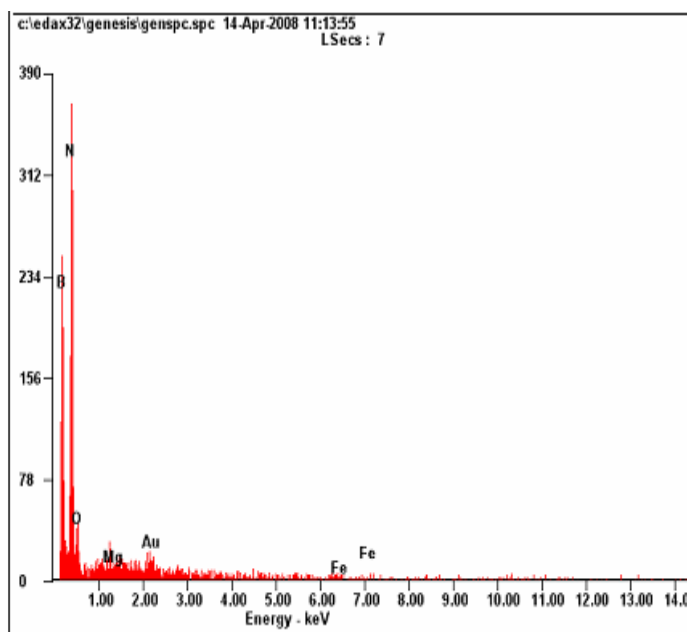
The atomic ratios of boron to nitrogen for different synthesized materials are tabulated in Table 3.1. It is observed that the ratios are close to each other and compatible with the chemical stoichiometric relation between boron and nitrogen except products having weight ratios of 1 and 0.5. In the samples with weight ratio ranges of 1 to 0.5, B to N atomic ratio is greater than one. This may be due to presence of unreacted boron in the synthesized materials.

Table 3.1 B to N atomic ratios of the products synthesized with different B:Fe₂O₃ weight ratios and boron sources at different temperatures.

Reaction temperature (C°)	B:Fe ₂ O ₃ weight ratio	Boron source	B:N atomic ratio
1400	15	Merck	0.84
1300	20	Sigma-Aldrich	1.01
1300	20	Merck	1.08
1300	15	Merck	0.87
1300	5	Merck	1.12
1300	1	Merck	2.61
1300	0.5	Merck	4
1200	15	Merck	1.13
1200	20	Sigma-Aldrich	1.22
1100	15	Merck	1.05
1000	15	Merck	0.95
900	15	Merck	0.91

3.2.4 Energy Dispersive X-ray Spectroscopy (EDX)

EDX spectrum of the product synthesized with boron to iron oxide weight ratio of 20 and Sigma-Aldrich boron source at 1300°C is shown in Figure 3.12. This figure illustrates the general analysis of the material surface. There are only boron, nitrogen, gold, magnesium, iron, and oxygen atoms. Since O₂ was adsorbed on the surface of the material, oxygen atom was observed in the spectrum. Au atom came from the coating of the material to supply conductivity. EDX spectra for other synthesized materials are given in Appendix F. Similar atoms were observed. In some spectra, carbon atom was also observed. This carbon atom came from CO₂ impurity adsorbed on the surface of the material.



<i>Element</i>	<i>Wt %</i>	<i>At %</i>
<i>B K</i>	40.54	47.58
<i>N K</i>	52.41	47.48
<i>O K</i>	05.95	04.72
<i>MgK</i>	00.23	00.12
<i>AuM</i>	00.64	00.04
<i>FeK</i>	00.23	00.05

Figure 3.12 EDX spectrum of BNNTs produced at 1300°C with B to Fe₂O₃ weight ratio of 20.

Atomic ratios of boron to nitrogen for the synthesized materials and comparison of these ratios with atomic ratios obtained from XPS are given in Table 3.2. It was observed that B to N atomic ratios were close to each other and close to one. These results agree well with the chemical stoichiometric ratio of B to N.

Table 3.2 Atomic ratios of boron to nitrogen for the materials synthesized with B to Fe₂O₃ weight ratio of 15 and boron purchased from Merck at different temperatures.

Reaction Temperature (°C)	B to N atomic ratio from EDX	B to N atomic ratio from XPS
1300	1.30	0.87
1200	1.22	1.13
900	1.09	0.91

Table 3.3 gives the atomic ratios of boron to nitrogen for the materials synthesized at 1300°C with different B to Fe₂O₃ weight ratios. The B to N atomic ratios in each weight ratio are close to one and these results agree well with the chemical stoichiometric ratio of B to N, except the sample having B to Fe₂O₃ weight ratio of 0.5. This may be due to analyzing different part of the same sample and presence of unreacted boron in the synthesized materials.

Table 3.3 Boron to nitrogen atomic ratios of BNNTs synthesized at 1300°C at different B to Fe₂O₃ weight ratios and boron purchased from Merck.

B to Fe₂O₃ weight ratio	B to N atomic ratio from EDX
0.5	5.90
1	1.03
5	1.06
15	1.30
20	1.00

The atomic ratio of boron to nitrogen for the materials synthesized at 1200°C with B to Fe₂O₃ weight ratio of 20 and boron purchased from Sigma-Aldrich is 1.12. This result agrees well with the chemical stoichiometric ratio of B to N and the result was closed to the atomic ratio obtained from XPS which was 1.20.

3.2.5 Scanning Electron Microscopy (SEM)

SEM images of BNNTs synthesized with B to Fe_2O_3 weight ratio of 15 and boron purchased from Merck at different reaction temperatures are given in Figure 3.13. Arrows on all images show some of boron nitride nanotubes. From the SEM images, it was observed that in all temperatures, at B to Fe_2O_3 weight ratio of 15, entangled BNNTs having closed tips were produced. The diameters of the synthesized nanotubes were nearly close to each other. The average diameters of the BNNTs seen in the images varied from 64 nm to 136 nm and the diameters of the BNNTs produced at different temperatures were closed to each other.

SEM images of BNNTs synthesized at 1300°C with boron purchased from Merck and B to Fe_2O_3 weight ratios are given in Figure 3.14. From the images, it was observed that BNNTs were produced in all weight ratios except 0.5. The nanotubes were entangled and bulbous and they had close tips. Their diameters varied from 66 nm to 136 nm and agreed with the diameters of BNNTs given in literature [32, 33, 38, and 40].

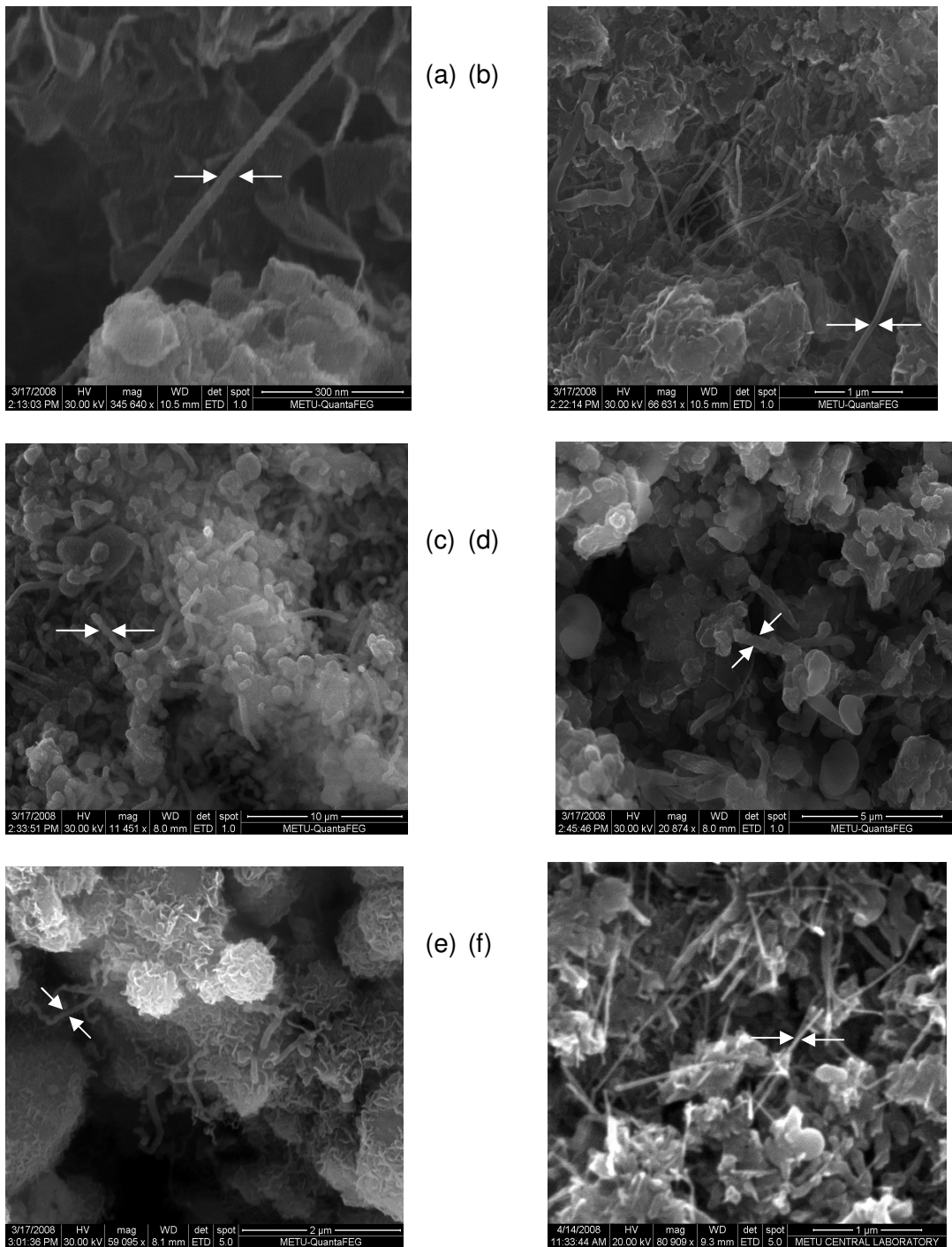


Figure 3.13 SEM images of BNNTs synthesized at B to Fe₂O₃ weight ratios of 15 with boron purchased from Merck at different reaction temperatures: (a) 1300 °C , (b) 1300 °C, (c) 1200 °C, (d) 1100 °C, (e) 1000 °C, and (f) 900 °C.

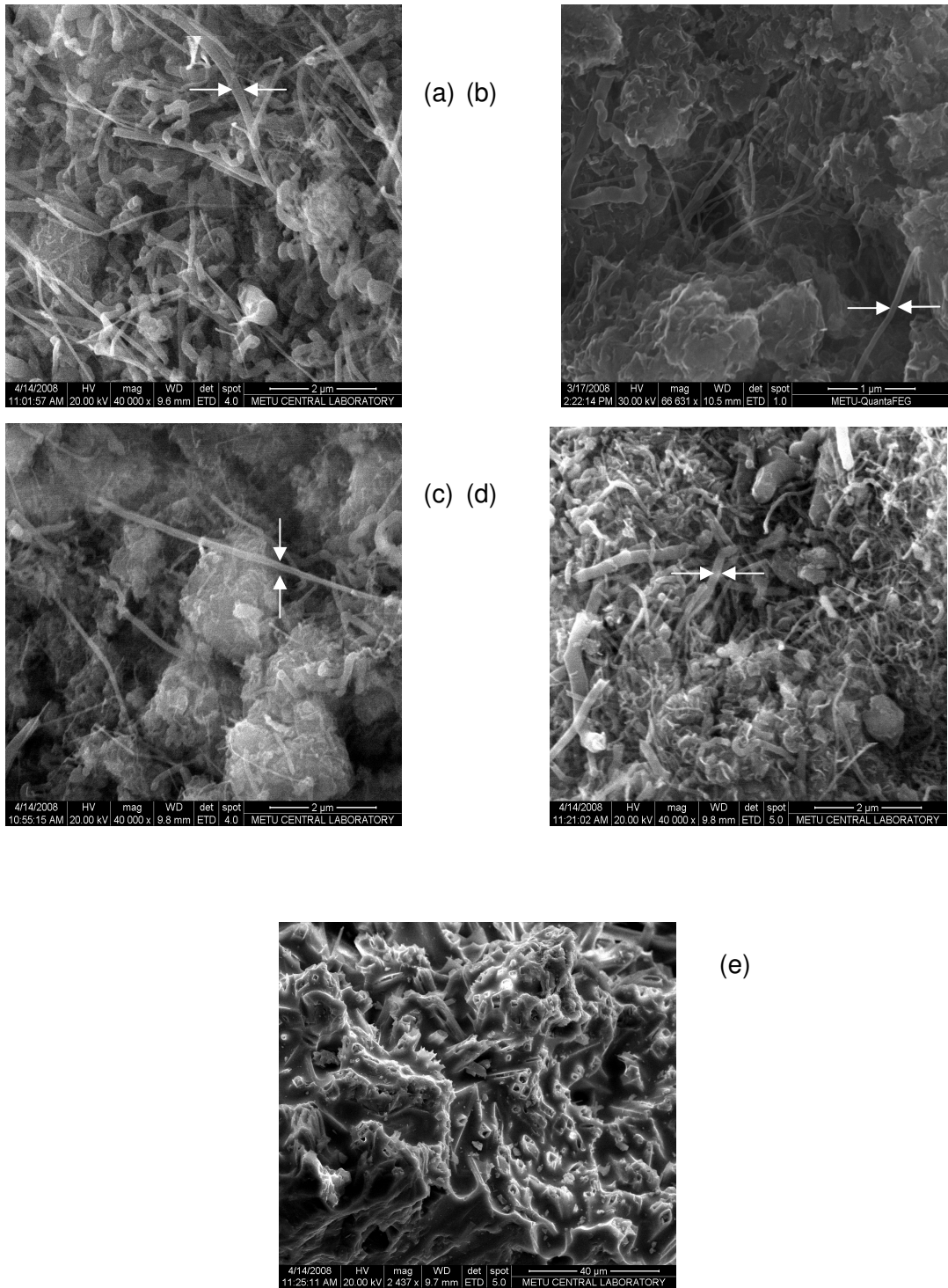


Figure 3.14 SEM images of BNNTs synthesized at 1300 °C with boron purchased from Merck and B to Fe₂O₃ weight ratios of (a) 20 (b) 15, (c) 5, (d) 1, and (e) 0.5.

In Figure 3.15 SEM images of BNNTs synthesized at 1200°C with boron purchased from Sigma-Aldrich with B to Fe₂O₃ weight ratio of 20. From the images, it was observed that entangled, bamboo-like BNNTs having closed tips were produced. Their diameters varied from 50 nm to 180 nm.

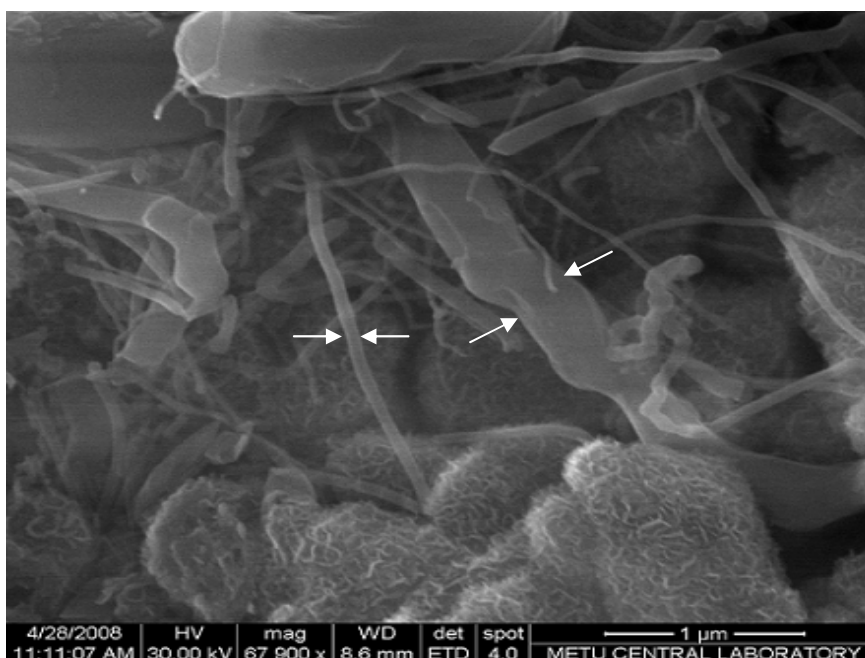
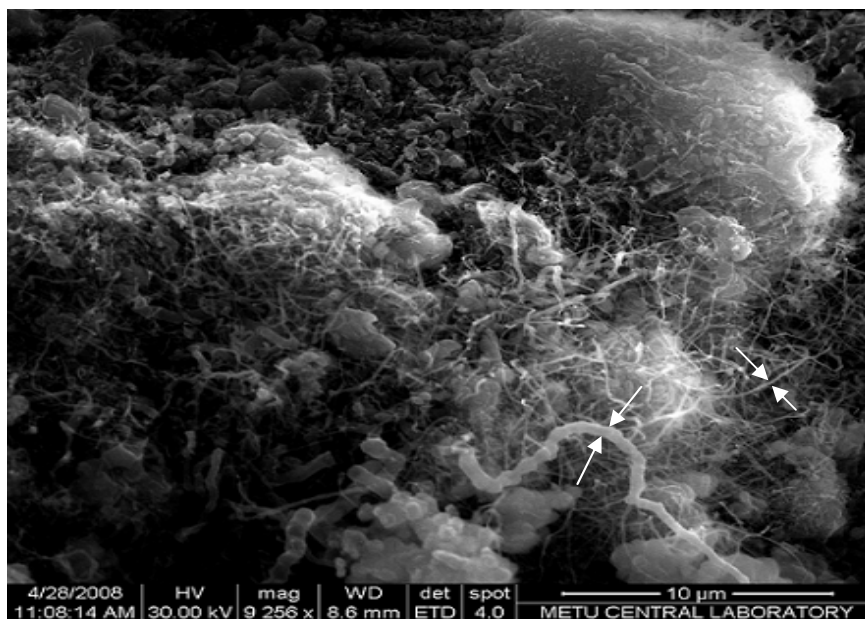


Figure 3.15 SEM images of BNNTs synthesized at 1200°C with boron purchased from Sigma-Aldrich and B to Fe₂O₃ weight ratio of 20.

3.2.6 Single Point Surface Area Measurement

Surface area measurements are most widely used for the characterization of porous materials. Single point surface areas of the products synthesized at different temperatures with B to Fe₂O₃ weight ratio of 15 are tabulated in Table 3.4. It was observed that the increase in reaction temperature caused an increase in the surface areas of the products.

Table 3.4 Single point surface areas of products synthesized at different temperatures with B to Fe₂O₃ weight ratio of 15.

Reaction Temperature (°C)	Surface Area (m ² /g)
1300	26.20
1200	18.80
1100	17.60
1000	8.80

3.2.7 Nitrogen Adsorption/Desorption Isotherms

The adsorption/desorption isotherms of the BNNTs synthesized at B to Fe₂O₃ weight ratio of 15 at 1300°C and 1200°C are given in Figure 3.16 and the adsorption/desorption isotherms of the BNNTs synthesized at B to Fe₂O₃ weight ratio of 5 at 1300°C is given in Figure 3.17.

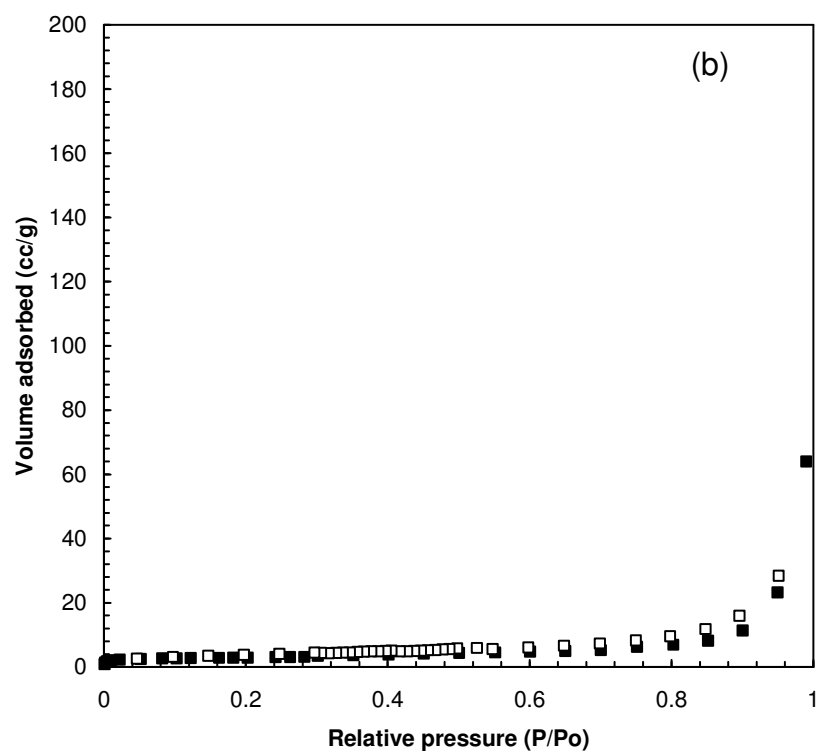
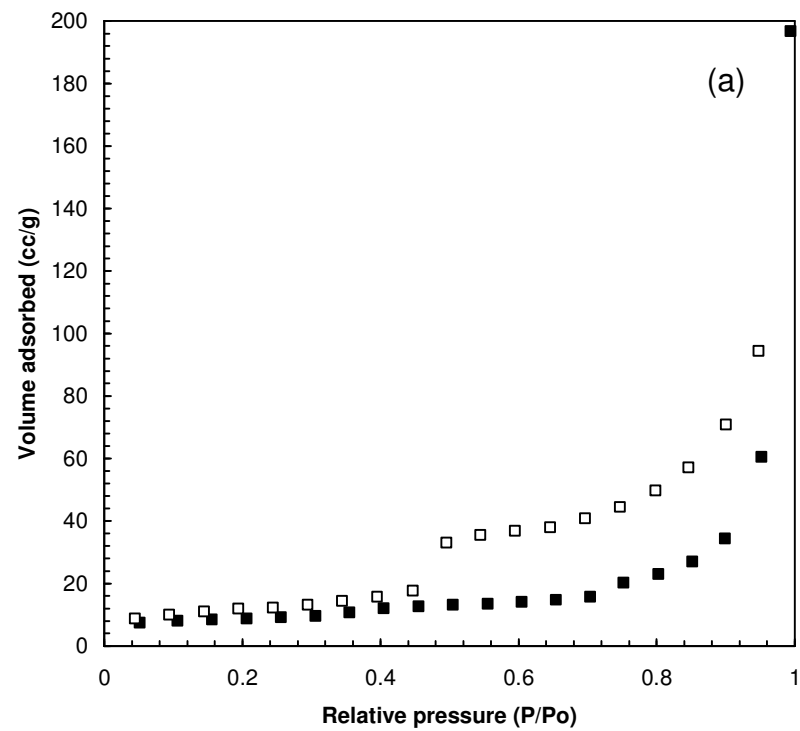


Figure 3.16 Adsorption/desorption isotherms of the BNNTs synthesized with B to Fe_2O_3 weight ratio of 15 at: (a) 1300°C and (b) 1200°C.

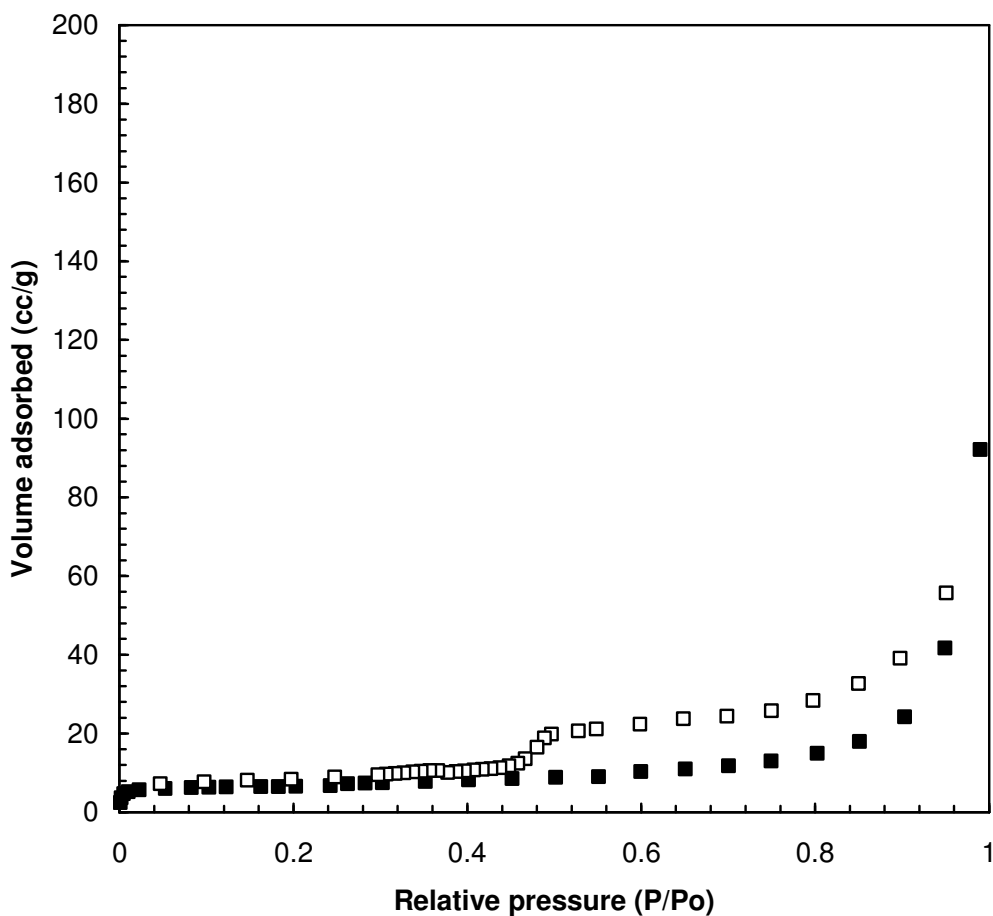


Figure 3.17 Adsorption/desorption isotherm of the BNNTs synthesized with B to Fe₂O₃ weight ratio of 5 at 1300°C.

According to the BDDT (Brauner-Deming-Deming-Teller) classification, the isotherm type of the BNNTs shown in Figures 3.16 and 3.17 corresponds to Type II isotherms. Type II isotherms are observed when adsorption occurs on nonporous powders or on powders with pore diameters larger than micropores [56]. From Figure 3.16, the volume of adsorbed nitrogen gas was found to be 90.51 cm³/g and 33 cm³/g at P/P_o value of 0.96 for 1300°C and 1200°C, respectively and the volume of adsorbed nitrogen gas was 8 cm³/g and 2.2 cm³/g at P/P_o value of 0.01 for 1300°C and 1200°C, respectively. The adsorbed gas volume at microporous region was 8.8% and 6.7% of the adsorbed gas volume at P/P_o of 0.96 for 1300°C and

1200°C, respectively. From Figure 3.17, the volume of adsorbed nitrogen gas was found to be 56.26 cm³/g at P/P_o of 0.96 and the volume of adsorbed nitrogen gas was 7.8 cm³/g at P/P_o value of 0.01. The adsorbed volume at microporous region (P/P_o<0.01) was 9% of the adsorbed volume at P/P_o of 0.96. From these values, it was concluded that solids contained nonconsiderable amounts of micropores.

The hysteresis formation was observed in the isotherms of these three samples. The adsorption of the gas first starts with micropores and then continues with mesopores. The adsorption and desorption mechanism occurs at the same time in micropores. While adsorption occurs by the condensation towards the walls of pores, desorption occurs by evaporation from the walls of pores. In mesopores, adsorption and desorption follow different ways. The filling of the mesopores occurs by the condensation on the wall of pores with formation of layers. On the other hand, desorption occurs by moving away from pore opening with the evaporation. Hence, in mesoporous region where the P/P_o >0.3, according to the de Boer, Type A hysteresis was observed. This type of hysteresis may be due to porous materials consisting of cylindrical-like pore channels [57]. In this study hysteresis opening became significant by the increase of temperature and the B to Fe₂O₃ weight ratio. The opening of the hysteresis became wider and this indicated the asset of the mesopores in a wider region.

From the Figure 3.16 and Figure 3.17, it was observed that the products contained mesopores. Total pore volumes and mesopore volumes of products are tabulated in Table 3.5. The total pore volume and mesopore volume were obtained from the desorption isotherm in Figure 3.16 and Figure 3.17 at P/P_o= 0.99 and P/P_o= 0.96, respectively by converting the desorped gas volume to the liquid volume. Mesopore volume of BNNTs produced at 1300°C was found to be 0.2 cm³/g (corresponding to 129 cm³ gas nitrogen/g) and mesopore volume of BNNTs produced at 1200°C was

found to be 0.059 cm³/g (corresponding to 38.2 cm³ gas nitrogen/g). Thus, the volume of mesopores decreased when the reaction temperature decreased. The total pore volumes of the pores were 0.3 cm³/g (corresponding to 197.9 cm³ gas nitrogen/g) and 0.099cm³/g (corresponding to 64.7 cm³ gas nitrogen/g) for the BNNTs produced at 1300°C and 1200°C, respectively. The decrease in reaction temperature caused a decrease in total pore volume of the BNNTs. From Figure 3.17, mesopore volume was found to be 0.102 cm³/g (corresponding to 66.37 cm³ gas nitrogen/g) and the total pore volume of the pores was 0.142 cm³/g (corresponding to 92.11 cm³ gas nitrogen/g). Thus, when the total and mesopore volumes of the products produced at different B to Fe₂O₃ weight ratios were compared, the decrease in the ratio caused a decrease in total and mesopore volumes of the BNNTs.

Table 3.5 Physical properties of the synthesized materials.

Reaction Temperature (°C)	B:Fe ₂ O ₃ Weight Ratio	Multipoint Surface Area (m ² /g)	Total Pore Volume (cm ³ liquid nitrogen/g)	Mesopore Volume (cm ³ liquid nitrogen/g)
1300	5	23.07	0.142	0.102
1300	15	30.70	0.300	0.200
1200	15	10.16	0.099	0.059

Multipoint BET surface areas of the BNNTs were calculated from the adsorption values between 0.05<P/P₀<0.30 and found to be 30.70 m²/g and 10.16 m²/g for the products synthesized at B to Fe₂O₃ weight ratio of 15 as at 1300°C and at 1200°C, respectively. The multipoint BET surface area of the BNNTs synthesized with B to Fe₂O₃ weight ratio of 5 at 1300°C was calculated as 23.07 m²/g. It was figured out that the decrease in

reaction temperature and the B to Fe₂O₃ weight ratio caused a decrease in surface area of BNNTs. The values were in an agreement with the ones obtained from single point measurement. The details of multipoint BET surface area calculations are given in Appendix G.

The pore size distributions (Figure 3.18-3.19) for the produced BNNTs were plotted using desorption data of BJH (Barrett-Joyner-Halenda) method at $0.35 < P/P_0 < 0.99$ corresponding to mesoporous site. For the BNNTs produced at 1300°C and 1200°C, the average mesopore diameter values were 37.93 Å and 37.98 Å, respectively and for the BNNTs produced at 1300°C with B to Fe₂O₃ weight ratio of 5 mesopore diameter was 39.07 Å. Very small peak at pore diameter of around 100 Å was observed. This peak indicated presence of little amount of macropores in all measured samples.

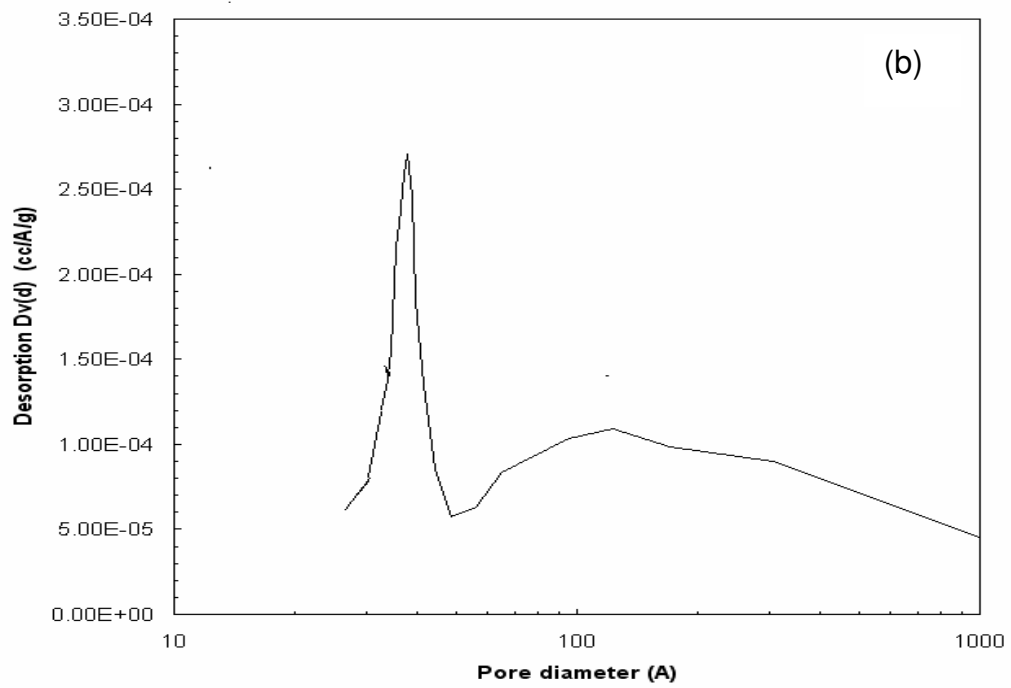
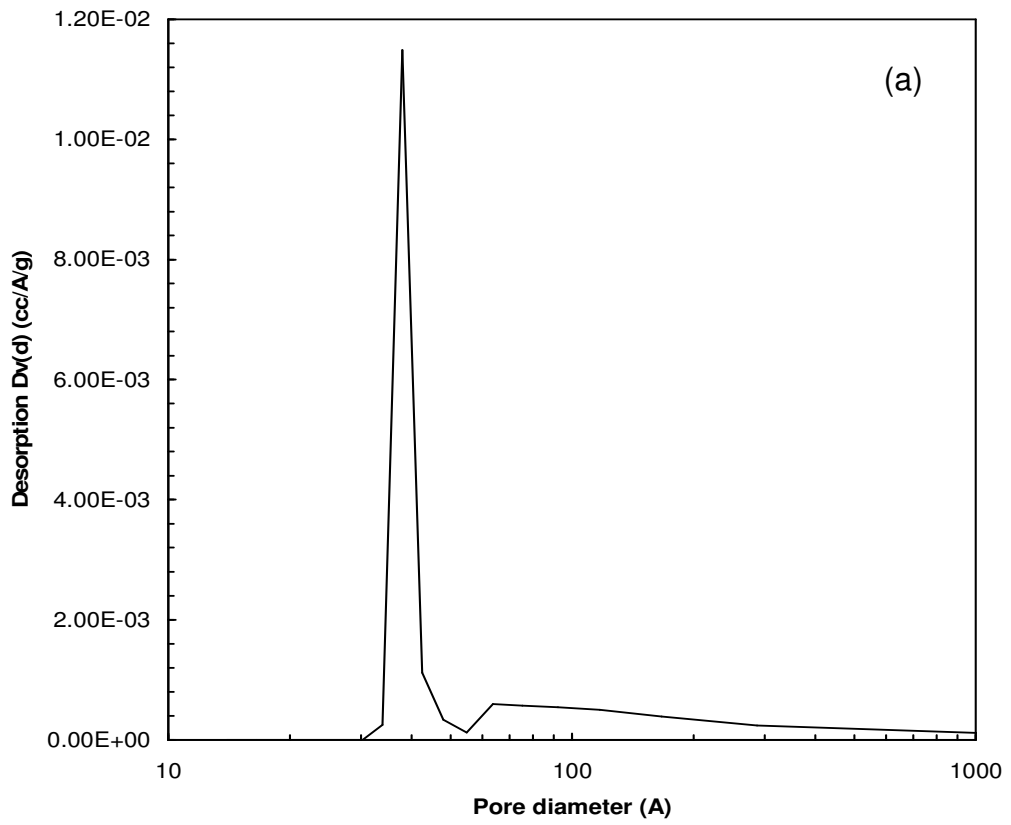


Figure 3.18 Pore size distributions for products produced at: (a) 1300°C and (b) 1200°C.

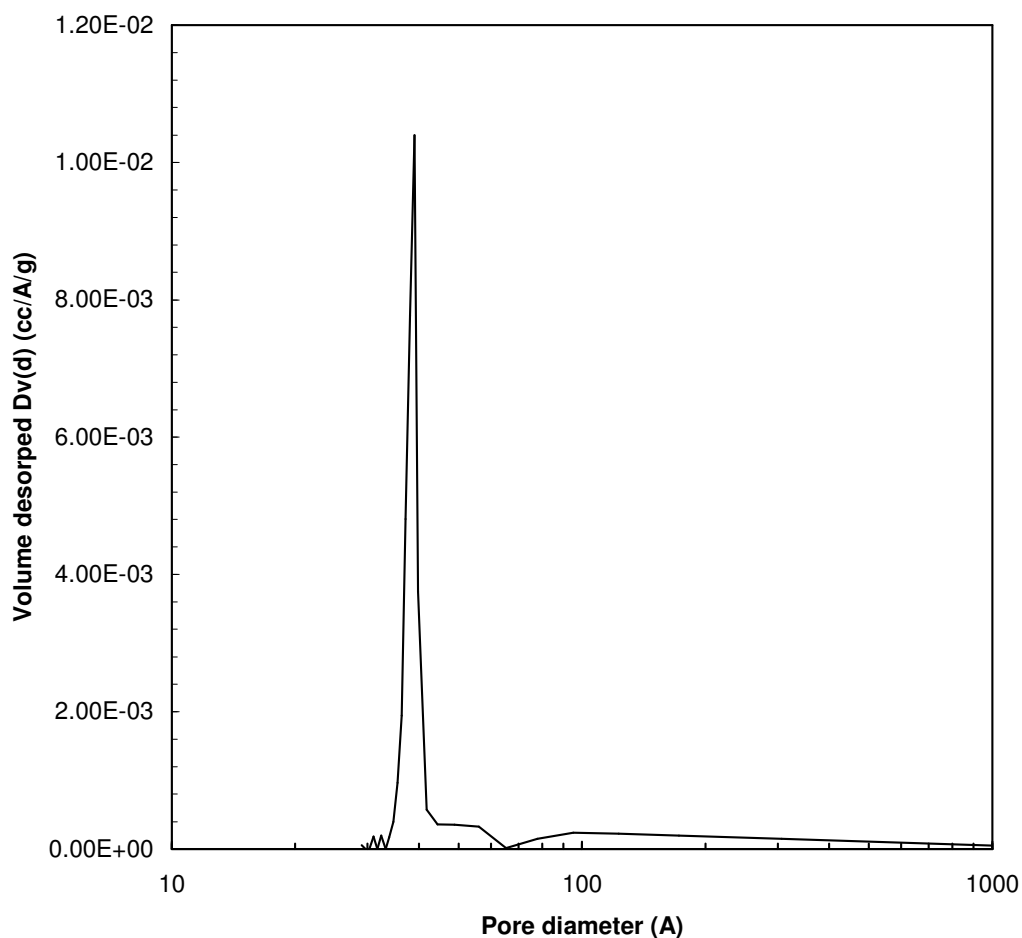


Figure 3.19 Pore size distribution for BNNTs produced at 1300°C with B to Fe₂O₃ weight ratio of 5.

3.3 Reproducibility of the Experimental Data

The reproducibility experiment is important to test the reliability of the experimental data. In order to determine the reproducibility of the data, two experiments were performed at the same conditions and then the results were compared. XRD patterns of the product synthesized with boron to iron oxide weight ratio of 15 at temperature of 1300°C are shown in Figure 3.20. In Figure 3.20.a, peaks observed at Bragg angle values of 25.9°, 41.9°, 43.7°, 50.0°, 55.1°, 76.2° correspond to hexagonal boron nitride and the peaks at Bragg angle values of 25.9°, 42.5°, 45.8°, 55.36°,

75.74° belong to rhombohedral boron nitride. In addition to hexagonal and rhombohedral boron nitride phases, cubic iron was also observed at Bragg angle values of around 44.65° and 65.2°. In Figure 3.20.b, peaks observed at Bragg angle values of 26.64°, 41.86°, 43.52°, 50.2°, 55.1°, 76.2° correspond to hexagonal boron nitride and the peaks at Bragg angle values of 26.64°, 42.7°, 45.44°, 55.12°, 75.72° belong to rhombohedral boron nitride. In addition to hexagonal and rhombohedral boron nitride phases, cubic iron was observed at Bragg angle values of around 44.6°, 64.88° and 82.44°. As a result, formation of hexagonal and rhombohedral boron nitride and cubic iron was observed for the reproducibility experiments. XRD patterns of BNNTs (Figure 3.20 a and b) were taken by using two different X-ray Diffractometers.

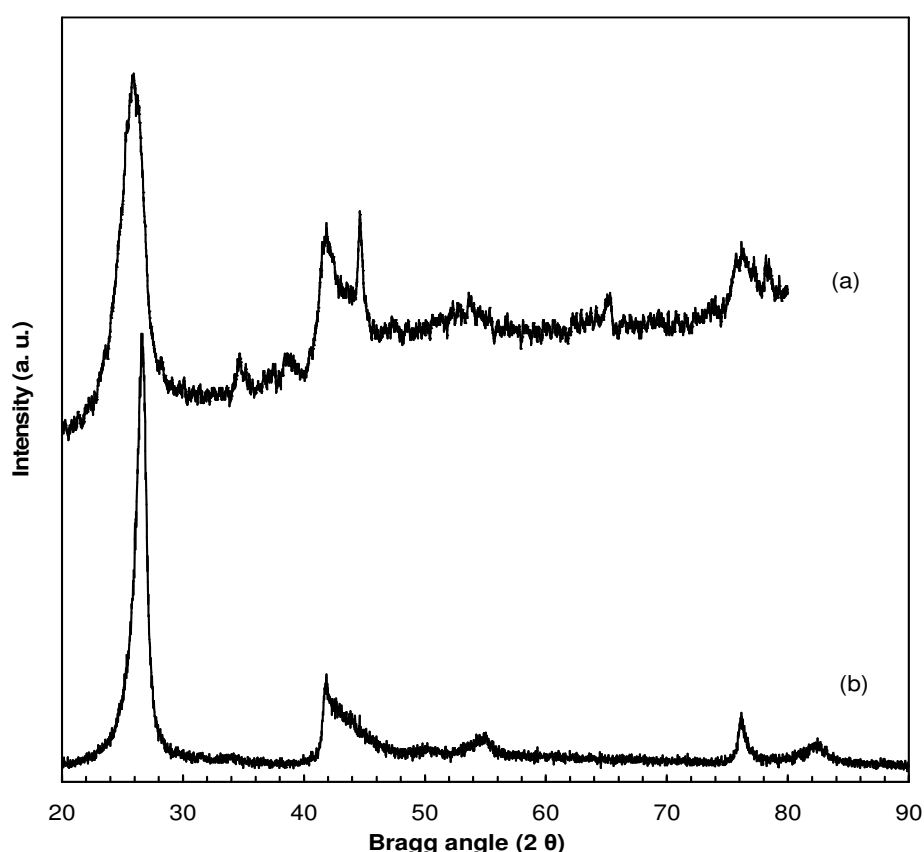


Figure 3.20 XRD patterns of BNNTs produced at 1300°C at B to Fe₂O₃ weight ratio of 15.

Figure 3.21 represents the FTIR spectra of the products synthesized with boron to iron oxide weight ratio of 15 at a temperature of 1300°C which were taken at different times. The peak heights' intensities were not the same because these spectra were taken at different times. But similar transmittance behavior was observed at the same wavenumbers. As shown in this figure, typical infrared peaks of boron nitride were observed at around 1370 cm^{-1} and 810 cm^{-1} which are assigned to the B-N stretching vibrations and B-N-B bending vibrations, respectively. The broad peak at wavenumbers between 2200 cm^{-1} and 2300 cm^{-1} belongs to boron. In addition to the peaks corresponding to boron nitride and boron, characteristic peak at 3210 cm^{-1} was also observed due to the water absorbed on the sample. There are other peaks at wavenumbers 547 cm^{-1} and 482 cm^{-1} , which belong to characteristic peaks of iron oxide.

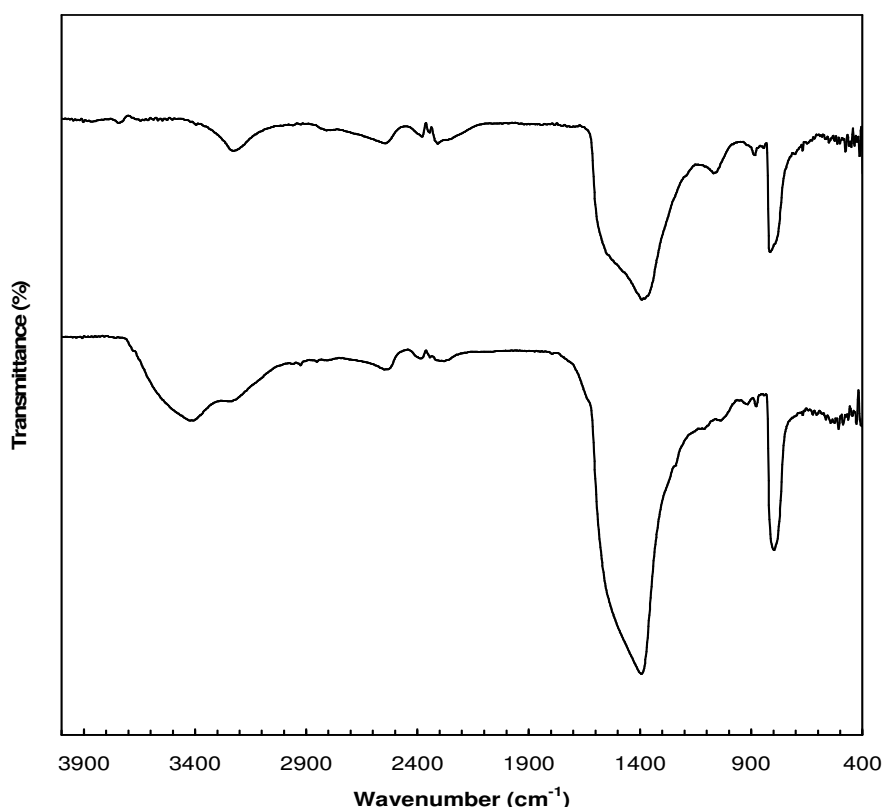


Figure 3.21 FTIR spectra of BNNTs produced at 1300°C at B to Fe_2O_3 weight ratio of 15.

CHAPTER 4

CONCLUSIONS

- Boron nitride nanotubes were successfully synthesized from the reaction of ammonia gas with the mixture of boron and iron oxide.
- From the mass spectrum of the reactor effluent stream, it was concluded that nitrogen formed in addition to hydrogen and water in the reaction of ammonia gas with the mixture of boron and iron oxide.
- Boron nitride nanotube formation reaction took place over 900 °C.
- Rhombohedral and hexagonal boron nitrides and iron were the solid phases formed in the operation temperature during the reaction of ammonia gas with the boron and iron oxide mixture.
- Crystallinity of the synthesized material increased with an increase in both temperature and boron to iron oxide weight ratio.
- The color and appearance of the product changed with temperature and boron to iron oxide weight ratio.
- From the XPS and EDX spectra, boron to nitrogen atomic ratios of the synthesized materials were found to be close to one.
- From the FTIR spectra, it was concluded that the amount of boron nitride increased with increase in boron to iron oxide weight ratio.

- Diameter of boron nitride nanotube did not change with temperature and weight ratio of boron to iron oxide. Entagled, hollow and bulbous boron nitride tubes were produced.
- The synthesized materials exhibited Type II isotherms.
- Surface area of the product decreased with decrease in both temperature and weight ratio of boron to iron oxide. On the other hand, its average mesopore diameter did not change with temperature and weight ratio of boron to nitrogen.
- The best temperature and weight ratio of boron to iron oxide to produce boron nitride nanotubes were found to be 1300 °C and 20, respectively.

CHAPTER 5

RECOMMENDATIONS

- The effect of temperature and the gas compositions on the reaction kinetics can be investigated.
- The rate expression of the production of BNNTs reaction can be found.
- Different catalysts can be used to investigate catalyst effect on the production of BNNTs.
- Experiments can be performed to get information about Fe_2O_3 acting as a catalyst or an oxygen supplier in the system.

REFERENCES

1. A.S. Milev, G. S. K. Kannangara, "Nanotechnology", in J. I. Kroschwitz., A. Seidel (Eds), Kirk-Othmer Encyclopedia of Chemical Technology, Fifth Edition, vol. 17, Wiley, NJ, 2005, pp 1-29.
2. Mac, Nanotubes and fullerenes for quantum computing, http://homepage.mac.com/jhgowen/research/nanotube_page/nanotubes.html, last accessed date: May 1, 2008.
3. Arkema, http://www.arkema.com/images/visuels/products/dossiers/nanotubes_en/types_nanotubes.gif, last accessed date: May 1, 2008.
4. Wilson, M., Kannangara, K., Smith, G., Simmons, M., Raguse, B., Nanotechnology, Basic Science and Emerging Technologies, Chapman & Hall / CRC, Australia, 2002.
5. Penn Engineering, What is a Carbon Nanotube, <http://www.seas.upenn.edu/mse/images/nanotube1.jpg>, last accessed date: May 1, 2008.
6. Iijima, S., "Helical microtubules of graphitic carbon", *Nature*, 354, p56, 1991.
7. Iijima, S., Ichihashi, T., "Single-shell carbon nanotubes of 1-nm diameter", *Nature*, 363, p603, 1993.
8. Bethune, D. S., Kiang, C. H., de Vries, M. S., Gorman, G., Savoy, R., Vazquez, J., Beyers, R., "Cobalt-catalysed growth of carbon nanotubes with single-atomic-layer walls", *Nature*, 363, (1993), 605.
9. Wikipedia, Carbon nanotube, http://en.wikipedia.org/wiki/Carbon_nanotube#Strength, last accessed date: May 1, 2008.

10. Cheaptubes, Properties and applications of carbon nanotubes.
http://www.cheaptubesinc.com/applications.htm#Strength_and_Elasticity, last accessed date: May 1, 2008.
11. Wikipedia, Potential applications of carbon nanotubes,
http://en.wikipedia.org/wiki/Potential_applications_of_carbon_nanotubes, last accessed date: May 1, 2008.
12. University of Michigan, Motivation for cubic BN,
<http://www.eecs.umich.edu/USL/MaterialScience/MotivationBN.html>, last accessed date: May 1, 2008.
13. Britannica, Boron nitride: hexagonal structures,
<http://www.britannica.com/eb/art-9370/Comparison-of-the-hexagonal-structures-of-graphite-and-boron-nitride?articleTypeld=1>, last accessed date: May 1, 2008.
14. Uminokai, Nanostructures of carbon and boron nitride
<http://uminokai.net/nanotube/intro.php?lg=en>, last accessed date: May 1, 2008.
15. Blasé, X., Rubio, A., Louie, S. G., Cohen, M. L., "Stability and band gap constancy of boron nitride nanotubes", *Europhys. Lett*, 28 (5), 335-340, 1994.
16. Suryavanshi, A. P., Yu, M., "Elastic modulus and resonance behaviour of boron nitride nanotubes", *Appl. Phys. Lett*, Volume 84, Number 14, 2527-2529.
17. Chopra, N. G., Zettl, A., "Measurement of the elastic modulus of a multi-wall boron nitride nanotube", *Solid state communications*, volume 105, No: 5, pp. 297, 1998.
18. Chen, Y., Zou, J., Campbell, S. J., Le Caer, G., "Boron nitride nanotubes: pronounced resistance to oxidation", *Appl. Phys. Lett*, volume 84, number 13, 2430-2432, 2004.
19. Ishigami, M., Aloni, S., Zettl, A., "Properties of boron nitride nanotubes", Scanning tunneling microscopy spectroscopy and related techniques: 12th international conf., 94-99, 2003.
20. Mpourmpakis, G., Froudakis, G. E., "Why boron nitride nanotubes are preferable to carbon nanotubes for hydrogen storage? An ab initio theoretical study", *Catalysis Today*, 120, 341-345, 2007.

21. Laude, T., "Boron nitride nanotubes grown by non-ablative laser heating: synthesis, characterization and growth processes", Phd Thesis, 2001.
22. Gogotsi, Y., Nanotubes and Nanofibers, Taylor&Francis Group, 2006.
23. Chopra, N. G., Luyken, R. J., Cherrey, K., Crespi, V. H., Cohen, M., L., Louie, S. G., Zettl, A., "Boron nitride nanotubes", *Science*, 269, 966-967, 1995.
24. Loiseau, A., Willaime, F., Demoncey, N., Schramchenko, N., Hug, G., Colliex, C., Pascard, H., "Boron nitride nanotubes", *Carbon*, Volume 36, No. 5-6, 743-752, 1998.
25. Narita, I., Oku, T., "Synthesis of boron nitride nanotubes by using NbB₂, YB₆ and YB₆/Ni powders", *Diamond and Related Materials*, 12, 1912-1917, 2003.
26. Yu, D., P., Sun, X. S., Lee, C. S., Bello, I., Lee, S. T., Gu, H. D., Leung, K. M., Zhou, G. W., Dong, Z. F., Zhang, Z., "Synthesis of boron nitride nanotubes by means of excimer laser ablation at high temperature", *Appl. Phys. Lett.*, Vol. 72, No. 16, 1966-1968, 1998.
27. Zhou, G. W., Zhang, Z. Bai, Z. G., Yu, D. P., "Catalyst effects on formation of boron nitride nano-tubules synthesized by laser ablation", *Solid State Communications*, 109, 555-559, 1999.
28. Laude, T., Matsui, Y., Marraud, A., Jouffrey, B., "Long ropes of boron nitride nanotubes grown by a continuous laser heating", *Appl. Phys. Lett.*, Vol. 76, No. 22, 3239-3241, 2000.
29. Lee, R. S., Gavillet, J., de la Chapelle, M. L., Loiseau, A., Cochon, J. L., Pigache, D., Thibault, J., Willaime, F., "Catalyst-free synthesis of boron nitride single-wall nanotubes with a preferred zigzag configuration", *Phys. Rev. B*, 64, 121405, 2001.
30. Chen, Y., Fitz Gerald, J., Williams, J. S., Bulcock, S., "Synthesis of boron nitride nanotubes at low temperatures using reactive ball milling", *Chem. Phys. Lett.*, 299, 260-264, 1999.
31. Chen, Y., Chadderton, L. T., Fitz Gerald, J., Williams, J. S., "A solid-state process for formation of boron nitride nanotubes", *Appl. Phys. Lett.*, 74, 2960-2962, 1999.

32. Bae, S. Y., Seo, H., W., Park, J., Choi, Y. S., Park, J. C., Lee, S. Y., "Boron nitride nanotubes synthesized in the temperature range 1000-1200 °C", *Chem. Phys. Lett.*, 374, 534-541, 2003.
33. Fengqiu, J., Chuanbao, C., Hong, X., Ziguang, Y., "Mechanosynthesis of boron nitride nanotubes", *Chinese J. Chem. Eng.*, 14 (3), 389-393, 2006.
34. Lourie, O., R., Jones, C. R., Bartlett, B. M., Gibbons, P. C., Ruoff, R. S., Buhro, W. E., "CVD growth of boron nitride nanotubes", *Chem. Mater.*, 12, 1808, 2000.
35. Ma, R., Bando, Y., Sato, T., "CVD synthesis of boron nitride nanotubes without metal catalysts" *Chem. Phys. Lett.*, 337, 61-64, 2001.
36. Tang, C. C, Lamy de la Chapelle, M., Li, P., Dang, H., Y., Fan, S. S., "Catalytic growth of nanotube and nanobamboo structures of boron nitride", *Chem. Phys. Lett.*, 342, 492-496, 2001.
37. Tang, C., Bando, Y., Sato, T., "Catalytic growth of boron nitride nanotubes", *Chem. Phys. Lett.*, 362, 185-189, 2002.
38. Tang, C., Bando, Y., Sato, T., Kurashima, K., "A novel precursor for synthesis of pure boron nitride nanotubes", *Chem. Comm.*, 12, 1290-1291, 2002.
39. Cai, P., Chen, L., Shi, L., Yang, Z., Zhao, A., Gu, Y., Huang, T., Qian, Y., "One convenient synthesis route to boron nitride nanotube", *Solid State Commn.*, 133, 621-623, 2005.
40. Yu, J., Bill, C., Li, P., Zhou, J., Chen, Y., "Influence of nitriding gases on the growth of boron nitride nanotubes", *J. Mater. Sci.*, 42, pp 4025-4030, 2007.
41. Tang, C. C., Ding, X. X., Huang, X. T., Gan, Z. W., Qi, S. R., Liu, W., Fan, S. S., "Effective growth of boron nitride nanotubes", *Chem. Phys. Lett.*, 356, 254-258, 2002.
42. Fu, J. J., Lu, Y. N., Huo, K. F., Wang, X. Z., Li, L., Hu, Z., Chen, Y., "The synthesis of boron nitride nanotubes by an extended vapour-liquid-solid method", *Nanotechnology*, 15, 727-730, 2004.
43. Rosas, G., Sistos, J., Ascencio, J. A., Medina, A., Perez, R., "Multiple-walled BN nanotubules obtained with a mechanical alloying technique", *Appl. Phys. A*, 80, 377-380, 2005.

44. Bechelacy, M., Bernard, S., Brioude, A., Cornu, D., Stadelmann, P., Charcosset, C., Fiaty, K., Miele, P., "Synthesis of boron nitride nanotubes by a template-assisted polymer thermolysis process", *J. Phys. Chem. C.*, 111, 13378-13384, 2007.
45. Hiden Analytical, RC RGA Analyser Operator's Manual, Manual Number: Ha-085-005.
46. Skoog D. A., Leary J. J., Principles of Instrumental Analysis, Fourth edition, Saunders College Publishing, USA, 1992.
47. Smith R.M., Busch K. L., Understanding Mass Spectra-A Basic Approach, John Wiley & Sons Inc., USA, 1999.
48. Binghamton University, X-Ray Analysis of a Solid, <http://materials.binghamton.edu/labs/xray/xray.html>, last accessed date: May 1, 2008.
49. Purdue University, Scanning Electron Microscope, <http://www.purdue.edu/REM/rs/sem.htm>, last accessed date: May 1, 2008.
50. Wikipedia, Scanning Electron Microscope, http://en.wikipedia.org/wiki/Scanning_electron_microscope, last accessed date: May 1, 2008.
51. Materials Evaluation and Engineering Inc., Energy Dispersive Spectroscopy, <http://www.mee-inc.com/eds.html>, last accessed date: May 1, 2008.
52. Wikipedia, Energy-dispersive X-Ray Spectroscopy, http://en.wikipedia.org/wiki/Energy-dispersive_X-ray_spectroscopy, last accessed date: May 1, 2008.
53. Stuart B., Modern Infrared Spectroscopy, John Wiley & Sons Inc., UK, 1996.
54. Nyquist R. A. & Kagel R. O., Infrared Spectra of Inorganic Compounds (3800-45 cm⁻¹), Academic Press, New York and London, 1971.
55. National Institute of Standards and Technology, NIST X-ray Photoelectron Spectroscopy Database, <http://srdata.nist.gov/xps/>, last accessed date: May 1, 2008.

56. Lowell S., Shields, J. E., Thomas M. A., Thommes M.,
Characterization of Porous Solids and Powders: Surface Area,
Pore Size and Density, Springer, Netherlands, 2006.
57. Lowell S., Shields J. E., Powder Surface Area and Porosity, Third
Edition, Chapman & Hall, New York, 1991.

APPENDIX A

VOLUMETRIC FLOW RATE CALIBRATION CURVES FOR ARGON AND AMMONIA ROTAMETERS

A.1 Calibration Curve for Argon Rotameter

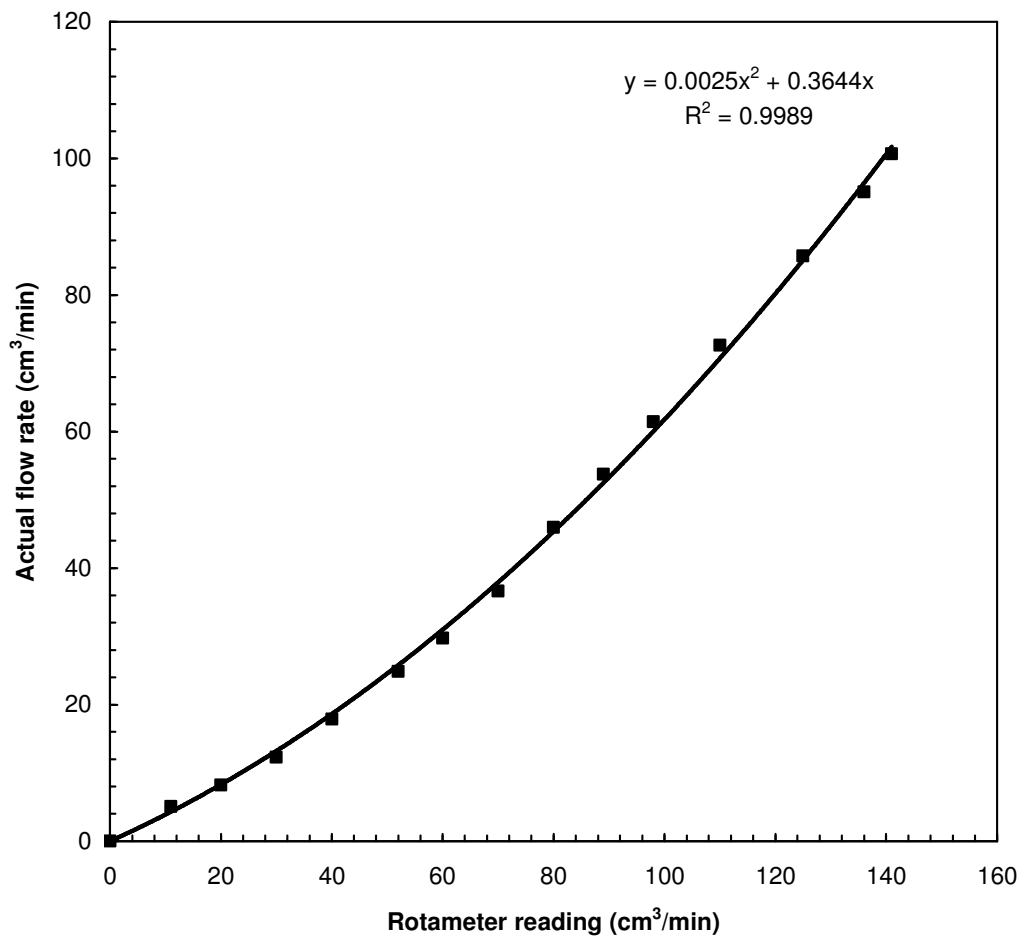


Figure A.1 Volumetric flow rate calibration curve for argon rotameter.

A.2 Calibration Curve for Ammonia Rotameter

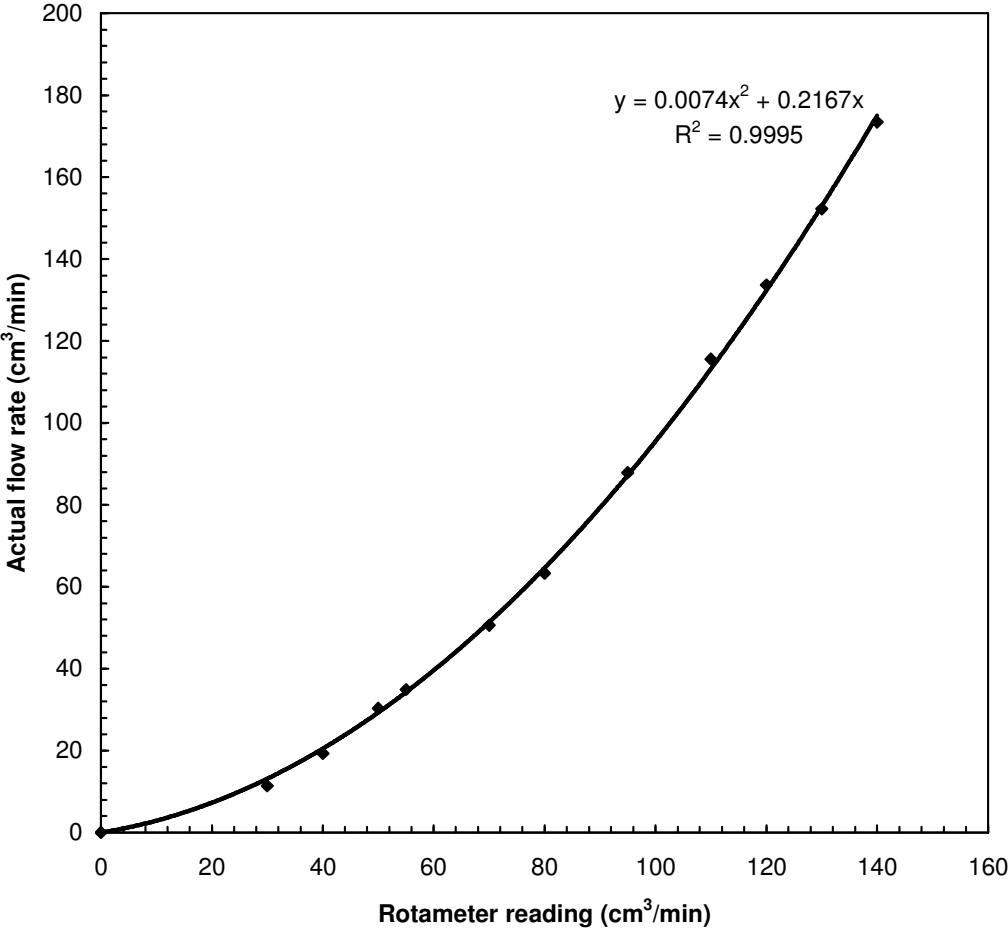


Figure A.2 Volumetric flow rate calibration curve for ammonia rotameter.

APPENDIX B

THE MASS SPECTROMETER CRACKING PATTERN DATA FOR THE SYSTEM GASES

The following cracking pattern data for the gases is obtained from the library of the Hiden Analytical HPR 20 Mass Spectrometer's software 'MASsoft'.

Table B.1 Mass spectrometer cracking pattern data for NH₃

Mass	Intensity (%)
14	2.2
15	7.5
16	80
17	100
18	0.4

Table B.2 Mass spectrometer cracking pattern data for Ar.

Mass	Intensity (%)
20	10.7
36	0.3
38	0.1
40	100

Table B.3 Mass spectrometer cracking pattern data for H₂

Mass	Intensity (%)
1	10
2	100

Table B.4 Mass spectrometer cracking pattern data for H₂O

Mass	Intensity (%)
2	0.7
16	1.1
17	23
18	100
19	0.1
20	0.3

Table B.5 Mass spectrometer cracking pattern data for N₂.

Mass	Intensity (%)
14	7.2
28	100
29	0.8

APPENDIX C

X-RAY DIFFRACTION DATA

C.1 X- ray Diffraction Data of Reference Compounds

The following X-ray diffraction data for reference compounds is obtained from the library of Philips model PW 1050 X-Ray Diffractometer's software. 'PCDFWIN'. XRD data for the reference compounds are tabulated in Table C.1.1-C.1.10

Table C.1.1 XRD data for hexagonal BN.

Catalog no:34-0421 Hexagonal BN Rad:CuKa1 (λ :1.5406)			
d	2 θ	Int	h k l
3.328	26.76	100	0 0 2
2.169	41.59	23	1 0 0
2.062	43.87	10	1 0 1
1.817	50.14	16	1 0 2
1.663	55.16	12	0 0 4
1.550	59.55	<2	1 0 3
1.319	71.41	5	1 0 4
1.252	75.93	13	1 1 0
1.172	82.17	14	1 1 2
1.134	85.51	<3	1 0 5
1.109	87.94	<3	0 0 6
1.084	90.53	<3	2 0 0
1.031	96.66	3	2 0 2
1.000	100.68	10	1 1 4
0.987	102.49	<3	1 0 6
0.908	115.93	<4	2 0 4
0.831	135.63	<4	0 0 8
0.830	136.14	4	1 1 6
0.819	139.99	<4	2 1 0
0.796	150.79	<4	2 1 2

Table C.1.2 XRD data for hexagonal BN.

Catalog no:45-0893 Hexagonal BN Rad:CuKa1 (λ :1.5406)					
d	2 θ	Int	h	k	l
3.330	26.74	100	0	0	2
2.170	41.58	26	1	0	0
1.820	43.69	10	1	0	1
1.670	50.07	27	1	0	2
1.320	54.93	12	0	0	4
1.250	59.59	2	1	0	3
3.330	71.40	8	1	0	4
2.170	76.08	19	1	1	0

Table C.1.3 XRD data for hexagonal BN.

Catalog no:45-0895 Hexagonal BN Rad:CuKa1 (λ :1.5406)					
d	2 θ	Int	h	k	l
3.330	26.74	100	0	0	2
2.170	41.58	11	1	0	0
2.070	43.69	37	1	0	1
1.820	50.07	11	1	0	2
1.670	54.93	12	0	0	4
1.550	59.59	11	1	0	3
1.320	71.40	3	1	0	4
1.250	76.08	5	1	1	0

Table C1.4 XRD data for hexagonal BN.

Catalog no:45-0896 Hexagonal BN Rad:CuKa1 (λ :1.5406)					
d	2 θ	Int	h	k	l
3.330	26.74	100	0	0	2
2.170	41.58	32	1	0	0
1.820	50.07	33	1	0	2
1.670	54.93	12	0	0	4
1.320	71.40	8	1	0	4
1.250	76.08	19	1	1	0

Table C.1.5 XRD data for cubic Fe.

Catalog no:87-0722 Cubic Fe Rad: CuK α 1 (λ :1.5406)					
d	2 θ	Int	h	k	l
2.022	44.76	100	1	1	0
1.430	65.16	16	2	0	0
1.167	82.52	30	2	1	1

Table C.1.6 XRD data for cubic Fe.

Catalog no:06-0696 Cubic Fe Rad:CuK α 1 (λ :1.5405)					
d	2 θ	Int	h	k	l
2.026	44.67	100	1	1	0
1.433	65.02	20	2	0	0
1.170	82.33	30	2	1	1
1.013	98.94	10	2	2	0
0.906	116.38	12	3	1	0
0.827	137.13	6	2	2	2

Table C.1.7 XRD data for rhombohedral boron nitride.

Catalog no:45-1171 Rhombohedral BN Rad:CuK α 1 (λ :1.5406)					
d	2 θ	Int	h	k	l
3.334	26.71	100	0	0	3
2.119	42.61	20	1	0	1
1.989	45.56	12	0	1	2
1.666	55.06	8	0	0	6
1.638	56.07	4	1	0	4
1.470	63.18	2	0	1	5
1.251	75.95	8	1	1	0
1.193	80.41	<3	1	0	7
1.172	82.11	11	1	1	3
1.112	87.66	<3	0	0	9
1.077	91.23	<3	0	2	1
1.059	93.22	<3	2	0	2
1.001	100.62	7	1	1	6
0.831	135.85	4	1	1	9
0.816	141.13	4	2	1	1
0.808	144.53	4	1	2	2

Table C.1.8 XRD data for cubic Fe.

Catalog no:89-4185					
Cubic Fe					
Rad:CuKa1 (λ:1.5406)					
d	2θ	Int	h	k	l
2.106	42.89	100	1	1	1
1.824	49.95	49	2	0	0
1.290	73.32	29	2	2	0
1.100	88.88	32	3	1	1

Table C.1.9 XRD data for cubic Fe.

Catalog no:88-2324					
Cubic Fe					
Rad:CuKa1 (λ:1.5406)					
d	2θ	Int	h	k	l
1.980	45.78	100	1	1	1
1.714	53.37	49	2	0	0
1.212	78.86	29	2	2	0

Table C.1.10 XRD data for Fe₂O₃.

Catalog no:33-0664					
Fe ₂ O ₃					
Rad:CuKa1 (λ:1.5406)					
d	2θ	Int	h	k	l
3.684	24.14	22	0	1	2
2.700	33.15	100	1	0	4
2.519	35.61	75	1	1	0
2.292	39.28	4	0	0	6
2.207	40.85	24	1	1	3
2.077	43.52	4	2	0	2
1.840	49.48	59	0	2	4
1.694	54.09	72	1	1	6
1.636	56.15	2	2	1	1
1.603	57.43	8	1	2	2
1.485	62.45	17	0	1	8
1.453	63.99	55	2	1	4
1.413	66.03	<2	[1	2	5]
1.349	69.60	6	2	0	8
1.311	71.94	21	1	0	10
1.306	72.26	12	1	1	9
1.259	75.43	17	2	2	0
1.227	77.73	9	3	0	6
1.214	78.76	4	2	2	3
1.189	80.71	11	1	2	8
1.163	82.94	12	0	2	10
1.141	84.91	17	1	3	4
1.103	88.54	17	2	2	6
1.076	91.34	5	0	4	2
1.055	93.71	18	2	1	10
1.042	95.24	<3	1	1	12
1.039	95.66	8	4	0	4
0.989	102.28	11	3	2	8
0.971	104.91	<3	2	2	9
0.960	106.61	14	3	2	4
0.958	107.02	11	0	1	14
0.951	108.08	14	4	1	0
0.931	111.51	6	4	1	3
0.920	113.59	6	0	4	8
0.908	116.04	15	1	3	10
0.899	117.75	3	3	0	12
0.895	118.69	9	2	0	14
0.878	122.42	18	4	1	6
0.864	125.92	3	2	3	8
0.854	128.75	9	4	0	10
0.843	131.87	16	1	2	14
0.839	133.23	10	3	3	0
0.808	144.44	13	3	2	10

C.2 XRD Data of Synthesized Materials

XRD data of the materials synthesized at different temperatures and different boron to iron oxide weight ratios are tabulated in Table C.2.1-C.2.14

Table C.2.1 XRD data for BNNTs produced at 1400°C with a B to Fe₂O₃ weight ratio of 15.

d	2θ	Intensity
3.31	26.90	100
2.16	41.65	9
2.11	42.83	12
2.06	43.87	13
1.98	45.75	9
1.81	50.29	4
1.66	55.00	5
1.66	55.18	4
1.24	76.20	5

Table C.2.2 XRD data for BNNTs produced at 1300°C with a B to Fe₂O₃ ratio of 15.

d	2θ	Int
3.42	25.97	100
2.15	41.89	47
2.02	44.65	49
1.99	45.37	19
1.67	54.78	16
1.63	56.05	11
1.42	65.19	14
1.25	75.91	16

Table C.2.3 XRD data for BNNTs produced at 1200°C with a B to Fe₂O₃ ratio of 15.

d	2θ	Int
3.35	26.53	100
2.15	41.82	31
2.12	42.53	29
2.08	43.40	13
1.98	45.61	16
1.83	49.78	11
1.66	55.13	14
1.25	76.01	14

Table C.2.4 XRD data for BNNTs produced at 1100°C with a B to Fe₂O₃ ratio of 15.

d	2θ	Int
3.37	26.37	100
2.16	41.72	45
2.12	42.59	29
2.09	43.14	33
2.04	44.32	33
1.99	45.34	22
1.82	49.92	21
1.67	54.71	26
1.43	64.87	19
1.25	75.91	26

Table C.2.5 XRD data for BNNTs produced at 1000°C with a B to Fe₂O₃ ratio of 15.

d	2θ	Int
3.34	26.63	100
2.17	41.47	54
2.15	41.85	57
2.11	42.82	39
2.08	43.37	45
2.01	44.98	71
1.84	49.35	28
1.83	49.57	43
1.68	54.24	36

Table C.2.6 XRD data for BNNTs produced at 900°C with a B to Fe₂O₃ ratio of 15.

d	2θ	Int
3.35	26.55	94
2.16	41.65	40
2.16	41.76	46
2.14	42.18	51
2.08	43.26	48
2.07	43.68	48
2.02	44.70	100
1.98	45.76	30
1.82	49.87	21
1.81	50.21	23
1.67	54.81	25
1.65	55.56	25
1.42	65.22	48
1.32	71.33	25
1.25	75.88	23
1.24	76.20	25

Table C.2.7 XRD data for BNNTs produced at 1300°C with a B to Fe₂O₃ ratio of 5.

d	2θ	Int
3.38	26.31	100
2.17	41.56	31
2.14	42.02	33
2.09	43.08	26
1.82	49.82	8
1.81	50.25	6
1.68	54.46	12
1.67	54.60	9
1.47	63.19	6
1.25	75.93	16
1.24	76.22	16

Table C.2.8 XRD data for BNNTs produced at 1300°C with a B to Fe₂O₃ ratio of 20.

d	2θ	Int
3.38	26.31	100
2.16	41.77	29
2.13	42.20	28
2.00	45.12	13
1.98	45.63	10
1.82	50.01	75
1.71	53.41	9
1.67	54.93	10
1.66	54.94	9
1.25	75.63	10
1.25	76.08	14
1.21	78.47	3

Table C.2.9 XRD data for BNNTs produced at 1300°C with a B to Fe₂O₃ ratio of 1.

d	2θ	Int
3.65	24.32	9
3.36	26.48	100
2.68	33.30	29
2.51	35.66	11
2.20	40.83	13
2.16	41.64	26
2.07	43.52	20
2.02	44.64	31
1.84	49.38	13
1.82	49.96	15
1.68	54.36	16
1.66	55.04	15
1.43	65.16	8
1.32	70.86	12
1.25	76.02	27
1.17	82.26	22

Table C.2.10 XRD data for BNNTs produced at 1300°C with a B to Fe₂O₃ ratio of 0.5.

d	2θ	Int
3.73	23.78	37
3.36	26.50	100
2.67	33.42	98
2.50	35.88	66
2.25	39.92	38
2.17	41.42	77
2.02	44.72	92
1.84	49.46	53
1.81	50.10	48
1.68	54.44	50
1.49	62.18	22
1.44	64.30	29
1.41	65.94	35
1.32	70.84	61
1.25	75.88	50
1.17	82.32	37

Table C.2.11 XRD data for BNNTs produced at 1300°C with a B to Fe₂O₃ ratio of 20 with boron source of Sigma-Aldrich.

d	2θ	Int
3.33	26.68	100
2.16	41.74	22
2.10	42.98	12
1.81	50.34	6
1.66	55.06	8
1.25	75.90	13
1.17	82.06	6

Table C.2.12 XRD data for BNNTs produced at 1200°C with a B to Fe₂O₃ ratio of 20 with boron source of Sigma-Aldrich.

d	2θ	Int
3.34	26.64	100
2.16	41.74	23
2.07	43.68	15
1.81	50.14	5
1.67	54.86	8
1.25	76.08	4
1.17	82.32	2

Table C.2.13 XRD data for BNNTs produced at 1100°C with a B to Fe₂O₃ ratio of 20 with boron source of Sigma-Aldrich.

d	2θ	Int
3.35	26.52	100
2.15	41.86	27
2.07	43.58	17
1.81	50.10	4
1.67	54.92	8
1.25	76.08	12
1.17	82.34	8

Table C.2.14 XRD data for BNNTs produced at 900°C with a B to Fe₂O₃ ratio of 20 with boron source of Sigma-Aldrich.

d	2θ	Int
3.33	26.74	100
2.15	41.88	34
2.06	43.78	36
2.02	44.70	40
1.82	49.9	14
1.67	54.78	16
1.66	55.08	14
1.43	65.06	9
1.24	76.12	18
1.17	82.07	14
1.17	82.14	21

APPENDIX D

FTIR SPECTRA OF BORON AND IRON OXIDE

FTIR spectra of the boron and iron oxide are given in Figure D.1 and Figure D.2.

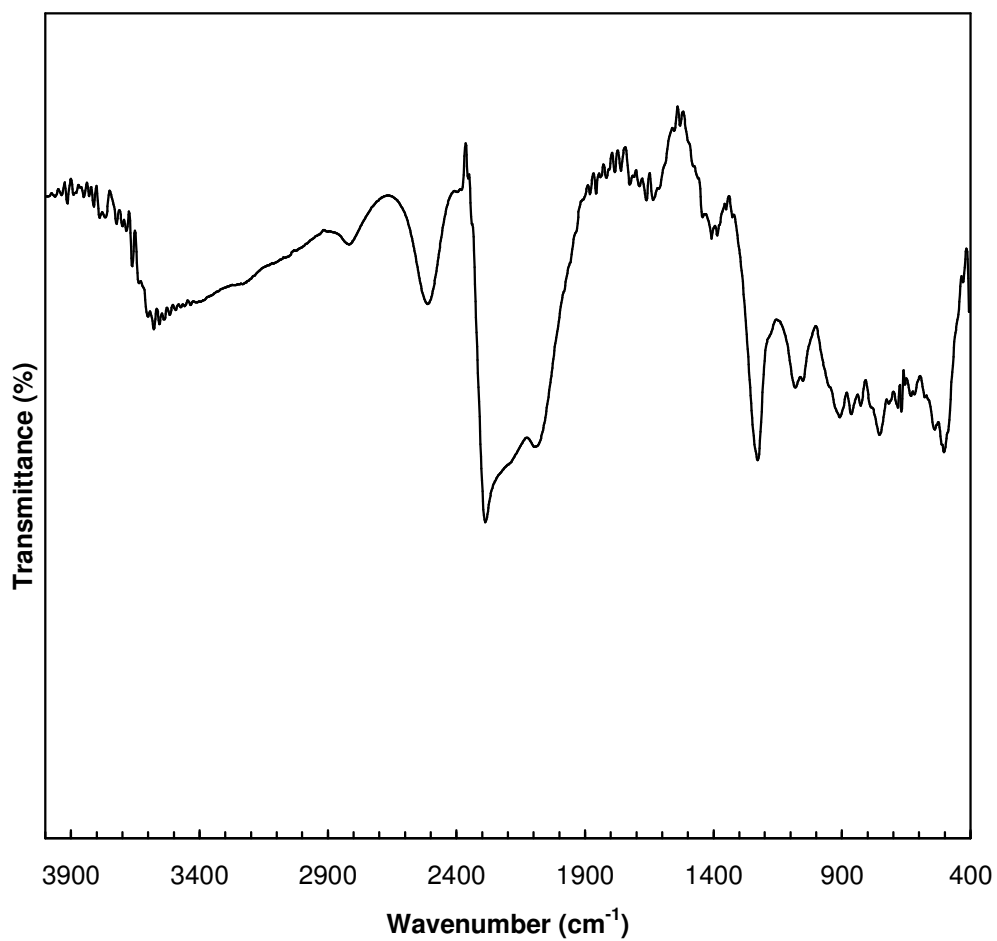


Figure D.1 FTIR spectrum of boron.

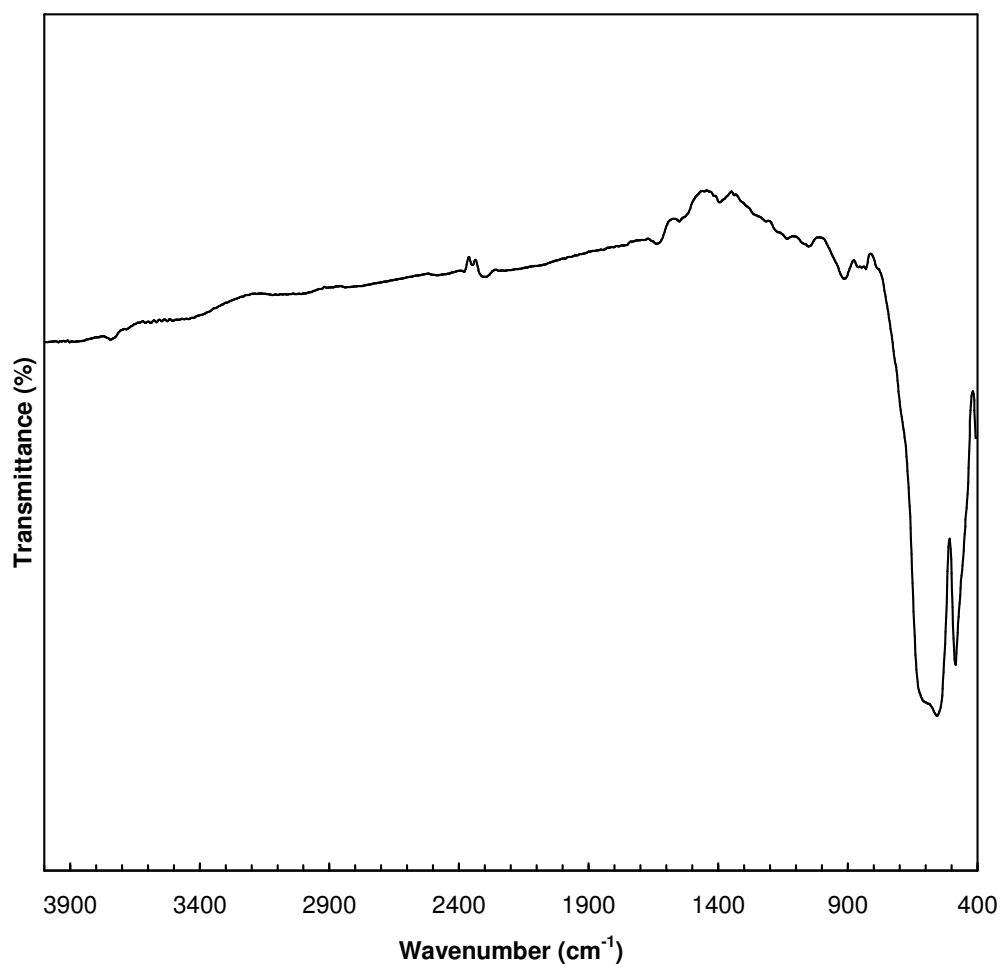


Figure D.2 FTIR spectrum of iron oxide.

APPENDIX E

XPS SPECTRA OF SYTHESIZED MATERIALS

XPS spectra of the materials synthesized at different temperatures with different boron to iron oxide weight ratios are given in Figures E1-E6.

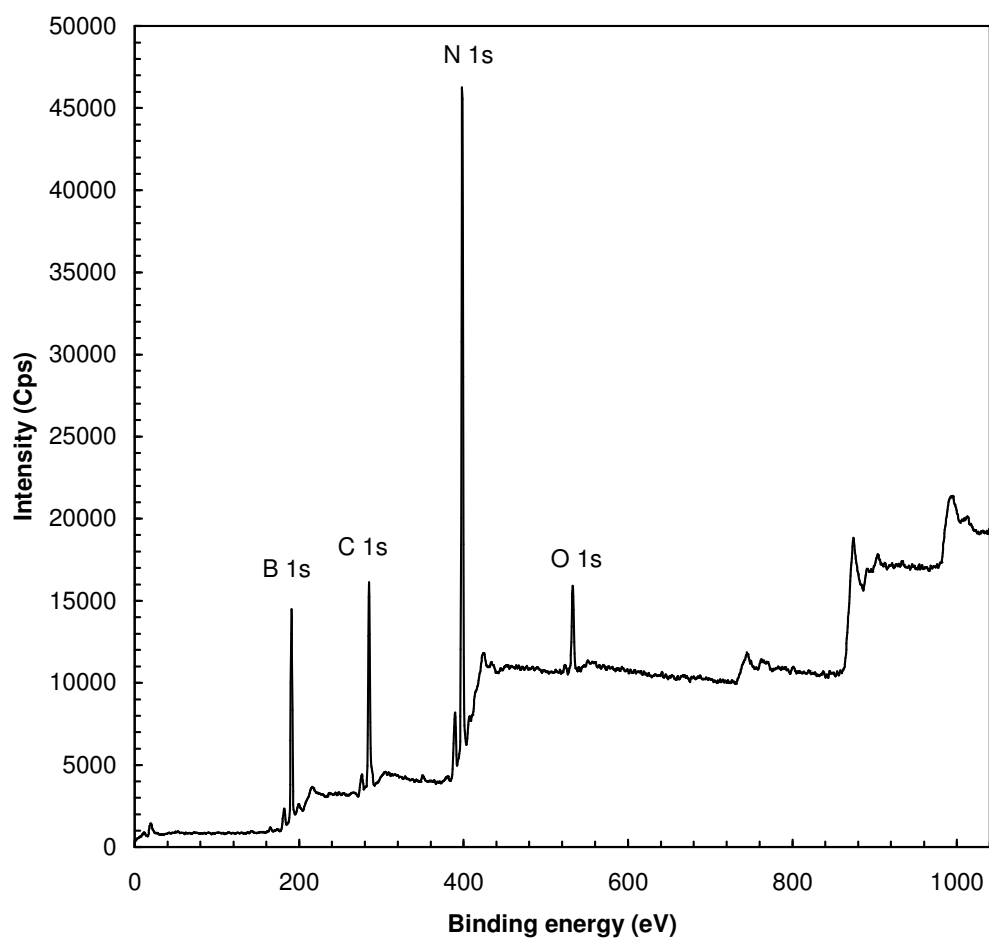


Figure E.1 XPS spectrum of BNNTs produced at 1400°C with B to Fe₂O₃ ratio of 15.

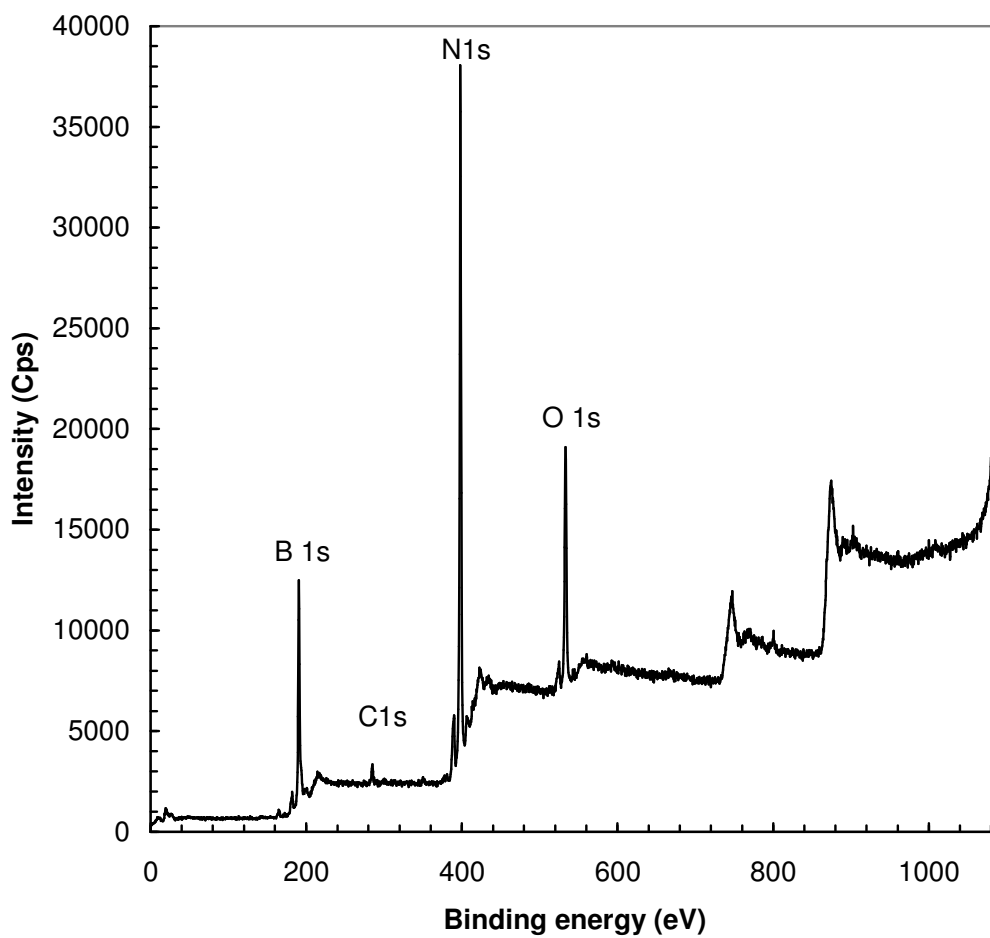


Figure E.2 XPS spectrum of BNNTs produced at 1200°C with B to Fe₂O₃ ratio of 15.

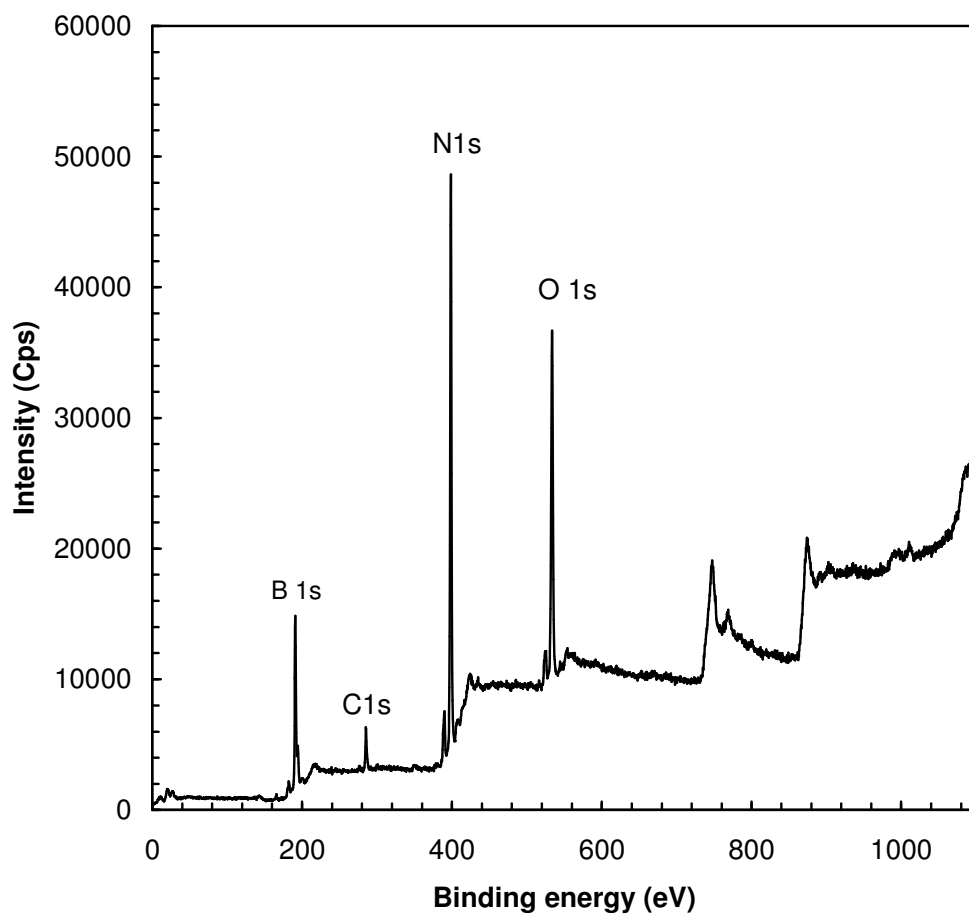


Figure E.3 XPS spectrum of BNNTs produced at 1100°C with B to Fe₂O₃ ratio of 15.

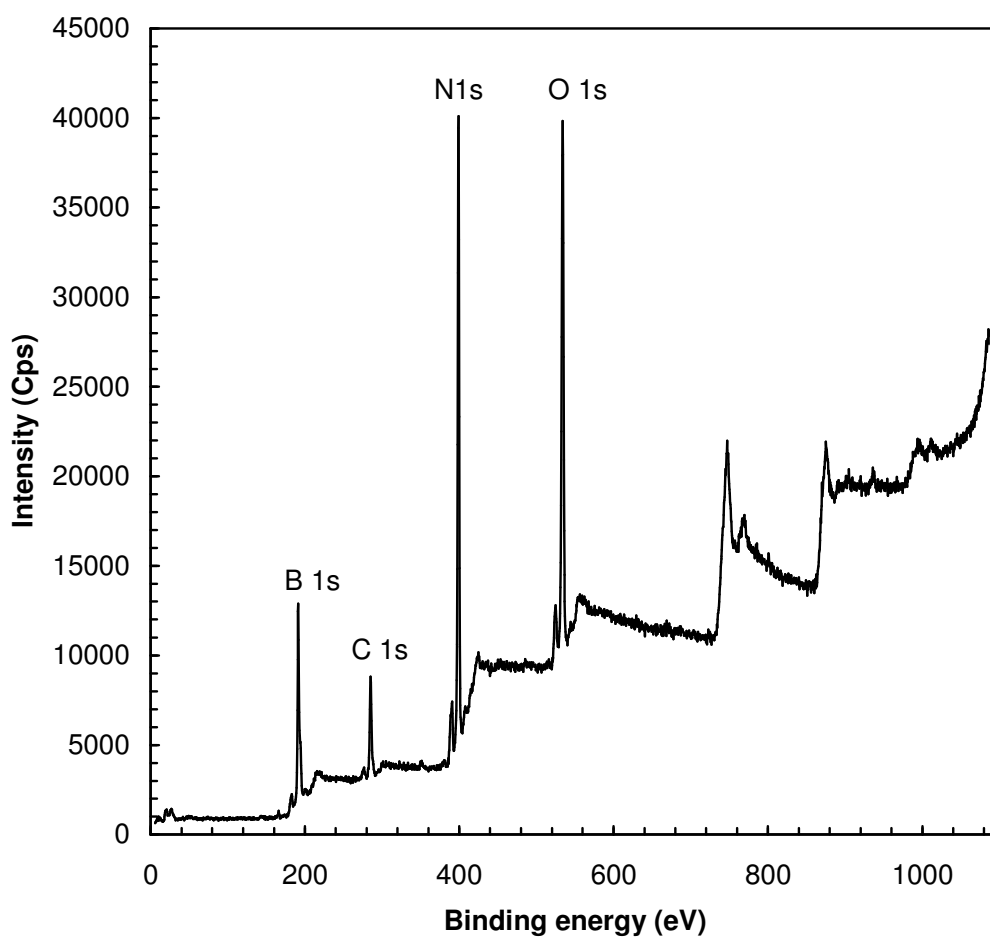


Figure E.4 XPS spectrum of BNNTs produced at 1000°C with B to Fe₂O₃ ratio of 15.

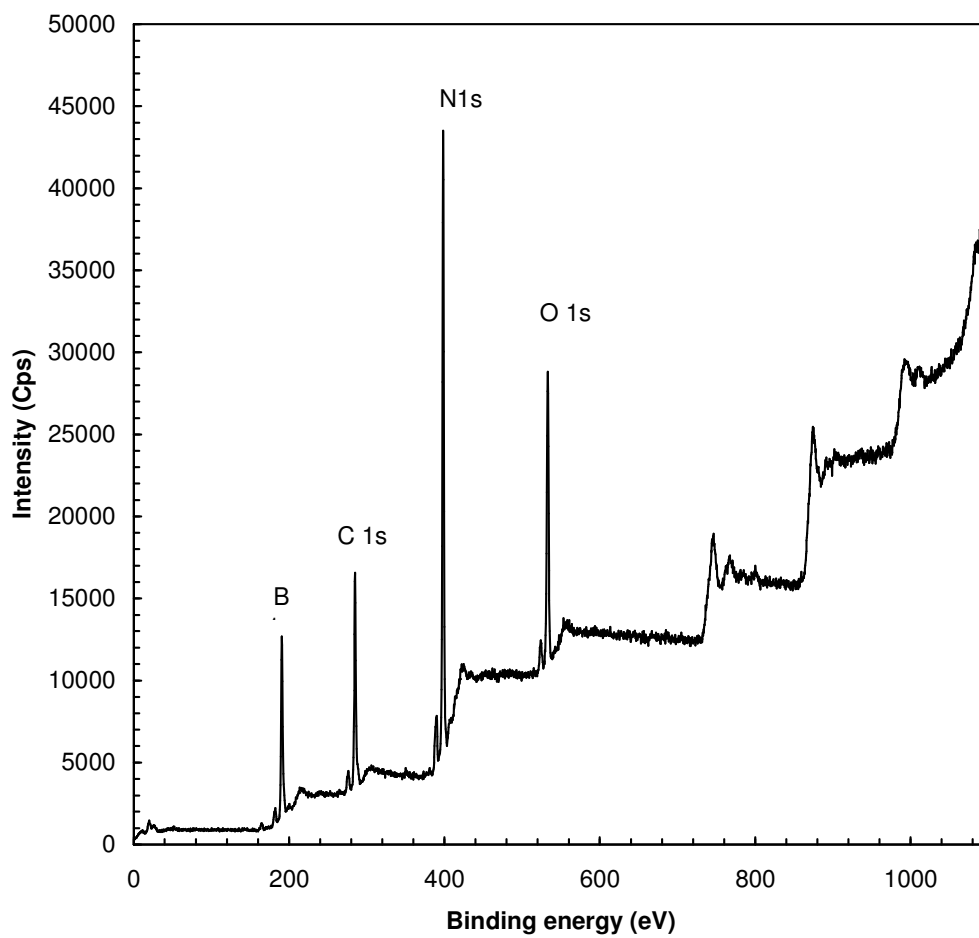


Figure E.5 XPS spectrum of BNNTs produced at 900°C with B to Fe₂O₃ ratio of 15.

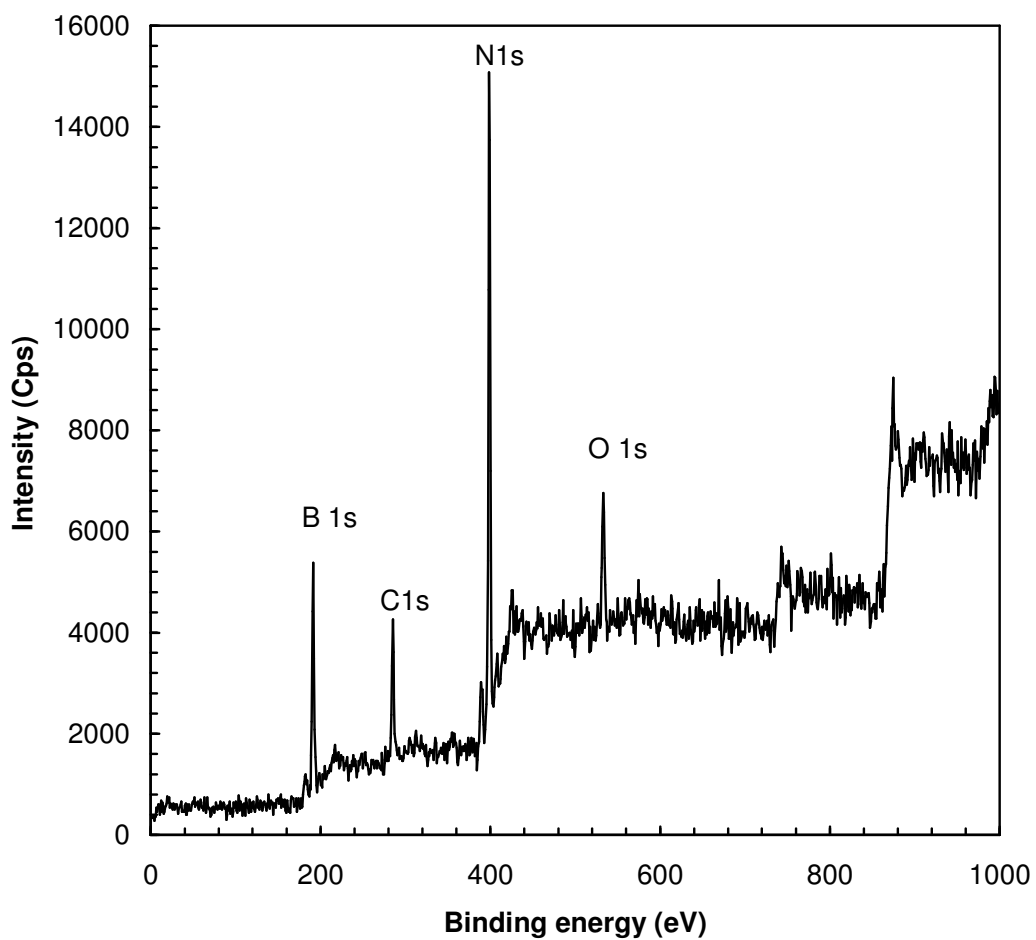


Figure E.6 XPS spectrum of BNNTs produced at 1300°C with B to Fe₂O₃ ratio of 20 with boron source of Sigma-Aldrich.

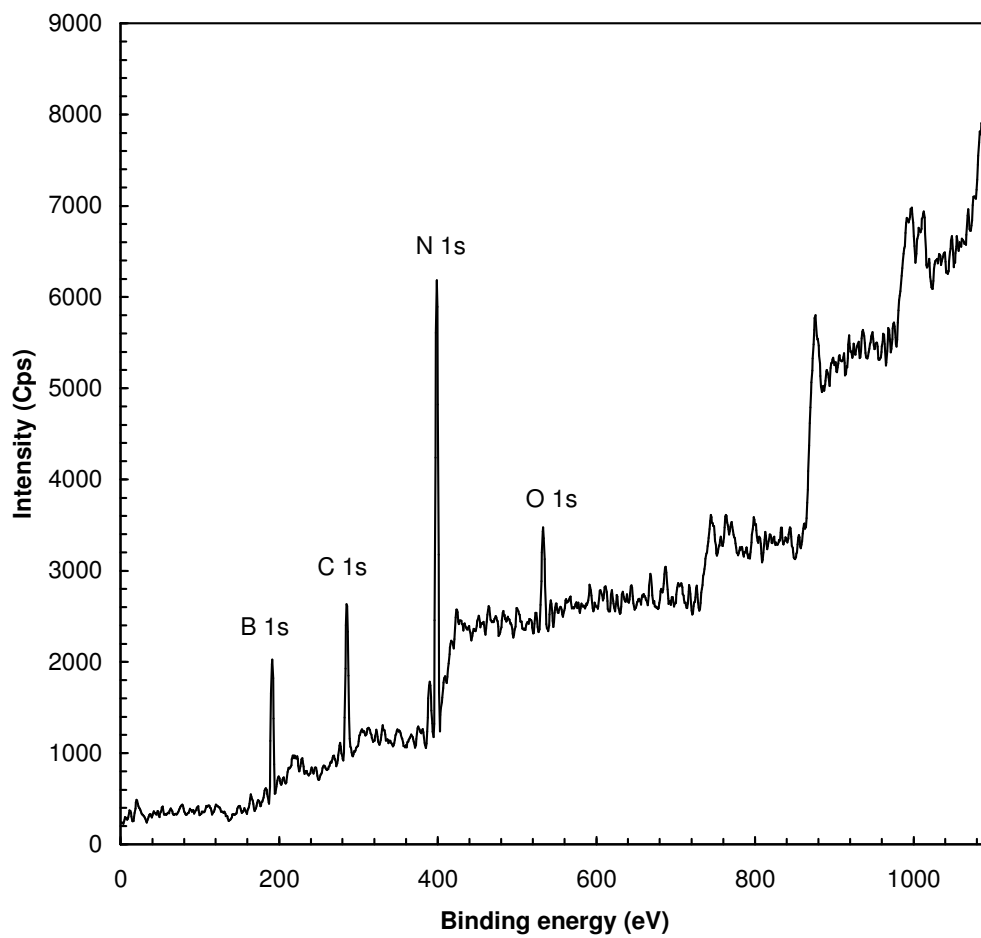


Figure E.7 XPS spectrum of BNNTs produced at 1300°C with B to Fe₂O₃ ratio of 20 with boron source of Merck.

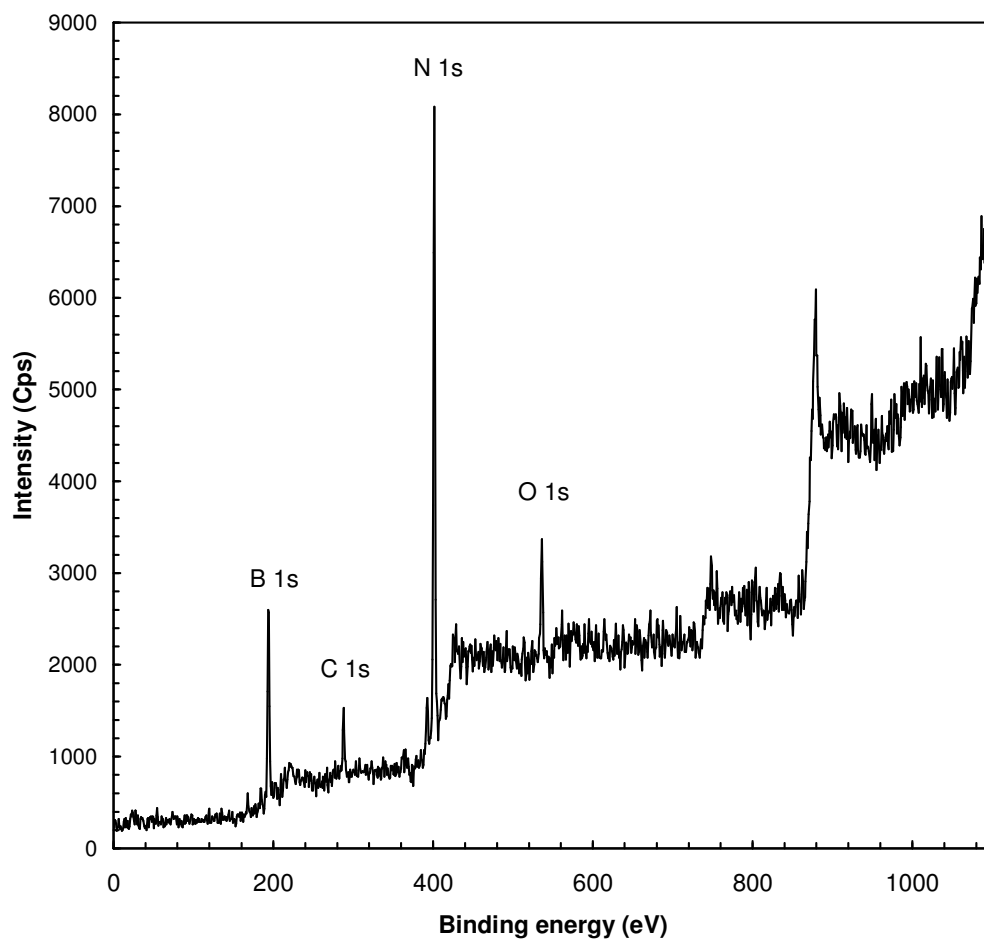


Figure E.8 XPS spectrum of BNNTs produced at 1300°C with B to Fe₂O₃ ratio of 5 with boron source of Merck.

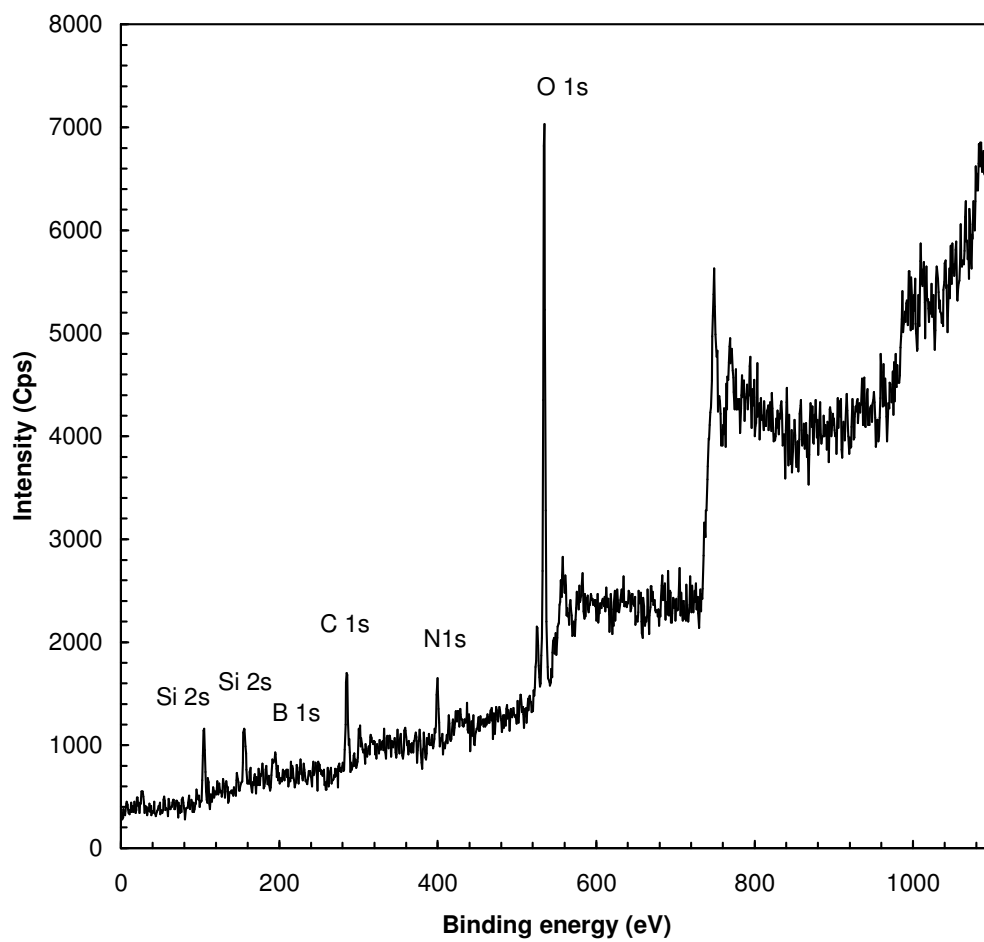


Figure E.9 XPS spectrum of BNNTs produced at 1300°C with B to Fe₂O₃ ratio of 1 with boron source of Merck.

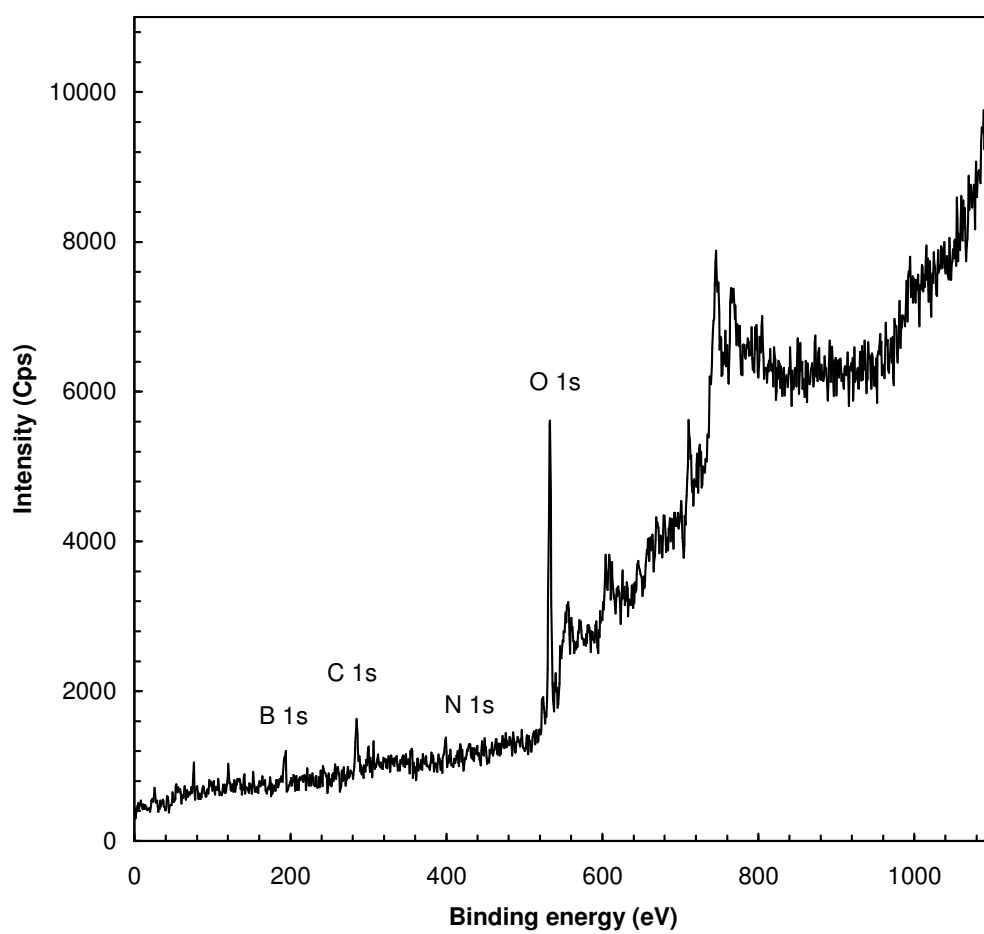


Figure E.10 XPS spectrum of BNNTs produced at 1300°C with B to Fe₂O₃ ratio of 0.5 with boron source of Merck.

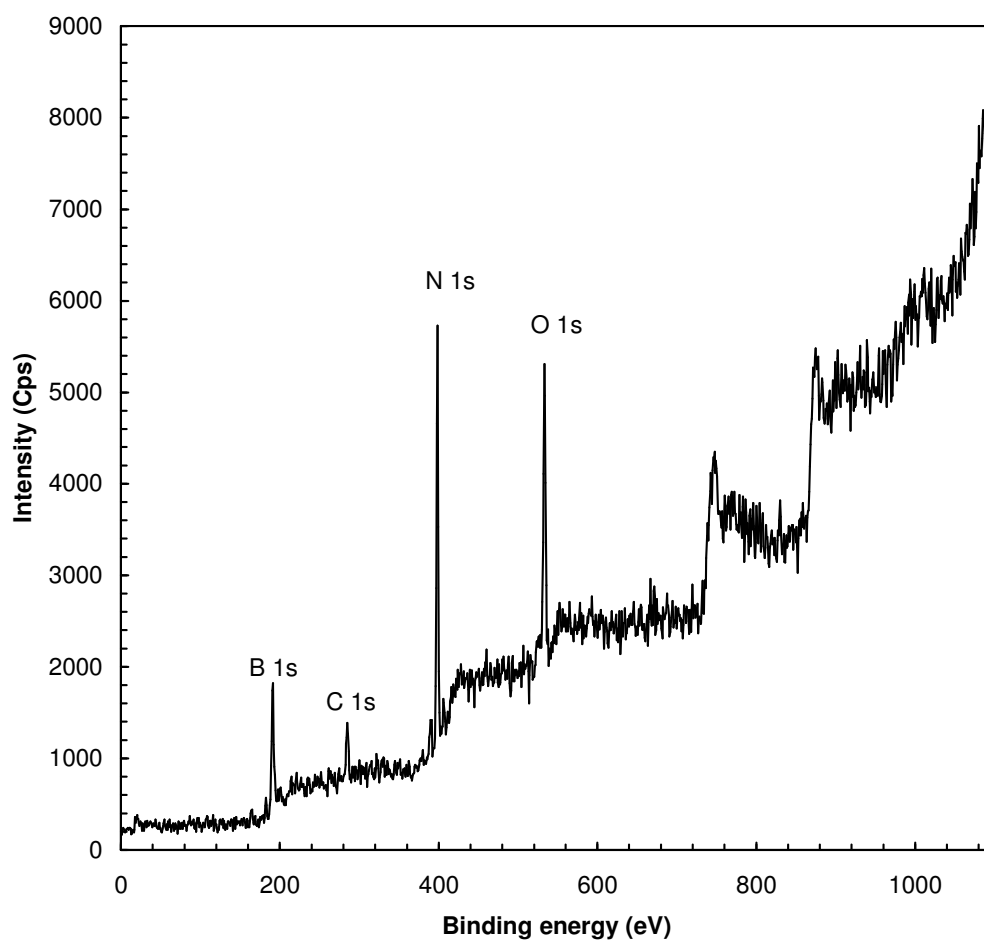
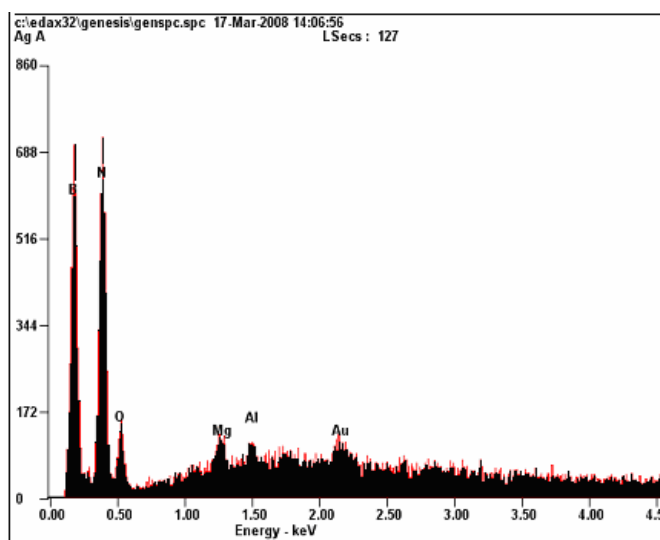


Figure E.11 XPS spectrum of BNNTs produced at 1300°C with B to Fe₂O₃ ratio of 20 with boron source of Sigma-Aldrich.

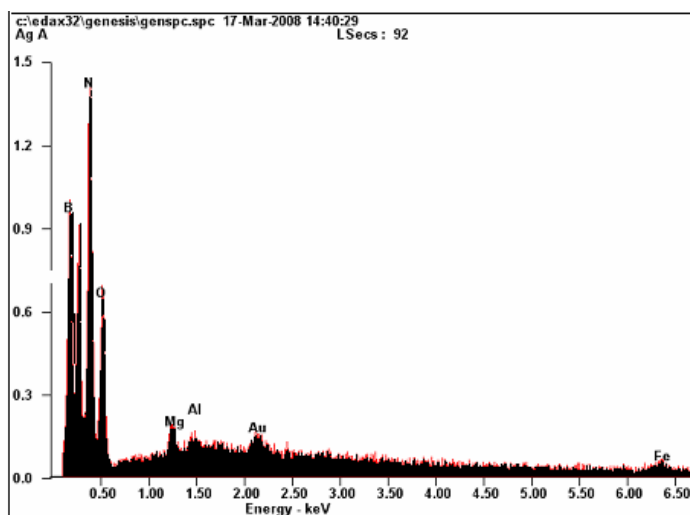
APPENDIX F

EDX SPECTRA OF PRODUCTS



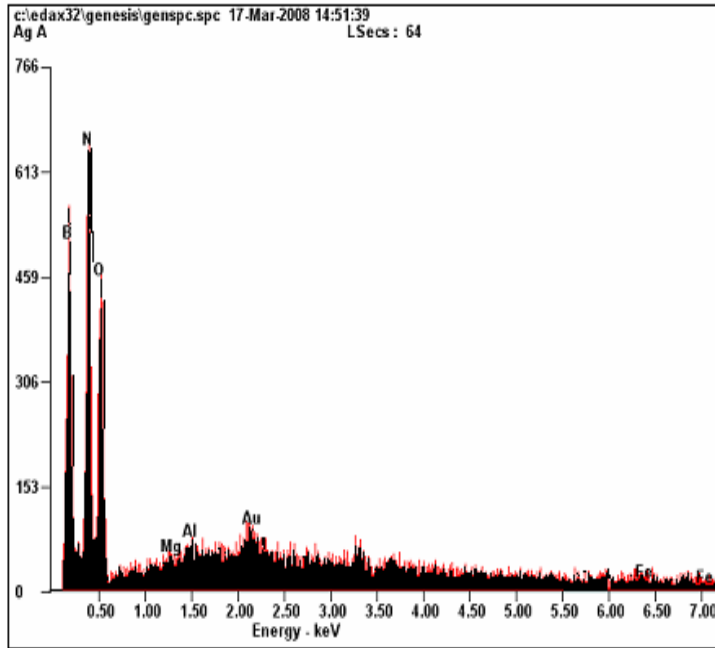
<i>Element</i>	<i>Wt %</i>	<i>At %</i>
<i>B K</i>	46.29	53.50
<i>N K</i>	46.28	41.28
<i>O K</i>	06.29	04.91
<i>Mg K</i>	00.38	00.19
<i>Al K</i>	00.17	00.08
<i>Au M</i>	00.60	00.04

Figure F.1 EDX spectrum of BNNTs produced at 1300°C with B to Fe₂O₃ weight ratio of 15.



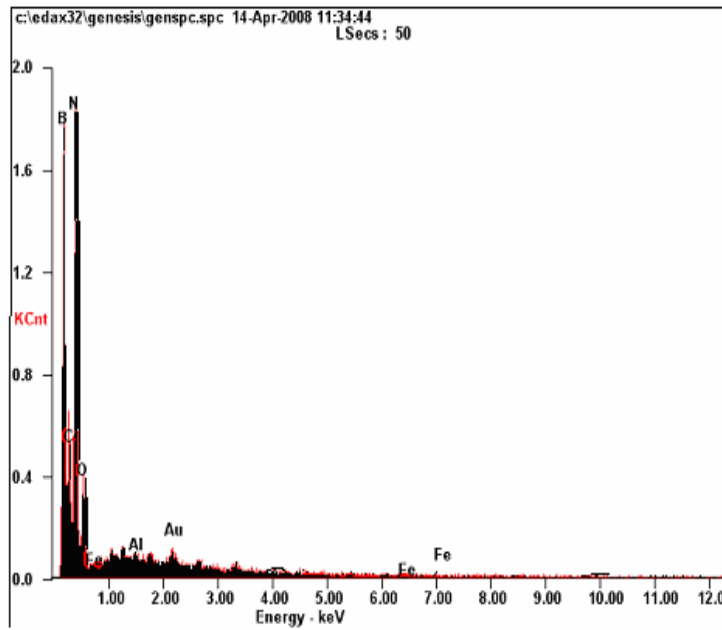
<i>Element</i>	<i>Wt %</i>	<i>At %</i>
<i>B K</i>	40.70	48.16
<i>N K</i>	43.13	39.39
<i>O K</i>	15.21	12.16
<i>Mg K</i>	00.33	00.17
<i>Al K</i>	00.10	00.05
<i>Au M</i>	00.33	00.02
<i>Fe K</i>	00.19	00.04

Figure F.2 EDX spectrum of BNNTs produced at 1200°C with B to Fe₂O₃ weight ratio of 15.



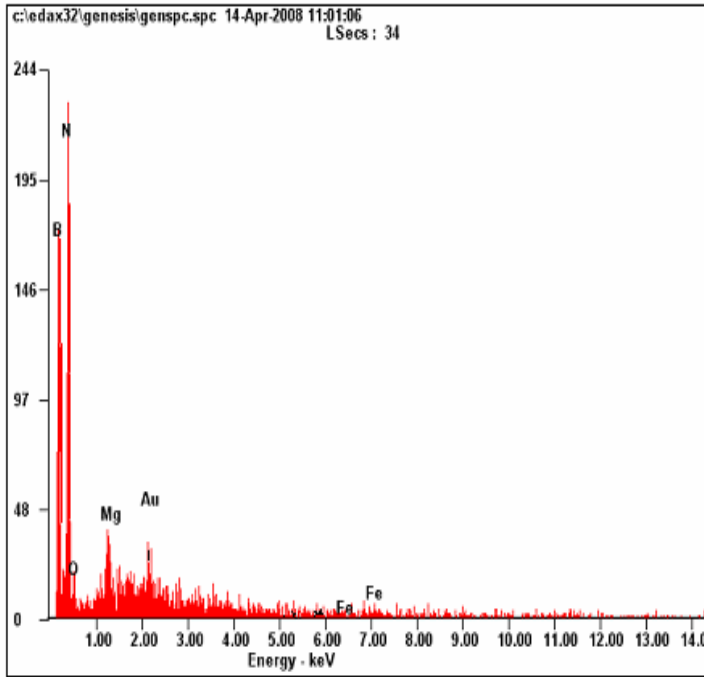
<i>Element</i>	<i>Wt %</i>	<i>At %</i>
<i>B K</i>	42.09	49.82
<i>N K</i>	37.80	34.54
<i>O K</i>	19.39	15.51
<i>MgK</i>	00.07	00.04
<i>AlK</i>	00.05	00.02
<i>AuM</i>	00.44	00.03
<i>FeK</i>	00.17	00.04

Figure F.3 EDX spectrum of BNNTs produced at 1200°C with B to Fe₂O₃ weight ratio of 20 with boron source from Sigma-Aldrich.



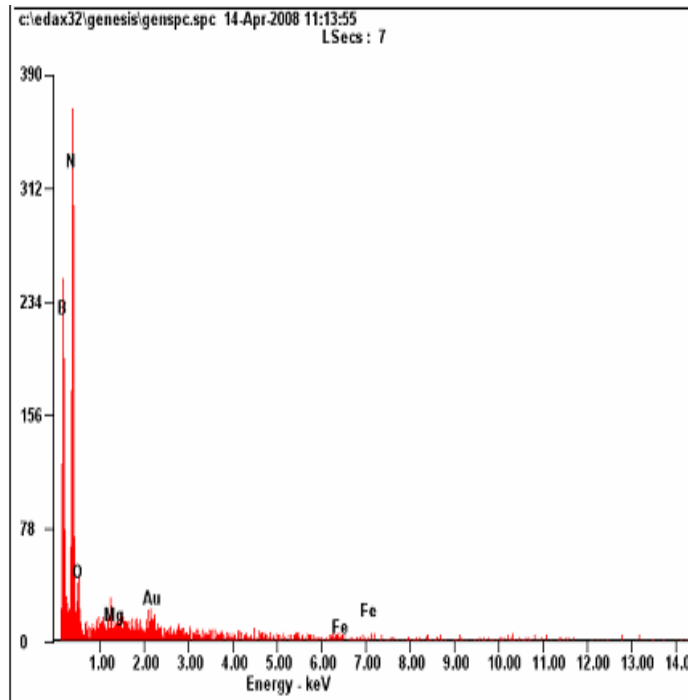
<i>Element</i>	<i>Wt %</i>	<i>At %</i>
<i>B K</i>	36.76	42.70
<i>C K</i>	12.40	12.97
<i>N K</i>	43.85	39.32
<i>O K</i>	06.25	04.91
<i>AlK</i>	00.06	00.03
<i>AuM</i>	00.51	00.03
<i>FeK</i>	00.16	00.04

Figure F.4 EDX spectrum of BNNTs produced at 900°C with B to Fe₂O₃ weight ratio of 15.



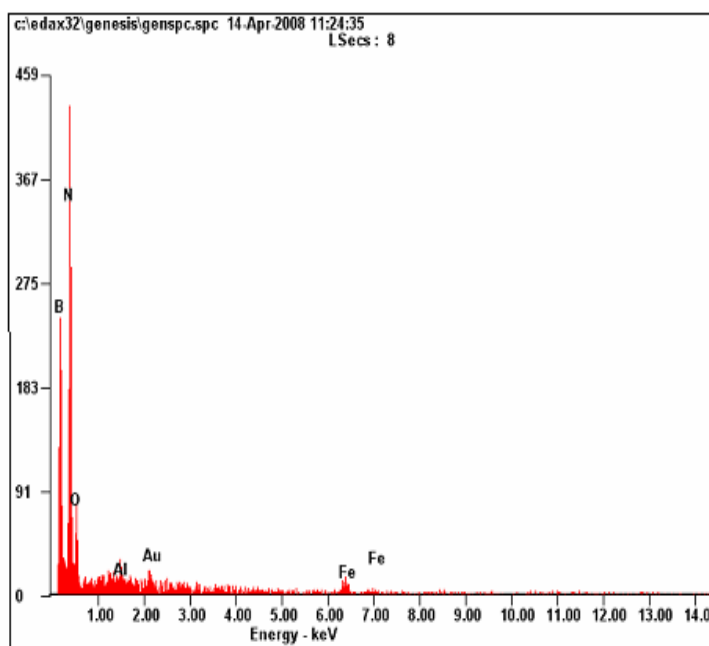
<i>Element</i>	<i>Wt %</i>	<i>At %</i>
<i>B K</i>	41.69	49.36
<i>N K</i>	50.96	46.57
<i>O K</i>	04.19	03.35
<i>MgK</i>	00.96	00.50
<i>AuM</i>	01.74	00.11
<i>FeK</i>	00.46	00.11

Figure F.5 EDX spectrum of BNNTs produced at 1300°C with B to Fe₂O₃ weight ratio of 5.



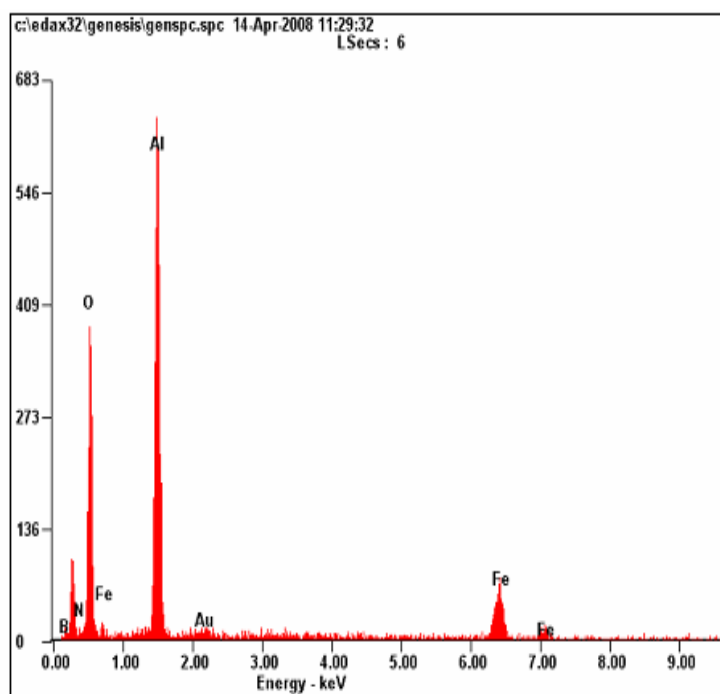
<i>Element</i>	<i>Wt %</i>	<i>At %</i>
<i>B K</i>	40.54	47.58
<i>N K</i>	52.41	47.48
<i>O K</i>	05.95	04.72
<i>MgK</i>	00.23	00.12
<i>AuM</i>	00.64	00.04
<i>FeK</i>	00.23	00.05

Figure F.6 EDX spectrum of BNNTs produced at 1300°C with B to Fe₂O₃ weight ratio of 20.



<i>Element</i>	<i>Wt %</i>	<i>At %</i>
<i>B K</i>	39.64	47.07
<i>N K</i>	50.00	45.83
<i>O K</i>	08.39	06.73
<i>Al K</i>	00.16	00.08
<i>Au M</i>	00.76	00.05
<i>Fe K</i>	01.05	00.24

Figure F.7 EDX spectrum of BNNTs produced at 1300°C with B to Fe₂O₃ weight ratio of 1.



<i>Element</i>	<i>Wt %</i>	<i>At %</i>
<i>B K</i>	14.04	24.32
<i>N K</i>	03.09	04.13
<i>O K</i>	41.24	48.28
<i>Al K</i>	27.02	18.76
<i>Au M</i>	01.60	00.15
<i>Fe K</i>	13.02	04.37

Figure F.8 EDX spectrum of BNNTs produced at 1300°C with B to Fe₂O₃ weight ratio of 0.5.

APPENDIX G

NITROGEN ADSORPTION/DESORPTION ISOTHERMS

G.1 BET Method

BET Method is a method that is used for determination of the surface area of the solid material and developed by Brauner, Emmet and Teller. It is a rule for the physical adsorption of gas molecules on a solid surface.

The multipoint surface area of the material is calculated from the BET equation (Eq. F.1). BET equation is obtained by extending the Langmuir theory (for monolayer adsorption) to multilayer adsorption. According to the BET, physical adsorption occurs on a solid in layers infinitely, there is no interaction between each adsorption layer and Langmuir theory is applied to the each layer.

$$\frac{1}{V[(P_o/P)-1]} = \frac{C-1}{V_m C} \left(\frac{P}{P_o} \right) + \frac{1}{V_m C} \quad (\text{F.1})$$

where;

C= isotherm constant depending on the pore structure of the adsorbate

V= volume adsorbed

V_m = volume adsorbed for monolayer coverage

P= equilibrium pressure

P_o = saturation vapor pressure of the adsorbate.

If the system obeys the BET model, plot of $1/[V(1-P/P_0)]$ versus (P/P_0-1) should give straight line for $0.05 < P/P_0 < 0.35$ and the slope of the plot gives $1/V_m C$ and the intercept of the plot gives $1/V_m$.

The total surface area is given by

$$S_g = \left[\frac{V_m N_o}{V} \right] \alpha \quad (\text{F. 2})$$

where,

S_g = total surface area

V_m = volume adsorbed for monolayer coverage

V = volume adsorbed

N_o = Avogadro's number, 6.02×10^{23} molecules/mol

α = value for the area covered by one adsorbed molecule

$$\alpha = 1.09 \left[\frac{M}{N_o \rho} \right]^{\frac{2}{3}} \quad (\text{F. 3})$$

where,

M = molecular weight

ρ = density of the adsorbed molecules

and $\alpha = 0.162 \text{ nm}^2/\text{molecule}$ for nitrogen

G.2 Single Point BET Method

For high values of C , the intercept of the BET equation is small compared to the slope and taken as zero. So, the BET equation becomes,

$$\frac{1}{V[(P_o/P)-1]} = \frac{C-1}{V_m C} \left(\frac{P}{P_o} \right) \quad (\text{F. 4})$$

Since the intercept is assumed to be vanished, equation F.4 becomes,

$$V_m = V(1 - P/P_o) \quad (\text{F. 5})$$

The total surface area measured by the single point method is calculated as follows:

$$S_t = \frac{PV_m N_o A_{cs}}{RT} \left(1 - \frac{P}{P_o} \right) \quad (\text{F. 6})$$

$$A_{cs} = 16.2 \times 10^{-20} \text{ m}^2 \text{ for nitrogen}$$